DISSERTATION

PROPAGATION OF THE SIDOARDJO MUD IN THE PORONG RIVER, EAST JAVA, INDONESIA

Submitted by

Neil Andika

Department of Civil and Environmental Engineering

In partial fulfillment of the requirements

For the Degree of Doctor of Philosophy

Colorado State University

Fort Collins, Colorado

Summer 2021

Doctoral Committee:

Advisor: Pierre Y. Julien

Neil S. Grigg
Robert Ettema
Sara Rathburn

ABSTRACT

PROPAGATION OF THE SIDOARDJO MUD IN THE PORONG RIVER, EAST JAVA, INDONESIA

The Sidoarjo Mud Volcano in East Java, Indonesia erupted on May 29, 2006. It caused controversy because of the impact of the mud volcano had on communities around it. The discharge of the mud volcano was 50,000 m^3/d (Harnanto, 2011) which comprised a 35% concentration of silt and clay. To mitigate the damage to surrounding regions, the Government of Indonesia diverted the mud to Madura Strait through the Porong River in 2016 (Hadimuljono, 2008). The objectives of this thesis are to: (1) understand the physical properties of mud from the mud volcano and its interaction with the water in the river; (2) carry out field measurements of sediment concentration along the Porong River for a model validation; (3) determine how the concentration of mud from the mud volcano varies along the river; (4) create a framework or guideline for the mitigation of a mud volcano disaster in the future.

Laboratory experiments were used to test the sediment properties. The experiments of turbidity and sediment concentration, C, concluded that the linear regression, $C = 5.297 \times Turbidity + 24$, was the best fitted regression. Flocculation tests in 2019 showed that the recorded deflocculated settling velocity for the sample of the Ginonjo Outlet was 0.013 mm/s which was approximately 2 times slower than the natural settling velocity of 0.028 mm/s. This value was one order slower than the general settling velocity for flocculated particles.

Two field measurement programs were completed, in July 2018 and in September 2019. The field programs in 2018 observed the sediment concentration along the Porong River at 106 cross-

sections and the point source sediment concentration at Ginonjo Outlet was 57,000 mg/l. It was found that the observed maximum sediment concentration ranged between 691 mg/l and 4,198 mg/l. The average sediment concentration at the downstream end of the Porong River on the other hand was 90 mg/l. The field program in 2019 captured the vertical sediment concentration profiles of the first 4 km of the Porong River. The highest near-bed sediment concentration was 1,500 mg/l at Line C cross-section 9. This was followed by 1,450 mg/l at Line C cross-section 6. These measurements showed that the sediment concentration are uniform along the Porong River except for the first 4 km where the bottom sediment concentration are higher.

There are three flow conditions based on the hydrograph of the Porong River: low flow with 45 m^3/s, medium flow with 250 m^3/s, and high flow with 2500 m^3/s. For low flow, the average flow velocity was 0.12 m/s and the shear velocity was 0.01 m/s. Results from the two-dimensional mixing model without settling was the fully-mixed concentration for low flow condition achieved at 4 km downstream from the outlet with a concentration of 470 mg/l. There was 380 mg/l difference between the model's result and the observed concentration.

The two-dimensional mixing and setting model without flocculation produced a result of sediment concentration of 195 mg/l at the downstream end of the Porong River. This came from the clay fraction which was about 48% of the total sediment. The sediment concentration difference between this model and the observed data was 105 mg/l. The two-dimensional mixing and setting model with flocculation was then used. The sediment concentration at the left bank side of the Porong River was about 90 mg/l, which matched the observed data. The gravel, sand and coarser silt fractions settled at the first 4 km of the study reach was also captured by the model. This result proved that the two-dimensional mixing and settling model with flocculation was a suitable model for the sediment propagation in Porong River.

ACKNOWLEDGEMENTS

All prise be to Allah, The One Almighty God and The Exalted. Because of His unlimited kindness, love, mercy, and guidance, I was able to finish this dissertation. Peace and salutation are uttered to our beloved Prophet Muhammad Peace Be Upon Him who has broung humanity to the light of Islam.

First and foremost, I am very grateful to Dr. Pierre Y. Julien as my advisor who gave me unending encouragement, helpful advice, and support throughout my Ph.D. program since 2015. I would like to thank the committee member: Dr. Neil S. Grigg, Dr. Robert Ettema, and Dr. Sara Rathburn for their outstanding contribution to this research. Also, I would like to thank CSU faculty including Dr. Timothy Gates, Dr. Darrell Fontane, Dr. Karan Venayagamoorthy, Dr. Mazdak Arabi, and Dr. Ellen Wohl for their valuable classes. I would also thank Linda Hinshaw, Laurie Alburn, and Susheela Mallipudi for their help and patience.

I am thankful for LPDP (Indonesia Endownment Fund for Education) for the financial support from my Master program to the extension for my Ph.D. program. Also, I would like to thank PPLS (Sidoardjo Mud Control Center – Indonesia) and Ministry of Public Work and Housing of the Republic of Indonesia for their help and assistance for my research.

I would like to send my gratitude for all my research mate and class mate including Marcos Palu, Chunyao Yang, Woochul Kang, Hwa Young Kim, Susan Cundiff, Weimin Li, Kristin LaForge, Kennard Lai, Corinne Horner, Tori Beckwith, Caitlin Fogarty, Dr. Jai Hong Lee, Dr. Seongjoon Byeon, Dr. Joonhak Lee, Dr. Eunkyung Jang, and Dr. Xudong Chen. I will miss our Seminar Series.

I am very thankful to my Indonesian friends in Fort Collins: Faizal Rohmat and Winda, Brandon Bernandus, Gabriel Kereh, Bagus Mahardika, Owen Carniege Limarta, Dhira Prasanti, Eka Noviana, Monika Aprianti, Aya Safira, Adji Witjaksono, Demison Tabuni, and all members of Permias Fort Collins for their friendship. We will conquer Indonesia together in near future. I would like to extend my gratitude to Mas Setyo Nugroho and Mbak Hesti, Mas Anton Pratama, Mbak Dessy Sapardina, Mas Ahmadin, and all Indonesian in Colorado for their support since I arrived in Colorado.

Finally, my deepest thanks to my beloved family, especially my parents M Basuki Hadimuljono and Kartika Nurani, my wife Aziza Widyani, my brothers and sisters, and all of my family members. Thank you for keep believing in me and keep giving me support. I love you all!

TABLE OF CONTENTS

LIST OF TABLES

LIST OF FIGURES

CHAPTER 1 INTRODUCTION

1.1 Background

The Sidoardjo Mud Volcano erupted on May 29, 2006 in East Java, Indonesia. In 2007, the eruption rate was 110,000 m^3/d and the volumetric sediment concentration increased to 70% (Mazzini et al., 2007). The average eruption rate had gradually decreased to 50,000 m^3/d since then (Harnanto, 2011). The Sidoardjo Mud Volcano, which is arguably the biggest onshore mud volcano recorded, caused devastation to the surrounding area. The Sidoardjo Mud Volcano caused at least 30,000 people to flee their homes and become refugees (McMichael, 2009), buried 10,000 houses and forced about 23 companies to shut down, as shown in **Figure 1**. The total economic loss based on data from the Ministry of Public Works of Indonesia report in 2007 was Rp 7.6 trillion, or about $565 million USD. On March 22, 2007, the impacted area, as determined by the National Mudflow Disaster Management Team (Tim Nasional Penanggulangan Semburan Lumpur Sidoardjo), was 650 ha.

A key issue was that the mud volcano was expected to flow at least until 2027 as the volume of mud was found to be consistently increasing inside the reservoir. Thus, containment measure was necessary. In addition, the Management Team discharged some portions of the mud to Madura Strait through the Porong River since November 2006 (Hadimuljono, 2008). The diversion were managed by Sidoardjo Mud Control Agency (or BPLS – Badan Penanggulangan Lumpur Sidoardjo) from 2007, and continued by Sidoardjo Mud Control Center (or PPLS – Pusat Pengendalian Lumpur Sidoardjo) from 2017. This catastrophic event raised several scientific and technical questions regarding the interaction between mud volcanoes and fluvial systems in heavily populated areas. Is the mud harmful to human health? Can human or living organism live

near the mud volcano? Does the presence of Sidoardjo Mud decrease the water quality of the Porong River?

Figure 1 *Mud flow drowned several settlements and infrastructures in Sidoardjo since 2006*

1.2 Problem Statement

The Porong River flows approximately 2 km away from the creater of the mud volcano. Because of its proximity, the river was used as a channel to transport the mud towards the Madura Strait. The mud was diluted before it was discharged into the Porong River, as shown in **Figure 2,** to reduce the sediment concentration into the Porong River. This action could change the river dynamic, by increasing the sediment concentration and disturbing the fish and native wildlife along the Porong River. In addition, this action also caused sedimentation in the Madura Strait. The overall impact however, varied at different sediment concentrations depending on the discharged mixture.

Figure 2 *The discharge of the mud mixture into the Porong River at the Pejarakan Outlet*

1.3 Research Objective

The overall objective of this research is to determine whether the diversion of the mud is a good idea or not from the technical stand point. The primary concerns of this research are the increase in the sediment concentration which includes: (1) turbidity over a range of discharges in the Porong River; (2) the high concentration of fine sediment; and (3) the size of mud particles and its settling processes. To achieve this objective, this research would:

1. Determine the properties of mud from the mud volcano and its interaction with the water in the Porong River, including the particle size distribution analysis, relationship between turbidity and suspended sediment concentration and flocculation/settling properties.
2. Carry out field measurements of turbidity and sediment concentration along the Porong River to the Madura Strait to test the computational models and understand the concentration distribution in the river.
3. Develop models for the propagation of suspended sediment with/without settling in the Porong River from the steady point source and determine how the sediment concentration varies aling the river.
4. Create a framework or guideline for the mitigation of a mud volcano disaster in the future and for any other related problem.

This research addresses a unique topic in terms of civil and environmental engineering namely the impacts of discharging mud mixture from the mud reservoirs into the Porong River. This topic carefully investigates and analyzes the dynamics of the sediment propagation along the Porong River and the sedimentation issue in the estuary and coastal area.

This dissertation consists of 8 chapters. Chapter 1 introduces the problems of Sidoardjo Mud Volcano and outlines the objectives of this research. Chapter 2 presents a review of previous

studies conducted on the topic and methods to approach the problems. Chapter 3 describes the study reach of this research. Chapter 4 focuses on the properties of the mud and the processes of interaction with a river, such as turbidity versus sediment concentration and flocculation. Chapter 5 covers the field measurements, including instantaneous sampling and vertical sediment concentration profiles. Chapter 6 presents the modeling component of the research, for example HEC-RAS and the two-dimensional mixing and settling model with/without flocculation for the suspended sediment propagation along the Porong River. Chapter 7 covers the management issues and recommendations based on the experiences from the Sidoardjo Mud Volcano. Finally, chapter 8 provides the conclusions of this research.

CHAPTER 2 LITERATURE REVIEW

2.1 Mud Volcano

Two geological terms describe piercement structures: mud diapirs and mud volcanoes. Mud diapirs are a slow, upward movement of sedimentary mass that does not reach the surface, while the latter term refers to a similar geological phenomenon on reaching the surface (Kopf, 2002). Mud volcanoes are created by thick sedimentary cover dominated by clay (i.e. smectite, illite or kaolinite), plastic shale layers and gas accumulation in the subsurface. They have excessively high pore pressure, rapid subsidence of sedimentary cover, tectonic activities, and flow of fluid mass along fractures (Milkov, 2000; Blouin et al., 2019). Some studies suggests that mud volcanoes are triggered by earthquake, particulary when the earthquake is at least 6 Mercalli scale and less than 100 km from the mud volcano (Mellors et al., 2007; Manga et al., 2009).

The development of mud volcanoes is explained as follows (Satyana and Asnidar, 2008): Stage 1 – deformation of mud shale, Stage 2 – upward movement of mud shale (mud diapirs), Stage 3 – mud shale extrusion to the surface (mud volcanoes), and Stage 4 – dormant period or end of shale extrusion. Dimitrov (2002) studied the shape and size of mud volcanoes. He found that the general shape of mud volcano is a conical mountain, as described in **Figure 3**. However, other forms such as flat cones, domes, and calderas have also been identified. The size varies from a few meters up to 500 m in heights and the diameter of the craters can reach up to 500 m, with the base width extending as far as 4 km.

There are over 900 onshore and 800 offshore mud volcanoes recorded (Dimitrov, 2002). In Indonesia, mud volcanoes can be found in Sumatra, Java, Semau, Rotti, Tanimbar, Sumba, Flores and Papua (Williams et al., 1984; Breen et al. 1986; Silver et al. 1986; Dimitrov, 2002; Kopf, 2002). The Bogor – North Serayu – Kendeng depression zone is the main location of mud diapirs

and mud volcanoes on the island of Java, as shown in **Figure 4**. The length and width of this zone is 1,000 km and 60 km, respectively, and starts from the Rangkasbitung area in West Java to Madura Strait in East Java. The list of mud diapirs and mud volcanoes in this zone includes (Satyana and Asnidar, 2008):

1. Ciuyah Mud Volcano in Kuningan, West Java.
2. North Serayu Diapirs.
3. Bledug Kuwu Mud Volcano Complex in Central Java, which consists of Bledug Kuwu, Bledug Kesongo, Bledug Kropak, and several others.
4. Sangiran Dome, near Surakarta, Central Java, which is an extinct mud volcano.
5. Mud Volcanoes in East Kendeng Zone, around Surabaya – Sidoardjo, East Java, which are Sidoardjo Mud Volcano (also called LUSI – Lumpur or Mud and Sidoardjo), Kalang Anyar, Pulungan, Gunung Anyar, Gresik, Socah, Porong, and several others.

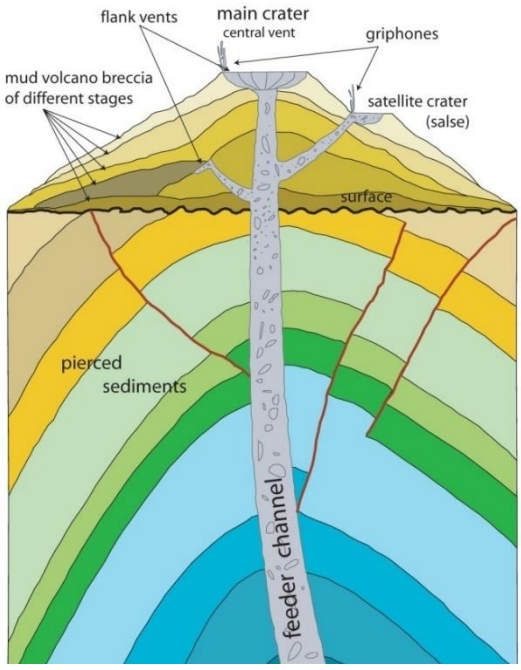

Figure 3 *Structure of a conical mud volcano (from Dimitrov, 2002)*

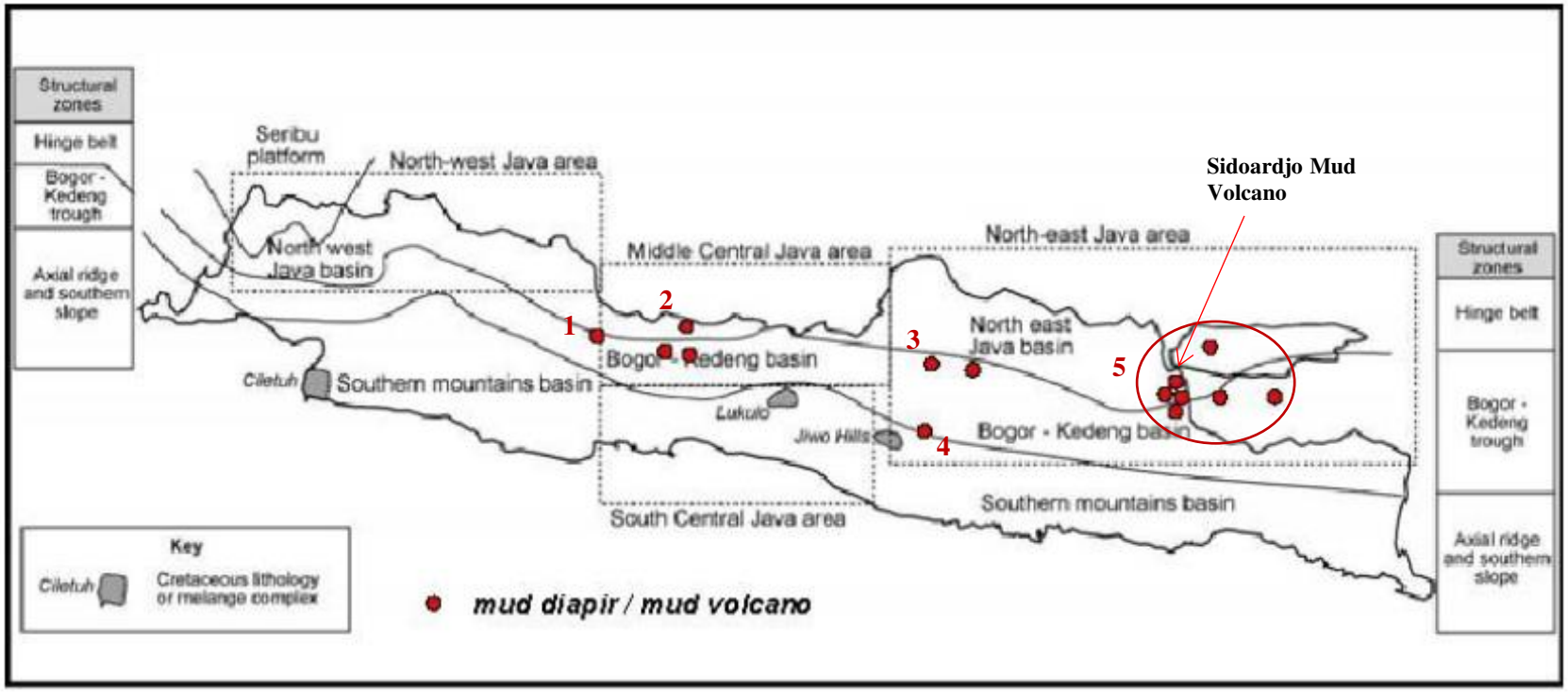

Figure 4 *The mud volcano distribution in the Bogor – North Serayu – Kendeng depression zone (after Satyana and Asnidar, 2008)*

2.2 Clay mineralogy

2.2.1 Structure of clay minerals

The term "clay material" refers to a group of phyllosilicate substance that derived from primary materials such as quartz, feldspar, micas, etc., which have been weathered by the Earth's surface (Brandon and Karathanasis, 2002). The foundation of all silicate structure is a four-sided building SiO_4^{4-} or tetrahedon, which consist of one Si^{4+} ions at its center and four O^2 ions at each apices. The horizontal connection of tetrahedron at the three corners creates an array called tetrahedral sheet. The other foundation is octahedron, which is an eight-sided building constructed by one cation (i.e. aluminum or magnesium) at its center and six O^2 ions surrounding the cation. A horizontal array of multiple octahedra is called octahedral sheet. The illustration of those essential foundations of silica structure are shown in **Figure 5**. Based on the formation and the number of tetrahedral and octahedral sheet in clay minerals, we can classified the clay minerals into 3 general group: 1:1 clay mineral, 2:1 clay mineral, and 2:1:1 clay mineral.

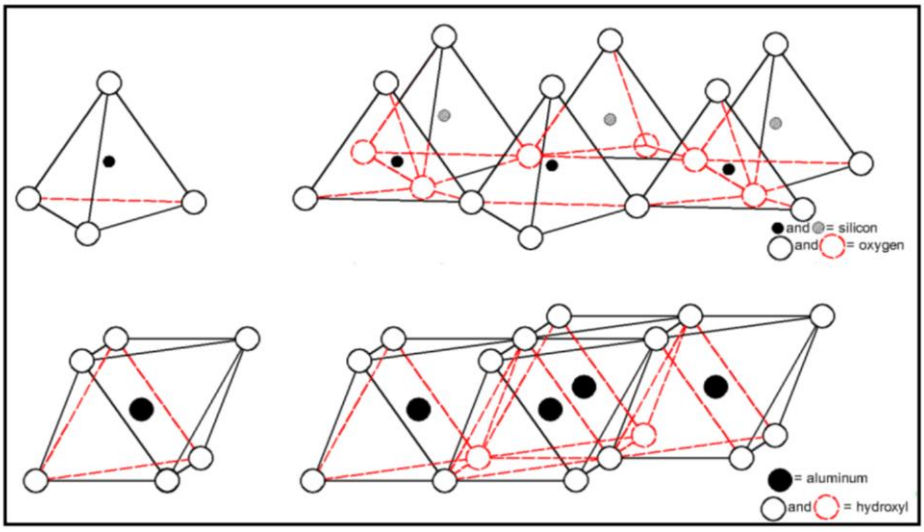

Figure 5 *Illustration of tetrahedron and tetrahedral sheel at top and octahedron and octahedral sheet at bottom (Aboubakr et al. 2013)*

A 1:1 clay mineral comprises one tetrahedral and one octahedral sheet as shown in **Figure 6**. The best representative of this type of clay mineral is kaolinite. Due to a tight hydrogen bonding between the two layers, the expansion capability of this clay mineral and the area of reactive surface are limited. The next type is a clay minerals with two tetrahedral and one octahedral sheets which is refered to a 2:1 clay mineral. There are many examples of this type of clay, but the three main groups are fine-grained mica, smectite and vermiculite. The last type is a clay mineral with two tetrahedral sheets, one octahedral sheet and one interlayer which is refered as 2:1:1 clay mineral or 2:2 clay mineral. The notable clay from this type is chlorite.

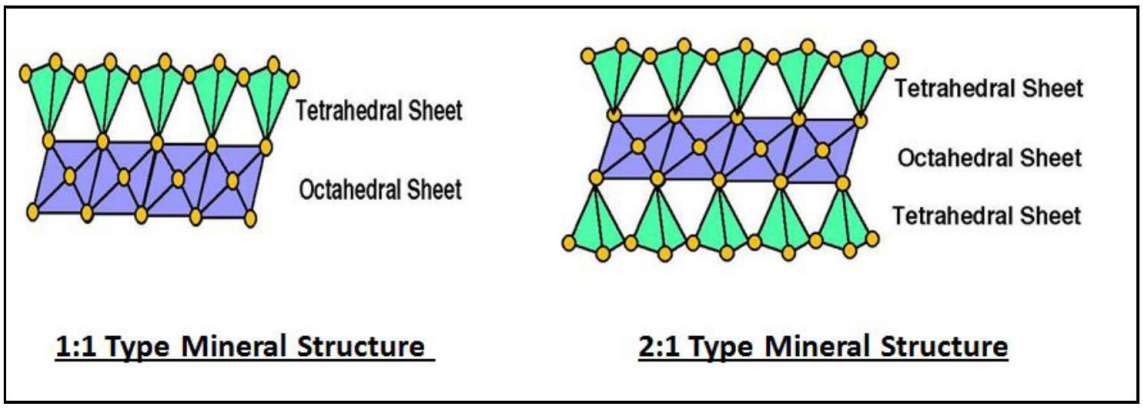

Figure 6 *Illustration of the silica structure for 1:1 clay mineral and 2:1 clay mineral (Sivakuga, 2001 at Marchuk, 2016)*

2.2.2 Properties and use of smectite clay mineral

The physicochemical properties of smectite clay material are related to the presence of exchangeable ions, the crystalline size, shape and arrangement. Several exchangeable ions are Ca, Mg, Na, H, and Li. Some of the members of smectite clay are montmorillonite, beidellite, nontronite, saponite and hectonite. Furthermore, illite has a similar structure with smectite, but with the presence of non-exchangeable K^+ ions.

If Ca and Mg are the predominant ions, the smectite is a non-swelling clay. However, if Na or Li are the predominant ions, the smectite has a high swelling capacity. This is because those ions help create a layer of water in the interlamellar surface in saturated condition as presented in **Figure 7**. Clay minerals with a strong swelling attribute are called active clay. In the clay industry, adding swelling properties into clay mineral can result in an activated clay. This can be done by replacing Ca or Mg ions with Na ion. The benefits of this are higher wet tensile strength and thermal resistance.

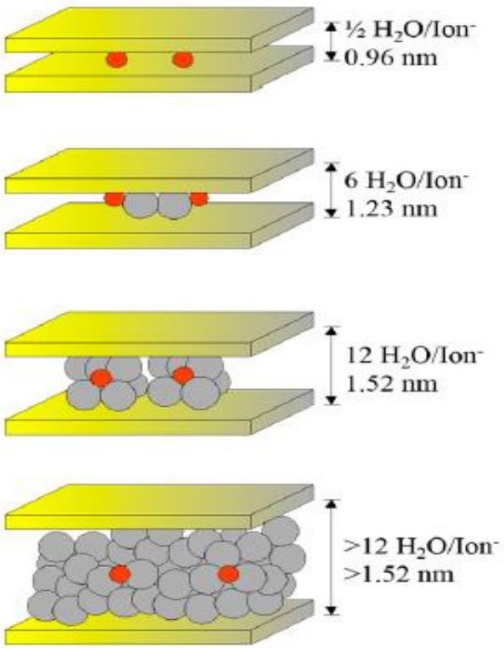

Figure 7 *Swelling mechanism of smectite (Aniekan et al., 2018)*

When a small amount of clay mineral is added into a large amount of water, its crystal composition separates and disperses. Furthermore, their electric potential cause the particles to repel each other. The term for this process is called colloidal or suspension. However, when the clay mineral present itself as a large concentration, the mixture becomes more viscous and has a high resistance to flow. Another unique property of clay mineral is thixotropy, which indicates a decrease in viscosity

when subjected to applied stress. Monmorillonite, saponite and hectonite are types of smectite that are viscous and thixotrpy because of the presence of sodium. Odom (1984) argued that smectite clay minerals in a single deposit can have either uniform or varied viscosity due to dispersibility and natural ion exchange.

Smectite clay minerals have been used in many processes and industries. Some notable uses are:

1. Foundry moulding sands. The metallurgy industry uses smectite in a mixture with sand and water to make sand plastic and cohesives. They harnesses the smectite properties such as compression strength, wet tensile strength, flowability and durability.
2. Drilling muds. The gas and oil industry uses smectite properties such as grit, viscosity, and rheological properties to lubricare and cool the drill bit.
3. Binding agents. The food industry combines Na or Ca smectites into the pelletization process to improve the nutrition of the animal while the iron ore industry combines the Na smectites into the pelletization process to absorb excess water from the ore.
4. Medicine. Smectites with zinc ion and magnesium ion accelerate the absorption of bacteria thereby accelerating wound healing (Sasaki and Yamamoto, 2017).
5. Grouting. Civil engineering practices use smectite for its viscosity, thixotropty, impermeability and plasticity properties. This action impedes water or waste in soils and provides non-mechanical support for excavator and construction of tunnel walls.
6. Water purification. Environmental practices employ actions to purify water from indurstrial oils and organic waste by applying dispersion and absorptive properties of smectites (Cody and Magauran, 1990).

2.3 Sidoardjo Mud Volcano

There are two theories surrounding the origins of the Sidoardjo Mud Volcano. They are: (1) it was a natural disaster which triggered by the Yogyakarta earthquake on May 27th, 2006 (Mazzini et al., 20017; Sawolo et al., 2009; Lupi et al., 2013); and (2) it was an underground blowout caused by an oil drilling failure (Banjar Panji-1 exploration well) by PT Lapindo Brantas (Manga et al., 2007; Tingay et al., 2008; Mori and Kano, 2009; Davies et al., 2007). Moreover, Mazzini et al. (2007) suggested that the mud volcano was strongly influenced by an earthquake that took place in Yogyakarta. His argument was based on a geochemical and field results that indicated an earthquake did take place. Sawolo et al. (2010) stated that the underground blowout did not occur in the exploration well based on a pressure analysis. Contrary to this theory is that the drilling process induced hydraulic fracturing or reactivated previously inactive faults, which increased pressure on the mud, thereby creating the conditions that led to the eruption of the mud volcano (Davies et al., 2010; Tingay et al., 2015).

Figure 8 shows the stratigraphy of soil from the Banjar Panji-1 exploration well in Sidoardjo. The exploration well was approximately 150 m from the main crater of the Sidoardjo Mud Volcano. This stratigraphy identifies the location of the mud. The extruded mud has a similar clay mineralogy composition as the sample from 1615 – 1828 m, taken from Upper Kalibeng 1 Formation. It is a bluish-gray clay and has a high level of smectite. The smectite could come from a smectite-rich layer in 1341 – 1432 m interval (Mazzini et al., 2007). Shirzaei et al. (2015) agreed that the mud comes from the Upper Kalibeng Formation, at depths beyond 3.5 km. Additionally, the main extruded gases from the crater are methane, carbon dioxide, and some hydrocarbons.

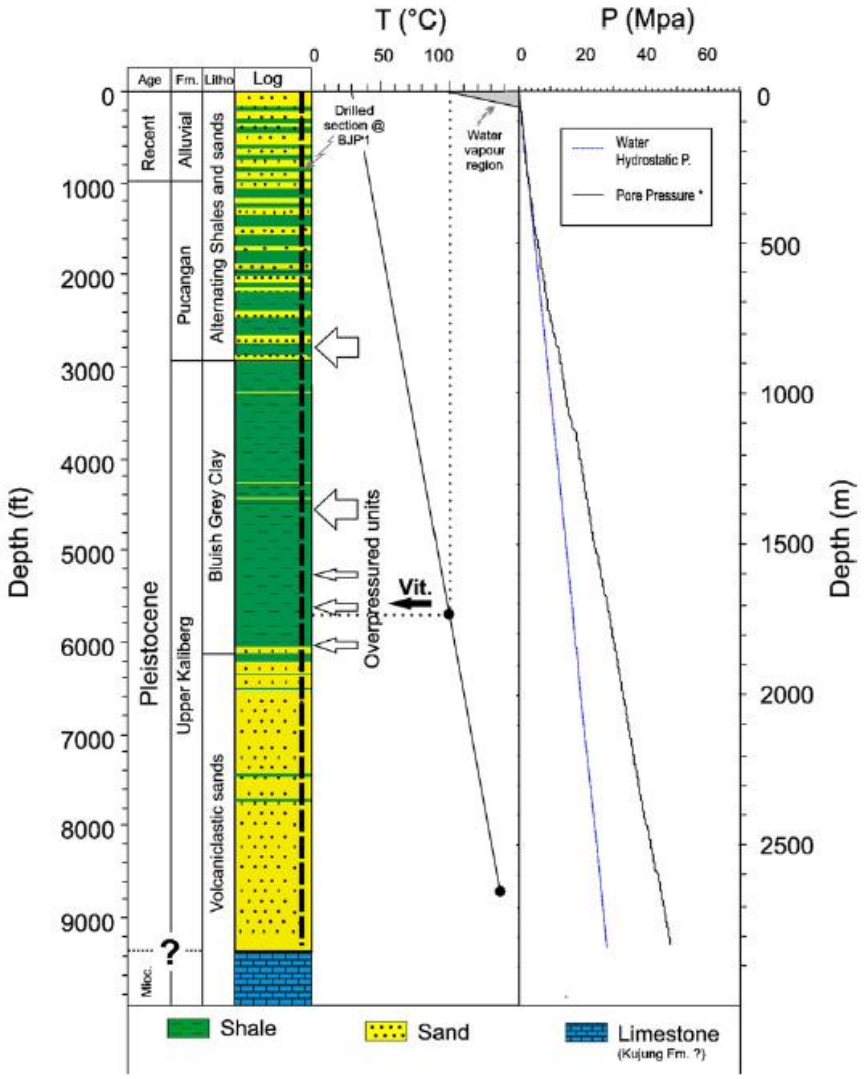

Figure 8 *Stratigraphy from Banjar Panji-1 exploration well in Sidoardjo, East Java (after Mazzini et al., 2007)*

Mazzini et al. (2007) also described the evolution of the Sidoardjo Mud Volcano. He suggested that at the beginning of the eruption, the mud volcano had an eruption rate of 5,000 m^3/d which had 60% water content. However, by December 2006, the eruption rate had peaked to 180,000 m^3/d and reached 110,00 m^3/d by June 2007. He went onto explain the relevance of the ellipsoid subsiding area around the mud volcano, which had an axis of 7x4 km while some other parts had an average subsidence rate of 1-4 cm/d. He argued that the subsidence can be caused by the weight

of the mud volcano itself or due to void gap left by the extruded mud (Usman et al., 2016). **Table 1** presents the simulated growth of Sidoardjo Mud Volcano with an assumed constant eruption rate of 90,000 m^3/d (Istadi et al., 2009).

Table 1 *Simulated growth of Sidoardjo Mud Volcano (after Istadi et al., 2009)*

Date	**Area (ha)**	**Volume (mil. m^3)**	**Peak of mud volcano* (m)**	**Subsidence at the crater* (m)**
Dec 1, 2007	832	54	20	-21
June 1, 2008	960	70	21	-30
Dec 1, 2008	1252	87	21	-39
June 1, 2009	1393	103	21	-47
Dec 1, 2009	1418	119	23	-55
June 1, 2009	1448	136	26	-63

* from original ground level

Typically, mud volcanoes only erupt for a few days (Mazzini et al., 2007). However, this is not the case with the Sidoardjo Mud Volcano. Given its unique characteristics, researchers have tried to predict its longevity. The estimated height of the Upper Kalibeng 1 Formation was 640 m and the area were 1.3 km^2 and 2 km^2 based on gravity and seismic data, respectively. Assuming a constant eruption rate of 100,000 m^3/d, it is predicted that the Sidoardjo Mud Volcano could last between 23 to 35 years (Istadi et al., 2009). According to the calculation of Davies et al. (2011), the mud volcano could last 26 years with a flow rate less than 0.1 Ml/day. This estimation was based on the Monte Carlo simulation. Rudolph et al. (2011) predicted, using a Gaussian model, that the Sidoardjo Mud Volcano has a 33% chance of lasting less than 21 years, a 50% chance chance of lasting less than 40 years, and a 67% chance of lasting less than 84 years.

2.4 Mud Properties

2.4.1 Settling velocity

When the density of a particle is greater than the density of the surrounding fluid, it moves downward. This movement is called settling while the speed is called settling velocity. The main driving force behind settling velocity is the gravity force or buoyant weight, which is a function of particle density and fluid density. The resistance force is the drag force, which is a function of particle size and shape and the viscosity of fluid (Cheng, 1997; Pejrup and Mikkelsen, 2009). Reichert et al. (2009) stated that the type of clay mineralogy affects the particles settling velocity. For example, particles with high smectice clay tends to have a slower settling velocity. This is due to dispersion. Sediment concentration also affects the settling velocity and a higher sediment concentration leads to a slower settling velocity (Vanoni, 1962; Cheng, 1997; Shen et al., 2016). Julien (2010) defined the settling velocity for natural particles is a function of dimensionless particle diameter d_*:

$$\frac{\omega}{\sqrt{(G-1)gd_s}} \cong \frac{8}{d_*^{1.5}}\left(\left(1+\frac{d_*^3}{72}\right)-1\right) \tag{1}$$

$$d_* = d_s\left[\frac{(G-1)g}{v_m^2}\right]^{\frac{1}{3}} \tag{2}$$

where d_s is the particle size, G is the specific gravity of the particle, and v_m is the kinematic viscosity of the fluid.

2.4.2 Flocculation

When numbers of very fine particles, such as silt and clay, are found in a river, they tend to hold together and form flocculated masses. This is due to electrochemical forces and high surface areas of clay particles. There are three factors that control the flocculation processes: sediment

concentration, turbulence and fluid salinity. Guo et al. (2017) found that the floc size is inversely proportional with turbulent shear, particularly with turbulent shear larger than 2-3 s^{-1}. Sutherland (2014) investigated the effect of salinity on clay settling and found that clay flocculation occurs at 10 ppt. The effect does not increase significantly beyond 10 ppt. However, high sediment concentration can discourage the flocculation processes of fine sediments. Flocculated settling velocity can range from 0.15 to 0.6 mm/s and usually occurs in particles that are less than 40 μm in size (Julien, 2010). Recall that clay particle has a sediment size equals or lower than 4 μm.

To investigate a flocculation procceses in a sediment sample, a deflocculant agent could be mixed into a sediment mixture and then the settling velocity of the micture was recorded. If flocculation occurs in the mixtures, the settling velocity of the mixture with the added deflocculant would be slower than the original mixture. A deflocculant comprises 35.70 g of sodium hexametaphosphate and 7.94 g of sodium carbonate when diluted in 1 liter of distilled water. Then 1 ml of this deflocculant is added for every 100 ml of sample (Guy, 1969; Vanoni, 1962; Julien and Mendelsberg, 2003).

Migniot (1989) proposed an equation to calculate the flocculated settling velocity ω_f:

$$\omega_f = \frac{250}{d_s^2}\omega \tag{3}$$

where d_s is the particle size in microns and ω is the settling velocity of disperse particles. To complement Equation 4, Winterwerp (1999) provided an empirical equation to approximate the floc size d_{flocc}:

$$\omega_f = 10 d_{flocc}^{1.5} \tag{4}$$

where ω_f is in mm/s and d_{flocc} is in mm.

2.4.3 Relationship between turbidity and sediment concentration

Turbidity is an optical property of water, which describes the ability of water to attenuate light through scattering and absorption (McCarthy et al., 2974). The scattering process is caused by suspended particles while absorption can be caused by dissolved matter and suspended particles (Gippel, 1989).

To date, turbidity measurements include: Nephelometric Turbidity Units (NTU), Formazine Nephelometric Units (FNU), Formazine Turbidity Units (FTU), and Formazine Attenuation Units). NTU and FNU are used for turbidity measurement with nephelometric instruments and formazine standard while FTU and FAU are used for turbidity measurements with generic turbidimeter and formazine standard. Furthermore, the International Organization for Standardization (2016) emphasized that NTU or FNU are more applicable for low turbidity water such as drinking water while FAU is more applicable for a turbid water such as waste waters. Since they use the same formazine standard, their values are the same (1 NTU = 1 FNU = 1 FTU = 1 FAU).

In civil engineering field works, turbidity can be used to estimate suspended sediment concentration because it is hard to continuously sample sediment concentration in storm events or in isolated sites. This approach is more accurate than using streamflow to estimate suspended sediment concentration (Christensen et al., 2002). Some attempts at using turbidity measurements to estimate suspended sediment concentration or the sediment load of streams have been recorded in Jansson (1992), Lewis (1996), Minella et al. (2008), Pavanelli and Bigi (2005), Pfannkuche and Schmidt (2003), and Riley (1998). The relationship between turbidity and suspended sediment concentration is affected by the accuracy of the instrument. Properties of suspended sediment and water, such as suspended particle size and shape, the color of water, composition of organic and

inorganic matters, and turbulence also play a role in affecting the accuracy of the result (Gippel, 1989). Therefore, calibration in laboratory or *in-situ* is important to develop an accurate result. Minella et al. (2008) stressed the importance of ensuring the accuracy of laboratory and *in-situ* calibration. To highlight their argument, they conducted an experiment in a small catchment areas in Rio Grandense plateau, Rio Grande do Sul, Brazil. They installed a locally-manufactured turbidimeter and Parshall flume to measure the turbidity and discharge, respectively, for 8 storm events between July 2004 and May 2005. *In-situ* calibration was done by collecting 458 suspended sediment samples with USDH-48 near the turbidimeter. They then measured the concentration through evaporation and paired it with the corresponding turbidity and discharge. Laboratory calibration was done by collecting different soils that represented the suspended sediment in the river, sieving it for the fine particles, weighing it, and finally diluting it in 1 liter river water. Then they recorded the concentration and turbidity of the samples. Half of the *in-situ* collected samples were used to derive the regression equation for turbidity as the independent variable and suspended sediment concentration as the dependent variable. The other half of the *in-situ* collected samples were used to determine an error of the regression equation. The error e was calculated by using the following equation:

$$e = \sqrt{\frac{(SSC_{calc} - SSC_{meas})^2}{n - 1}} \tag{5}$$

where SSC_{calc} is the predicted or calculated suspended sediment concentration from turbidity value, SSC_{meas} is the observed or measured suspended sediment concentration, and n is the number of samples. The error between *in-situ* and laboratory calibration were $\pm$122 mg/l and -601 mg/l, respectively, which indicates that the *in-situ* calibration is superior to the laboratory calibration. **Figure 9** supports these results particularly where the predicted suspended sediment

concentrations were similar to the observed concentration with some underestimated values at high concentration for *in-situ* calibration. On the other hand, the predicted concentration was overestimated for laboratory calibration. The dilution effect for turbid water, which was for samples beyond the maximum limit of the instrument, can cause further error in laboratory calibration (Pavanelli and Bigi, 2005).

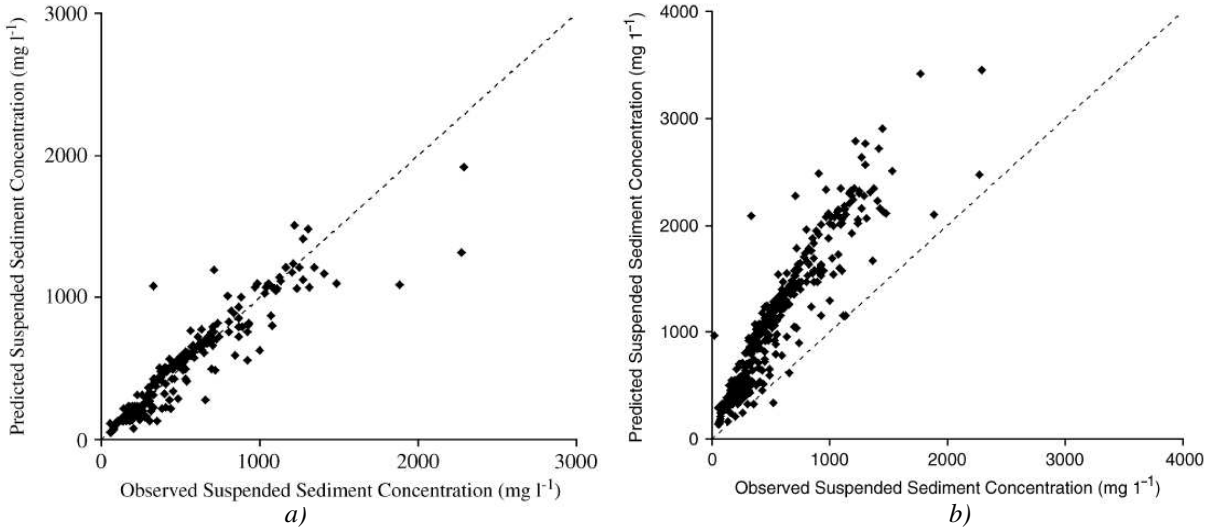

Figure 9 *Comparison of the observed and predicted suspended sediment concentration for (a)* in-situ *calibration, and (b) laboratory calibration (after Minella et al., 2008)*

In laboratory experiments, Holliday et al. (2003) found that turbidity measurements can be used to accurately estimate the suspended sediment concentration. However, the presence of sand or larger particles can cause an underestimated or inaccurate estimations (Riley, 1998). These studies followed on work conducted by Foster et al. (1992) on the effects of particle size on the relationship between turbidity and sediment concentration in Midland UK as shown in **Figure 10**.

Table 2 and **Figure 11** summarize the relationship between turbidity in NTU, FTU, or TUR and suspended sediment concentration (SSC) or total suspended sediment (TSS) or suspended

particulate matters (SPM) in mg/l. The coefficient of determination or r^2 represents the variability of the data compared to the relationship or the regression line.

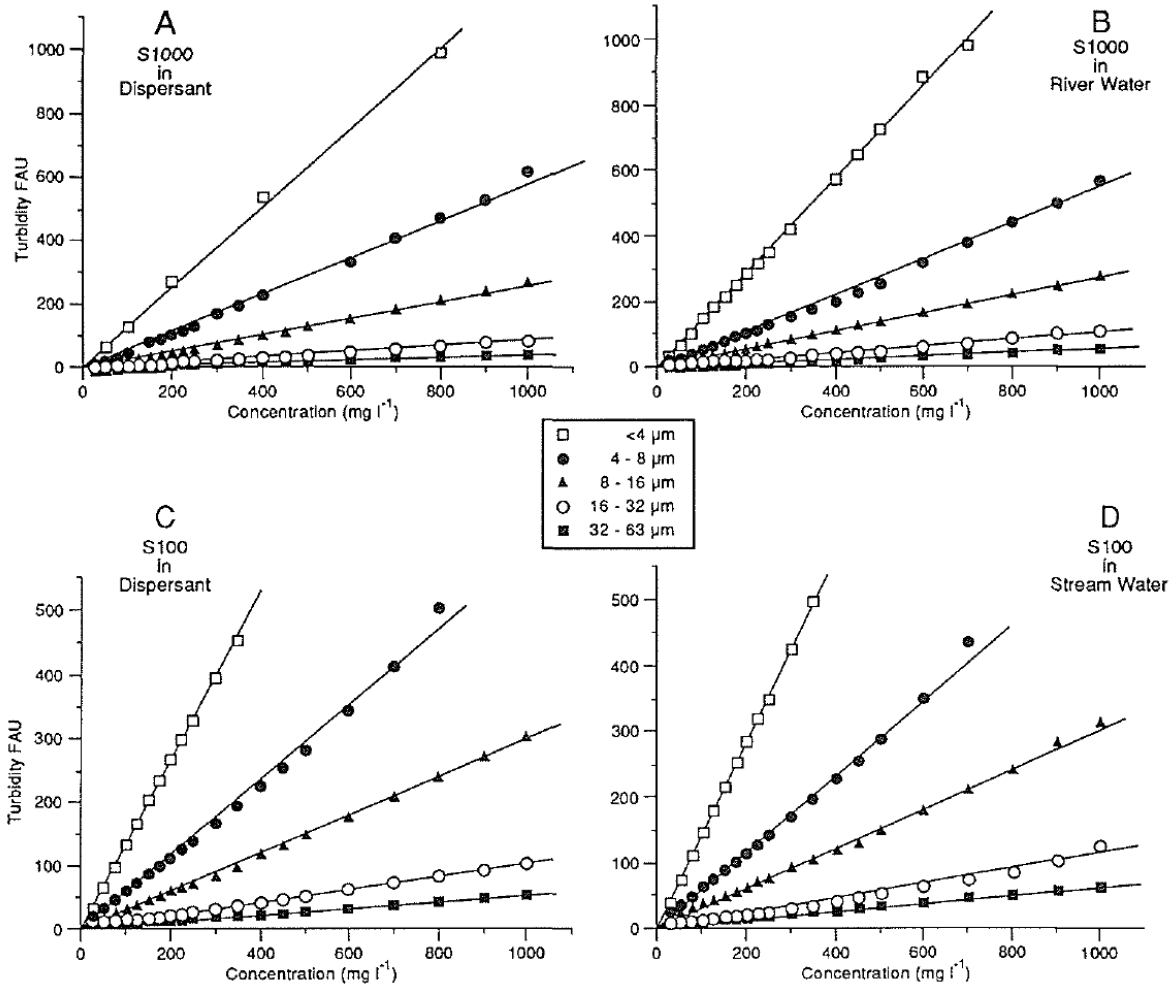

Figure 10 *The relationship of turbidity and suspended sediment concentration for 5 particle size fractions prepared in dispersant and river water with S100 and S1000 optical turbidimeter (Foster et al., 1992)*

Table 2 *Summary of the relationship between turbidity and sediment concentration from previous studies*

	Location and Reference	Relationship	R^2	Remarks
1	Doce River, Brazil by Palu and Julien (2019)	$NTU = 2 \times C$	0.98	
2	Cecil A_p soil by Holliday et al. (2003)	$NTU = 0.4833 \times TSS^{1.012}$	0.9987	Whole soil
		$NTU = 1.0283 \times TSS^{1.0282}$	0.9991	Silt + clay
		$NTU = 0.7733 \times TSS^{0.9336}$	0.9996	Clay
3	N'djili Basin, Congo by Ndolo Goy (2015)	$\log TSS = 0.9269 \times \log NTU + 0.613$	0.9955	2005
		$\log TSS = 0.9327 \times \log NTU + 0.6306$	0.9838	2013
4	Ranger Uranium Mine, Australia by Riley (1998)	$Sed\ Con\ = 0.6 \times 10^{-6} \times Turb^{1.166}$	0.58	
5	Elbe River, Germany by Pfannkuche and Schmidt (2003)	$SPM = 0.695 \times NTU + 15.20$	0.6	
6	Sillaro Torrent, Italy by Pavanelli and Bigi (2005)	$SSC = 0.65 \times 10^{-6} \times NTU + 0.00278$	0.79	Fresh sample
		$SSC = 0.60 \times 10^{-6} \times NTU + 0.00142$	0.98	1 month old sample
7	Avorezinha, Brazil by Minella et al. (2008)	$SSC = 0.098 \times TUR^{2.313}$	0.86	*In situ*
		$SSC = 0.569 \times TUR^{2.039}$	0.807	Laboratory
8	Geeburg Creek by Gippel (1989)	$FTU = 1.22 \times TSS - 9.70$	0.858	Corrected for color
9	Singapore by Daphne et al. (2011)	$TSS = 0.7992 \times NTU$	0.8009	For sample with $TSS < 80\ mg/l$

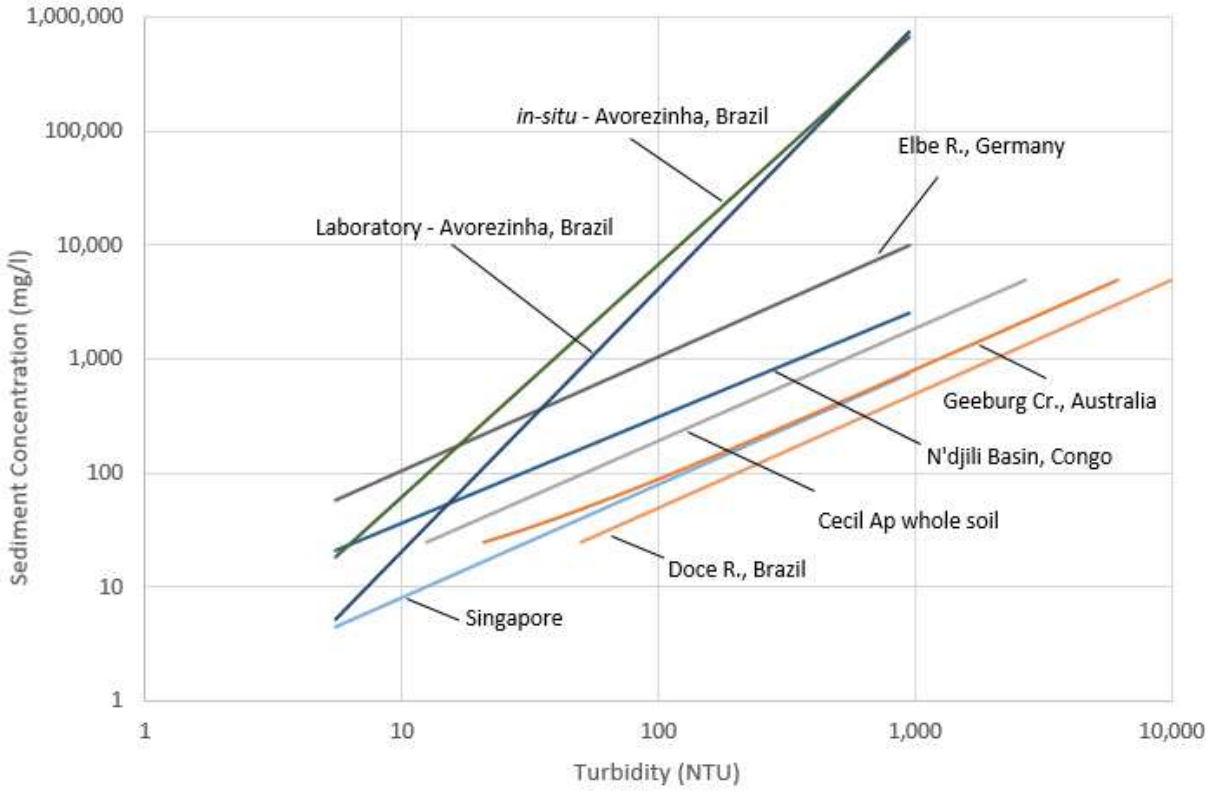

Figure 11 *The relationship between turbidity and sediment concentration from previous studies*

2.4.4 Properties of Sidoardjo mud

It is important to understand the characteristics of the mud from the mud volcano. A preliminary study about the characteristics of Sidoardjo mud was conducted by Plumlee et al. (2008). They found that the mud contained mostly clay minerals (73.6%) followed by quartz (8.3%) and feldspar (5.6%). Smectite and illite are the dominant clay minerals. Results from the particle size analysis are shown in **Figure 12**. Mostly particles are finer than 10 μm.

Using a scanning electron microscope, Harnanto (2011) also tested Sidoardjo mud to understand its physical and chemical properties. It was found that the mud particles had a thickness of 0.01-0.05 μm, a width up to 5 μm, and a specific mass of the mud is between 1,240 to 1,370 kg/m^3. The levels of CaO, Al_2O_3, SiO_2, and Fe_2O_3 were 1.8-2.7%, 17.96-19.96%, 44.5-49.7%, and 4.95-6.02%, respectively, which means that it is not possible to use Sidoardjo mud for cementing purposes.

Indrawan et al. (2013) analyzed the incipient motion of the Sidoardjo mud and found that consolidation time plays a bigger role than flow depth. The highest critical shear stress of the mud was found to be 0.843 N/m^2 after 14 days of consolidation at 3 m in depth. This produced the following equation where τ_{cr} is in N/m^2 and ρ_{dry} is in kg/m^3:

$$\tau_{cr} = 3 \times 10^{-6}\left(\rho_{dry}\right)^{1.74} \tag{6}$$

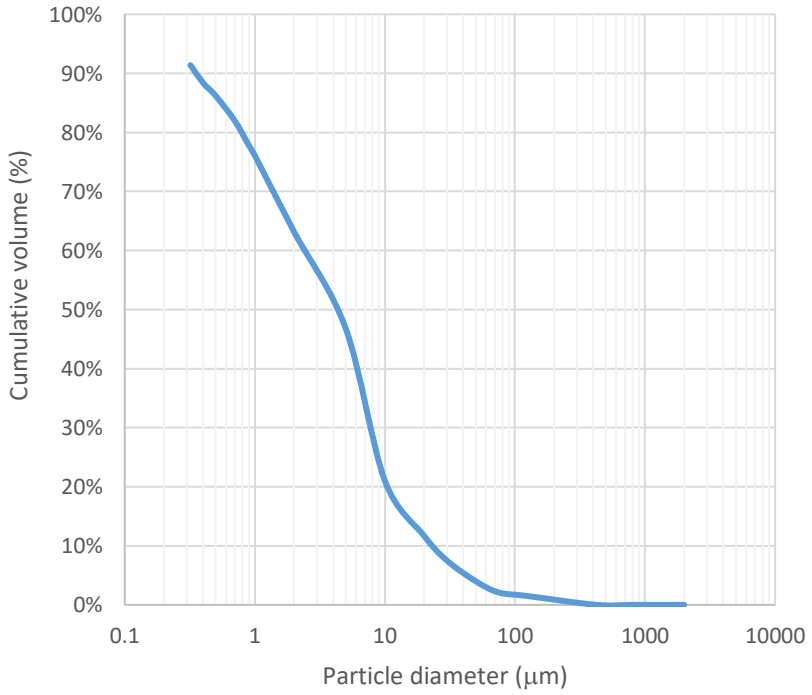

Figure 12 *Particle size distribution of Sidoardjo mud (after USGS, 2008)*

2.5 Sediment Transport in Rivers

2.5.1 Mixing processes

When sediments or contaminants are discharged into a river, they undergo three mixing stages (Fischer et al., 1979; Jung et al., 2019). The first stage is a mixing process controlled by momentum and buoyancy, the second stage is lateral mixing caused by the turbulence in the river, while the third stage is longitudinal dispersion which diminishes the longitudinal concentration gradient.

The mixing processes, particularly the second stage, can be analyze using the advection-diffusion equation The complete three-dimensional advection-diffusion equation is:

$$\underbrace{\frac{\partial C}{\partial t}}_{\text{mass change}} + \underbrace{\boxed{u\frac{\partial C}{\partial x} + v\frac{\partial C}{\partial y} + w\frac{\partial C}{\partial z}}}_{\text{advective}} = \underbrace{\dot{C}}_{\text{phase change}} + \underbrace{\boxed{(D+\varepsilon_x)\frac{\partial^2 C}{\partial x^2} + (D+\varepsilon_y)\frac{\partial^2 C}{\partial y^2} + (D+\varepsilon_z)\frac{\partial^2 C}{\partial z^2}}}_{\text{Diffusion and turbulent mixing}} \quad (7)$$

where C represents the mass concentration, D is the molecular diffusion, and ε represents the turbulent mixing coefficient. Phase change, $\dot{C}$, is applied on nonconservative substance which could undergoes the internal mass change such as sedimentation, decay or chemical reaction (Julien, 2010). The molecular diffusion D is negligible compared to the turbulent mixing in rivers. In this research, the author would replace the x, y, and z coordinates correspond to the longitudinal, transversal and vertical direction, respectively ($\varepsilon_x = K_d, \varepsilon_y = \varepsilon_t,\ and\ \varepsilon_z = \varepsilon_v$).

Fischer et al. (1979) proposed empirical functions for the longitudinal dispersion coefficient, vertical and transversal mixing coefficient, K_d, ε_v and ε_t, respectively for natural channels in m^2/s:

$$K_d \cong 0.011\frac{U^2W^2}{hu_*} \quad \varepsilon_v \cong 0.067\, hu_* \quad \varepsilon_t \cong 0.6\, hu_* \quad (8)$$

where U is the mean flow velocity, W is the channel width, h is flow depth and u_* is the shear velocity on average equals to $\sqrt{ghS}$ with g is the gravitational acceleration and S is the energy

slope. The use of dispersion coefficient is more appropriate than turbulent mixing coefficient because the mass motion, due to molecular diffusion and shear flow (advective motion), is additive and it is often hard to differentiate (Aris, 1956).

The first-order approximation of time and length scales of longitudinal dispersion, vertical and transversal mixing are:

$$X_d = \frac{(500hu_*)}{U} \quad X_v = \frac{hU}{0.1u_*} \quad X_t = t_t V = \frac{W^2 U}{hu_*} \tag{9}$$

$$t_d \cong \frac{X_d^2}{500hu_*} \quad t_v \cong \frac{h}{0.1u_*} \quad t_t = \frac{W^2}{hu_*} \tag{10}$$

The three-dimensional advection diffusion equation can be simplified in the case of straight channels. Assume that the most dominant process occurs in the longitudinal x direction, which for steady point sources implies $v = w \cong 0 \quad and \quad K_d \cong 0$. Turbulent flow in natural channels lets us to neglect the molecular diffusion, and after vertical mixing complete, we can assume $\varepsilon_v \cong 0$.

For a nonconservative substance, the term $\dot{C}$ in the advection-diffusion equation will not be zero This is due to internal mass change such as settling or decay. For example, in stagnant fluid, the advection-diffusion equation and the solution are:

$$\frac{\partial C}{\partial t} = -kC \tag{11}$$

$$C_i = C_0 e^{-kt} \tag{12}$$

$$C_i = C_{0i} e^{-\frac{X\omega_i}{hU}} \tag{13}$$

where k is the decay or settling rate, $C_{o,i}$ is the initial or upstream sediment concentration of fraction i, C_i is the downstream sediment concentration of fraction i, X is the distance, h is flow depth, U is the flow velocity, and ω_i is the settling velocity of the fraction i. The value of settling

rate k for suspended sediment can be defined as $k = \omega/h$ where ω is the fall velocity and h is the flow depth. Meanwhile, the time t can be defined as X/U.

The analytical solution of one-dimensional advection-diffusion equation with settling for instantaneous mass injection is:

$$C(x,t) = \frac{m_p}{2\sqrt{\pi K_d t}} e^{-\frac{(x-Ut)^2}{4K_d t} - kt} \tag{14}$$

The analytical solution proposed by O'Loughlin and Bowmer (1975) for infinite duration of continuous mass injection was:

$$C(x,t) = \frac{C_0}{2}\left[e^{\frac{Ux}{2K_d}(1-\Gamma)} erfc\left(\frac{x - Ut\Gamma}{2\sqrt{K_d t}}\right) + e^{\frac{Ux}{2K_d}(1+\Gamma)} erfc\left(\frac{x + Ut\Gamma}{2\sqrt{K_d t}}\right)\right] \tag{15}$$

$$\Gamma = \sqrt{1+4\eta} \quad ; \quad \eta = \frac{kK_d}{U^2} \tag{16}$$

In case of a mass injection of finite duration τ into a channel system, the previous analytical solution (Chapra, 1997; Julien, 2018; Palu, 2019) can be used while the mass is being injected ($t < \tau$). For $t > \tau$, the analytical solution for sediment concentration C is:

$$C(x,t) = \frac{C_0}{2}\left\{e^{\frac{Ux}{2K_d}(1-\Gamma)}\left[erfc\left(\frac{x - Ut\Gamma}{2\sqrt{K_d t}}\right) - erfc\left(\frac{x - U(t-\tau)\Gamma}{2\sqrt{K_d(t-\tau)}}\right)\right]\right. \tag{17}$$

$$+\left[e^{\frac{Ux}{2K_d}(1+\Gamma)} erfc\left(\frac{x + Ut\Gamma}{2\sqrt{K_d t}}\right)\right.$$

$$\left.\left. - e^{\frac{Ux}{2K_d}(1+\Gamma)} erfc\left(\frac{x + U(t-\tau)\Gamma}{2\sqrt{K_d(t-\tau)}}\right)\right]\right\}$$

$$\Gamma = \sqrt{1+4\eta} \quad ; \quad \eta = \frac{kK_d}{U^2} \tag{18}$$

where C_0 is the initial sediment concentration, U is the mean flow velocity, K_d is the longitudinal dispersion coefficient, and k is the settling rate.

For a conservative substance (assuming no settling of the fine volcano mud), the phase change $\dot{C}$ is assumed equal to 0 (Julien 2018). We can further simplify the advection-diffusion equation to:

$$\frac{\partial C}{\partial t} + U\frac{\partial C}{\partial x} = \varepsilon_t \frac{\partial^2 C}{\partial y^2} \tag{19}$$

The analytical solution of the simplified advection diffusion equation for infinitely wide channel due to continuous mass flux injection $\dot{m}$ is (Fischer et al., 1979):

$$C(x,y) = \left[\frac{\dot{m}}{h\sqrt{4\pi\varepsilon_t x U}}\right] e^{-\frac{y^2 U}{4\varepsilon_t x}} \tag{20}$$

Most rivers cannot be assumed as an infinitely wide channel. Additional consideration due to channel boundaries should be added with the method of superposition as illustrated in **Figure 13**. If the sediment source located at $X = 0$ and both banks located at $X = \pm L$, by adding imaginary sources at $X = \pm 2L, \pm 4L, \pm 6L, \ldots, \pm nL$, a zero concentration gradient at the boundaries could be achieved (or $\partial C/\partial y = 0$ at $y = 0$ and $y = W$). Assume y_0 is the location of mass injection. The solution of the simplified advection diffusion equation after considering the boundaries of the channels is:

$$\frac{C}{C_b} = \frac{1}{\sqrt{4\pi x'}} \sum_{n=-\infty}^{\infty} \left\{ \exp\left[-\frac{(y' - 2n - y_0')^2}{4x'}\right] + \exp\left[-\frac{(y' - 2n + y_0')^2}{4x'}\right] \right\} \tag{21}$$

$$C_b = \frac{\dot{m}}{UhW} \quad x' = \frac{x\varepsilon_t}{UW^2} \quad y' = \frac{y}{W} \quad y_0' = \frac{y_0}{W} \tag{22}$$

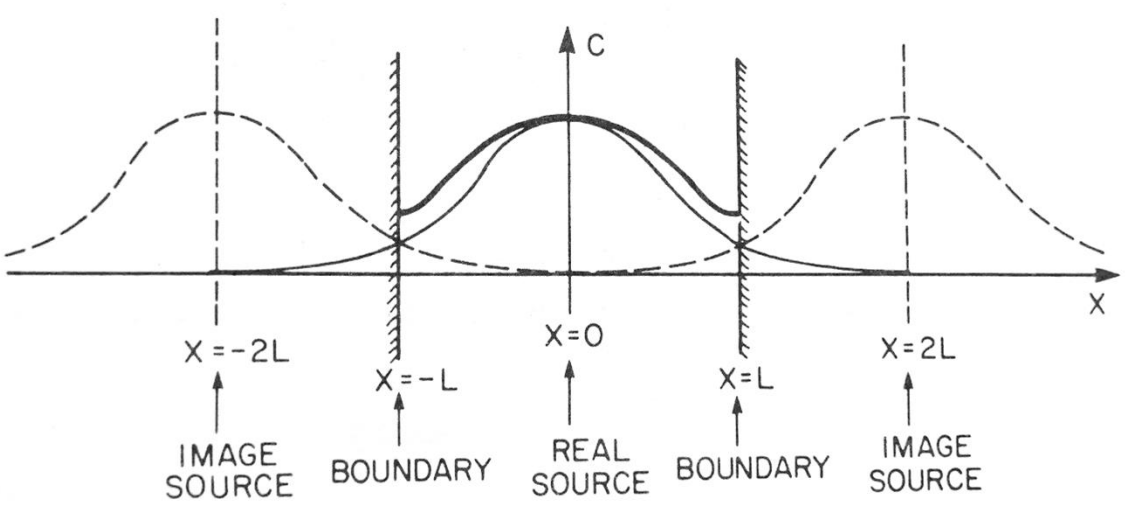

Figure 13 *Illustration of additional channel boundaries (after Fischer et al., 1979)*

C_b was defined as the fully-mixed sediment concentration, which is calculated from:

$$C_b = \frac{C_{outlet} \times Q_{outlet} + C_{river} \times Q_{river}}{Q_{outlet} + Q_{river}} \tag{23}$$

Furthermore, the one-dimensional advection-diffusion equation with settling factor is (Chapra, 1997; Palu, 2019):

$$\frac{\partial C}{\partial t} + U\frac{\partial C}{\partial x} = K_d \frac{\partial^2 C}{\partial x^2} - kC \tag{24}$$

Palu (2019) recently proposed a new approach to calculate the flood hydraulic diffusivity K_d:

$$K_d = \left[\frac{1 - 0.444Fr^2}{2n\sqrt{S_0}}\right]\left(\frac{0.6C_e}{Fr\sqrt{g}}\right)^{10/3} \tag{25}$$

Where Fr is the Froude number, n is Manning's coefficient, S_0 is the bed slope, and C_e is the floodwave celerity which is βU with β is 5/3 and U is the depth-average flow velocity.

The value of Manning's coefficient n had been studied previously (Chow, 1959). It can be determined by using Manning's equation such as,

$$U = \frac{1}{n} R^{\frac{2}{3}} S_f^{\frac{1}{2}}$$

where U is the depth-average flow velocity, R is the hydraulic radius, and S_f is the friction slope of the flow. Another method to determine the Manning's coefficient n is using **Table 3** to choose a value of n for an appropriate description of the river or channel.

Table 3 *The value of Manning's coefficient (after Brunner, 2016)*

	Type of Channel	Minimum	Normal	Maximum
A.	**Natural Streams – Main Channels**			
	a. Clean, straight full, no rifts or deep pools	0.025	0.030	0.033
	b. Same as above, but more stones and weeds	0.030	0.035	0.040
	c. Clean, winding, some pools and shoals	0.033	0.040	0.045
	d. Same as above, but some weeds and stones	0.035	0.045	0.050
	e. Same as above lower stages, more ineffective slopes and sections	0.040	0.048	0.055
	f. Same as "d" but more stones	0.045	0.050	0.060
	g. Sluggish reaches, weedy, deep pools	0.050	0.070	0.080
	h. Very weedy reaches, deep pools, or floodwats with heavy stands of timber and brush	0.070	0.100	0.150
B.	**Excavated or Dredged Channel**			
1.	Earth, straight and uniform			
	a. clean, recently completed	0.016	0.018	0.020
	b. clean, after weathering	0.018	0.022	0.025
	c. gravel, uniform section, clean	0.022	0.025	0.03
	d. with short grass, few weeds	0.022	0.027	0.033
2.	Earth, winding and sluggish			
	a. No vegetation	0.023	0.025	0.030
	b. Grass, some weeds	0.025	0.030	0.033
	c. Dense weeds or aquatic plants in deep channels	0.030	0.035	0.040
	d. Earth bottom and rubble side	0.028	0.030	0.035
	e. Stony bottom and weedy banks	0.025	0.035	0.040
	f. Cooble bottom and clean sides	0.030	0.040	0.050

2.5.2 Suspended sediment transport

One of the most important parameters in sediment transport is the Rouse number, Ro. This parameter, proposed by Rouse (1937), defines the ratio of downward particle movement due to settling and upward particle movement due to turbulent mixing (Ettema, 2006). The sediment concentration C at point z can be determine from the Rouse equation:

$$\frac{C}{C_a} = \left(\frac{h-z}{h}\frac{a}{h-a}\right)^{Ro} \tag{26}$$

$$Ro = \frac{\omega}{\beta_s \kappa u_*} \tag{27}$$

where C_a is reference sediment concentration at reference point a from bed level, ω is the settling velocity of particles, β_s is the momentum coefficient which is assumed to equal 1 for uniform flow (Chow, 1959), κ is the von Kármán constant which equals to 0.4, and u_* is the shear velocity.

The Rouse equation is usually employed to construct a sediment concentration distribution or vertical sediment concentration profile. Researchers such as Hunt (1954), Tanaka-Sugimoto (1958), Ni and Wang (1991), Mazumder and Ghoshal (2006), and Xhu et al. (2017) have used this equation to estimate the sediment concentration profile. The latter used empirical model while the others used mathematical model such as the diffusion equation. Kineke and Sternberg (1989) suggested that data obtained from *in-situ* methods, through a microcamera to capture the actual floc size or settling cylinder to measure the settling velocity, works better than data estimated from the particle size distribution of sediment sample. This is particularly the case when predicting the sediment concentration distribution.

Akalin (2002) tried to determine the Rouse number by plotting the suspended sediment concentration versus $(h-z)/z$ as shown in **Figure 14**. Parameter $(h-z)/z$ is the ratio of the distance from the top and distance from the bottom of the point of interest. He used suspended

sediment data collected from the Lower Mississippi River and found that the Rouse number is the slope of the power function of the suspended sediment soncentration. He also found that the water temperature has an inverse effect on the Rouse number due to the change of water viscosity.

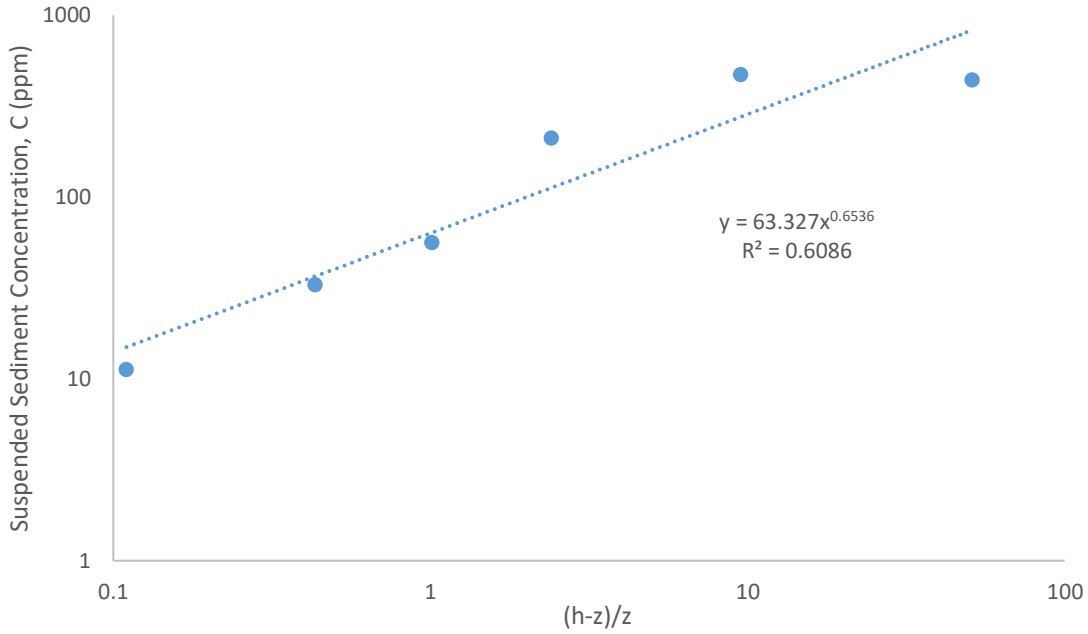

Figure 14 *Proposed method to determine Rouse number (after Akalin, 2002)*

Julien (2010) classified the mode of sediment transport in rivers based on the Rouse number, as shown in **Table 4**. The bed load is a mode of sediment transport which is dominated by a coarser sediment load at a thin layer near the bed level. The bed load condition is indicated by a high Rouse number ($Ro > 5$) which means that the settling velocity ω is much higher than the upward movement due to turbulence. The bed load was studied by Meyer-Peter and Muller (1948), van Rijn (1984a), and Kociuba (2017). On the other hand, a suspended load is dominated by fine sediment in suspension, as put forward by van Rijn (1984b), Yang et al. (1996), Shah-Fairbank et al. (2011), and Vercruysse at al. (2017). In the case of suspended load, the settling velocity of the

particles and the Rouse number are small ($Ro < 1.25$). This is also the view of Allen et al. (1979) and Shi (2010) who studied the tidal effects to the transport of suspended sediment. Between the two modes of sediment transport is a mixed load which both bed load and suspended load contribute to the total load.

Table 4 *Classification of the mode of sediment transport*

Ro	$\boldsymbol{u_*/\omega}$	**Mode of Sediment Transport**
$> \mathbf{12.5}$	< 0.2	No motion
$\cong \mathbf{12.5}$	$\cong 0.2$	Incipient motion
$\mathbf{12.5 - 5}$	$0.2 - 0.5$	Bed load
$\mathbf{5 - 1.25}$	$0.5 - 2$	Mixed load
$< \mathbf{1.25}$	> 2	Suspended load

The sediment load by size fraction can be calculated by using the following equation (Julien, 2010),

$$q_b = \sum \Delta p_i q_{bi} \tag{28}$$

Where Δp_i is the relative weight of fraction *i* of the sediment and q_{bi} is the unit sediment discharge for fraction *i.*

There are field measurement techniques to analyzed suspended sediment (Hamilton et al., 1999; Wren et al., 2000; Julien, 2010; Armijos et al., 2015), such as:

1. Water sampling methods; a direct measurement of suspended sediment concentration employed by taking water (or sample) from the site. This method includes instantaneous sampling, point sampling and depth-integrated sampling.

2. Optical methods; an indirect measurement where instruments, such as nephelometer and transmissometers, record light backscatters or attenuation.
3. Acoustic Methods; another indirect measurement where instruments capture the backscatter noises of particles.

Armijos et al. (2015) proposed additional field measurement protocols such as separation of the turbidity measurement and the Rouse profile for fine and coarse sediment. He argued that particularly for coarse sediment, at least one measurement of turbidity and sample for granulometry at less than 1 m from bed level are needed. The recorded Rouse number for fine sediment ranged from 0.01-0.03 while for coarse sediment ranged from 0.25-0.6.

2.5.3 Suspended sediment transport in Porong River

Hermawan (2012) studied the discharge of the Porong River, which was used to transport mud into the estuary. HEC-RAS was used to simulate the sediment transport of the Porong River for several discharge scenarios ranging from 10 to 600 m^3/s. Using the Toffaleti transport function, he found that a minimum discharge of 200 m^3/s was required to transport the mud mixture to the Madura Strait. Based on the incipient motion analysis, at least 126 m^3/s was needed to flush the bed of the Porong River and 270 m^3/s was needed to flush away all the mud, including the settled mud, to the estuary of the Porong River (Indrawan et al., 2013).

Degradation was recorded at several locations along the Porong River, particularly between the upstream and the middle reach, which was about 4 m between October 2008 to February 2009. It was caused by a much lower sediment inflow from the upstream region than the transport capacity of the Porong River (Harnanto, 2011). Degradation mainly occurs during the wet season from November to April and aggradation occurs from June to November. The degradation and aggradation did not decrease the flood capacity of the Porong River because the deposition material

could be easily flushed away by the flood during the wet season (Kure et al., 2014). Hernawan and Budiono (2013), however, observed sediment sorting for each size fraction. Sand fraction was found along the thalweg of Porong River while silts and clays were found near the bank of the Porong River. They concluded that while the mud was found in the Porong River estuary, no mud from the mud volcano was found in the outskirt of the Porong River estuary. The deposition of sediment at the mouth of the Porong River was caused by the confluence of a high river discharge and a high tidal and monsoon-induced flow, which hindered the transport processes (Hoekstra, 1988). This accounted for the final location of the mud is on flat slope areas at a depth of 20-60 m in Madura Strait (Usman et al., 2016).

Several studies have been conducted to estimate the concentration of pollutants (for example the suspended sediment concentration) in the Porong River and its estuary. Jennerjahn et al. (2013) compared the level of contaminants in the Porong River and its estuary before and after the eruption. They collected data from 1991-1998. The research team conducted another assessment in 2002-2003 and another one in 2008. In 2008, the TSS had increased by 1 to 2 orders of magnitude during the dry and wet seasons compared to the 1991-1998 and 2002-2003. The maximum TSS during the dry and wet seasons of 2008 are 967 mg/l and 2,299 mg/l, respectively. This was observed 9 km from the mouth of the Porong River.

The modeling of contaminants along the Porong River after the Sidoardjo Mud Volcano was conducted by Suntoyo et al. (2015), using the Mike 21 Hydrodynamics and Ecolab module. The model had 10 simulation days with 240 time steps. This simulation was validated with the measurement data from the downstream end of the Porong River. The maximum TSS from the simulation was 300 mg/l, which is lower than the water quality standard.

Based on the imagery from ASTER 2005-2008, Landsat5 TM 1994, and Landsat 7 ETM+ 2003, the sediment concentration (TSS) ranged between 50-100 mg/l in 1994-2005 and 100-150 mg/l in 2006. It increased to >200 mg/l in 2007-2008 as a result of the mud volcano (Pahlevi and Wiweka, 2010). Another estimation method for TSS was proposed using the Sentinel-2 imagery (Bioresita et al., 2018) where the Laili algorithm for Landsat imagery was adapted. The imagery from January 12, 2016 as shown in **Figure 15** denotes a black area at the left side which is masked land and the gray area is the coastal area. To validated the algorithm, 9 *in-situ* data were collected on April 20, 2016 (marked with plus sign) and compared to the 9 extracted points from the Sentinel-2 imagery. The minimum, mean and maximum value of TSS from this analysis were 14.8 mg/l, 19 mg/l and 55.9 mg/l, respectively, with a correlation of 0.72

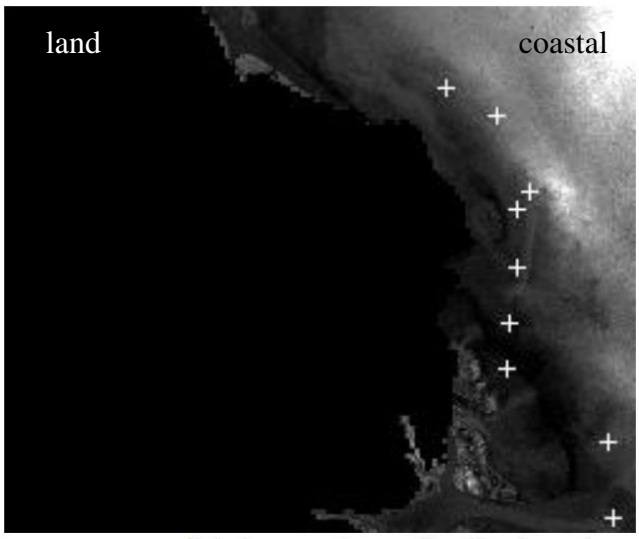

Figure 15 *Sentinel-2 imagery of the Porong River in infrared (Bioresita et al., 2018)*

A high level of contaminants was also found in the lower reach of the Porong River. Example of this were TSS, aluminum, and iron, which has harmful effects on the fast growing Mozambique Tilapia (*Oreochromis mossambicus*). Damage to this species was indicated by a lower density of

melanophores in the scales of the fishes found in the downstream reach, as compared to scales from the fishes found in the upstream reach of the Porong River (Hidayati et al., 2017).

CHAPTER 3 SITE DESCRIPTION

3.1 Sidoardjo Mud Reservoir

The mud reservoir is the area that contains the extruded mud from the Sidoardjo Mud Volcano. The mud volcano is located in Renokenongo Village, the district of Porong, within the regency of Sidoardjo, East Java as shown in **Figure 16**. More specifically, there are two craters of the Sidoardjo Mud Volcano at 7º31'36.99"S and 112º42'41.90"E as shown in **Figure 17**. The volume of the mud reservoir was about 40 million m^3 with an area of 565 ha, a perimeter of 11 km and a height of embankment of 15 m.

Figure 16 *The location of Sidoardjo Mud Volcano*

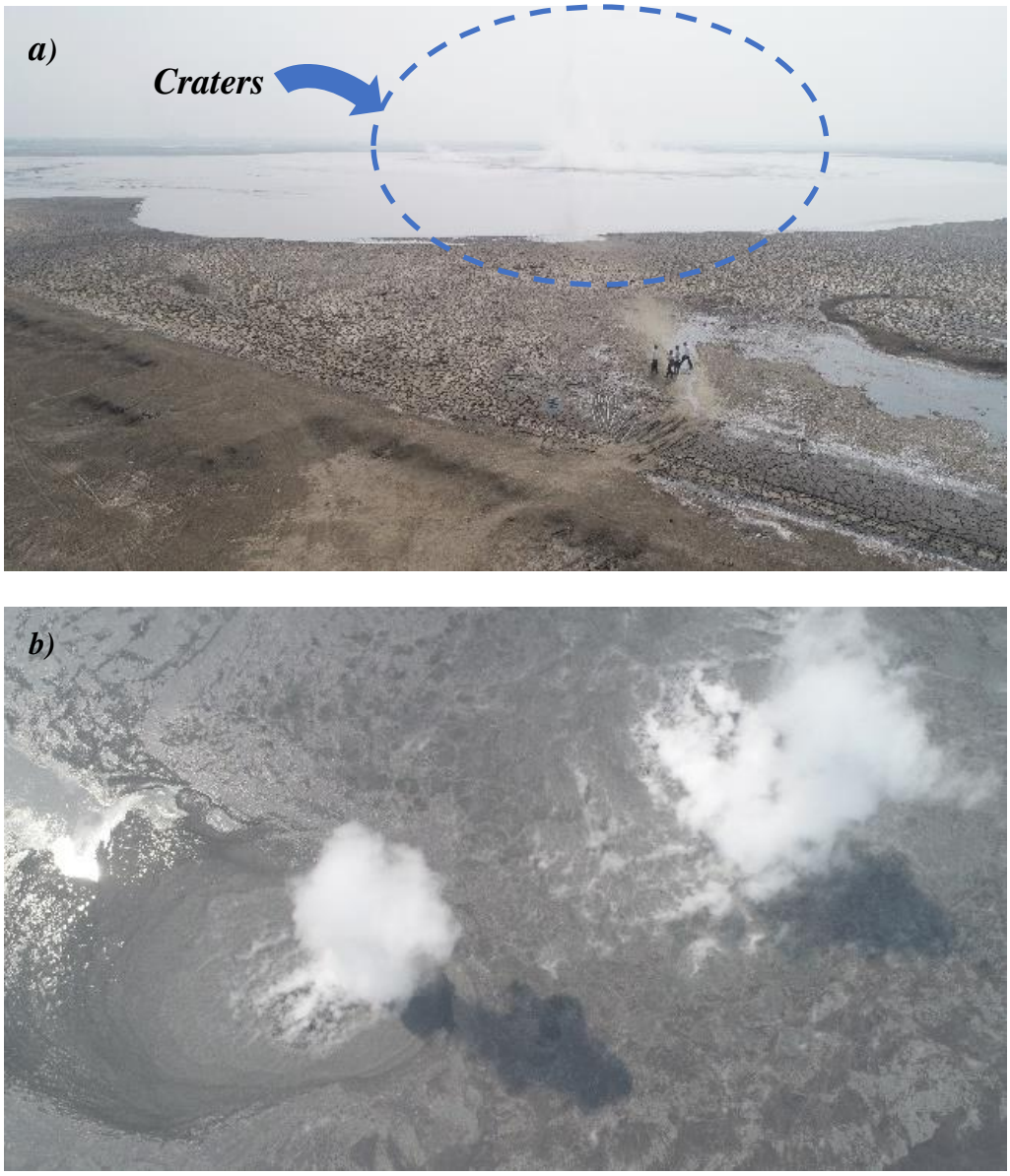

Figure 17 *The recent photos of Sidoardjo Mud Volcano: a) bird view of the mud reservoir with the main crater in the circle; b) the main crater of the Sidoardjo Mud Volcano*

Figure 18 shows the evolution of the Sidoardjo Mud Volcano. The yellow arrow indicates the main crater of the Sidoardjo Mud Volcano and the blue arrow indicates the flow direction of the Porong River. In June 2006, the affected area was about 135 ha but the damage was still spreading. From July 2010 to August 2018 as the figure shows, the mud volcano stabilized. Communities were relocated and the mud reservoir had been constructed.

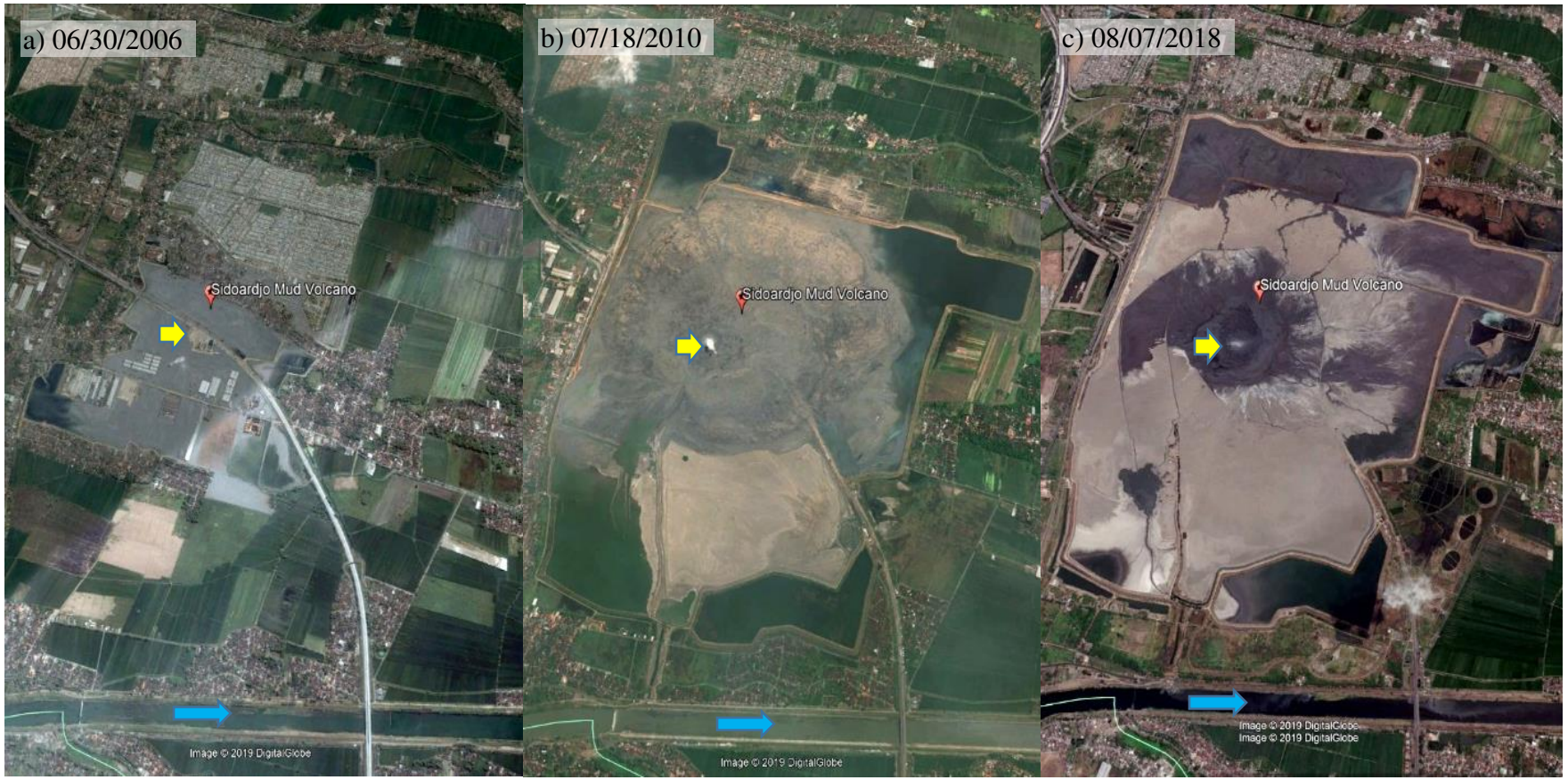

Figure 18 *The evolution of Sidoardjo Mud Volcano taken with Google Earth (from left to right are pictures in 06/30/2006, 07/08/2010 and 08/07/2018, respectively)*

Figure 19 presents an embankment or mud reservoir map as managed by the Sidoardjo Mud Control Agency in 2016. This was the public agency tasked with overseeing management and mitigation of the mud volcano. The mud reservoirs were divided into several ponds based on the location of former villages before the eruption. They are clockwise: Kedungbendo pond, Glagaharum pond, Renokenongo pond, and Siring/Jatirejo pond. The agency also named the embankments based on the order in which they were constructed. They start from P1 to P100. The first 20 embankment points were located near the main crater and submerged due to the constant eruption and subsidence. The most important points on the embankment are P25 (Jatirejo pond) and P43 (Renokenongo pond). These are the location where pipes were installed to divert the mud. There were 2 dredges at P25 (Jatirejo pond) and 4 dredges at P43 (Renokenongo pond). The name of the outlet for P25 is Pejarakan Outlet (PO), located 16 km from the estuary while the outlet for P43 (Renokenongo pond) is Ginonjo Outlet (GO), located 1 km downstream of the Pejarakan Outlet. The recorded sediment concentration of the Pejarakan Outlet at the survey time was 40,000 mg/l or $C_v = 0.015$, and the concentration of Ginonjo Outlets is 57,000 mg/l or $C_v = 0.022$.

Figure 19 *The 2016 Embankment maps of the mud reservoir*

3.2 Porong River

The Porong River is a tributary of Brantas River. The Porong River starts from Lengkong Baru Weir in Mojokerto, East Java and is 50 km in length. The average bed slope is 28 cm/km. The Porong River also receives water from Sadar Creek and Kambing Creek. For this research, the study reach starts from upstream of the Ginonjo Outlet to its estuary at Madura Strait as indicated by the blue bold line in **Figure 20**. The length of the study reach is 15.8 km. The Ginonjo and Pejarakan Outlet's pipe, are located on the left bank of the Porong River. Two important structures near the study reach area are: a Porong station, which is 1.2 km upstream of Pejarakan Outlet, records the stage of the Porong River and a scour protection structure devised to protect an upstream bridge.

The quality of water is set out in Regulation 82 in 2001 (Indonesian Government, 2001). The maximum total suspended sediment (TSS) for the Porong River as a class II river is 50 mg/l.

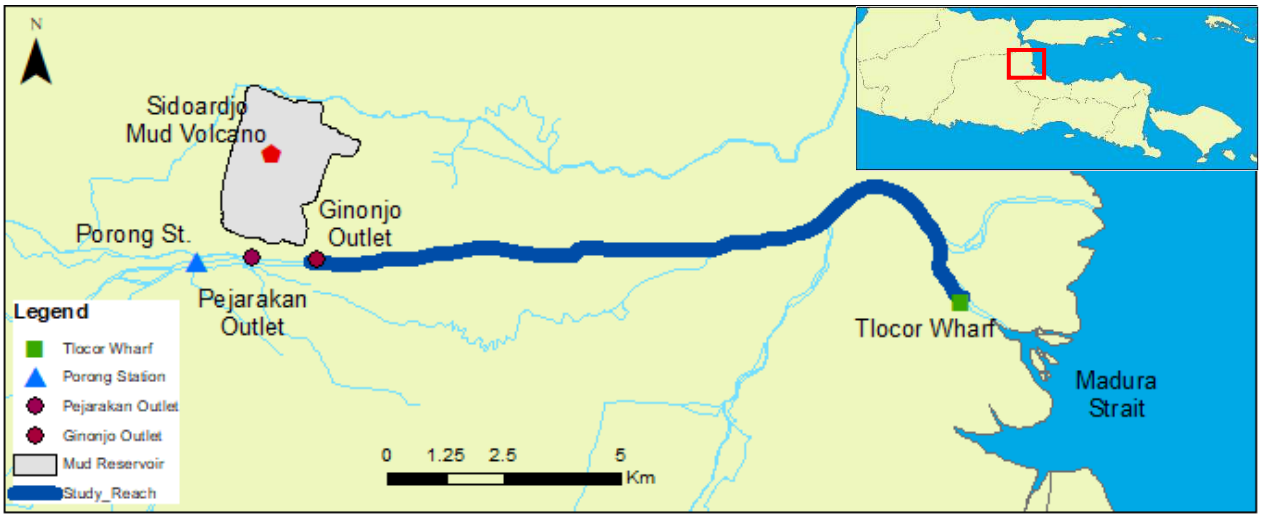

Figure 20 *Plan view of the study reach in Porong River*

3.2.1 Hydrographs of the Porong River

Figure 21 sets out the hourly discharges based on data acquired from January 1, 2012 to December 31, 2016. The flow of duration curve is presented in **Figure 22**. The wet season usually starts from November to April while the dry season goes from May to October. The highest hourly discharge between 2012 and 2016 occurred on April 19th, 2013 at 14:00 where it reached 2,446.2 m^3/s. The lowest hourly discharge occurred in November 2nd, 2012 at 22:00 where it reached 14.5 m^3/s. Based on the hydrograph of the Porong River, the author decided to focus on three flow conditions: low flow Q_l at 45 m^3/s, medium flow Q_m at 250 m^3/s, and high flow Q_h at 2500 m^3/s.

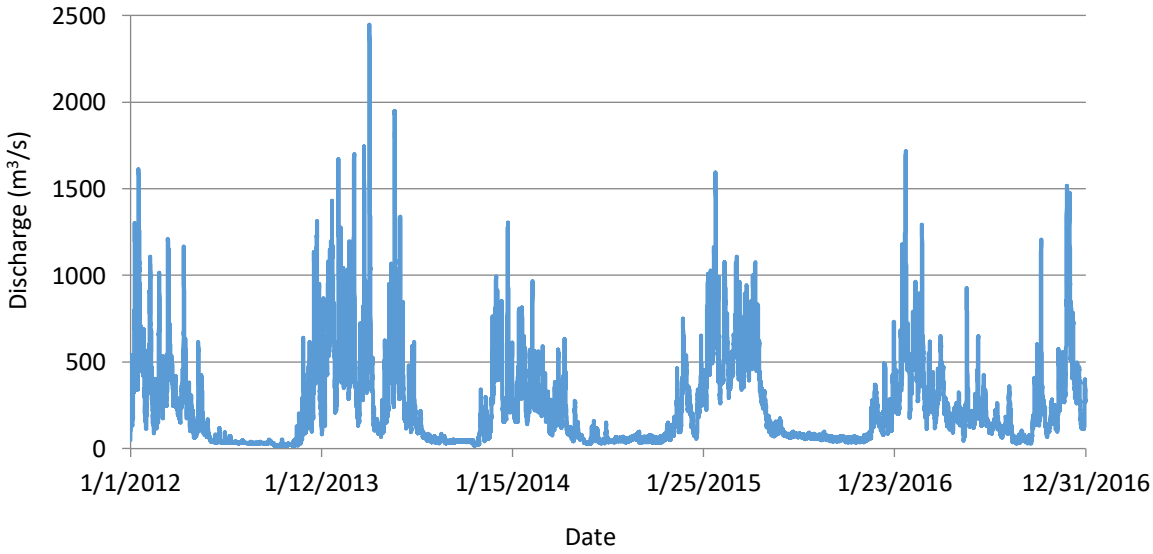

Figure 21 *Hourly discharges of the Porong River based on Porong Station from 2012 to 2016*

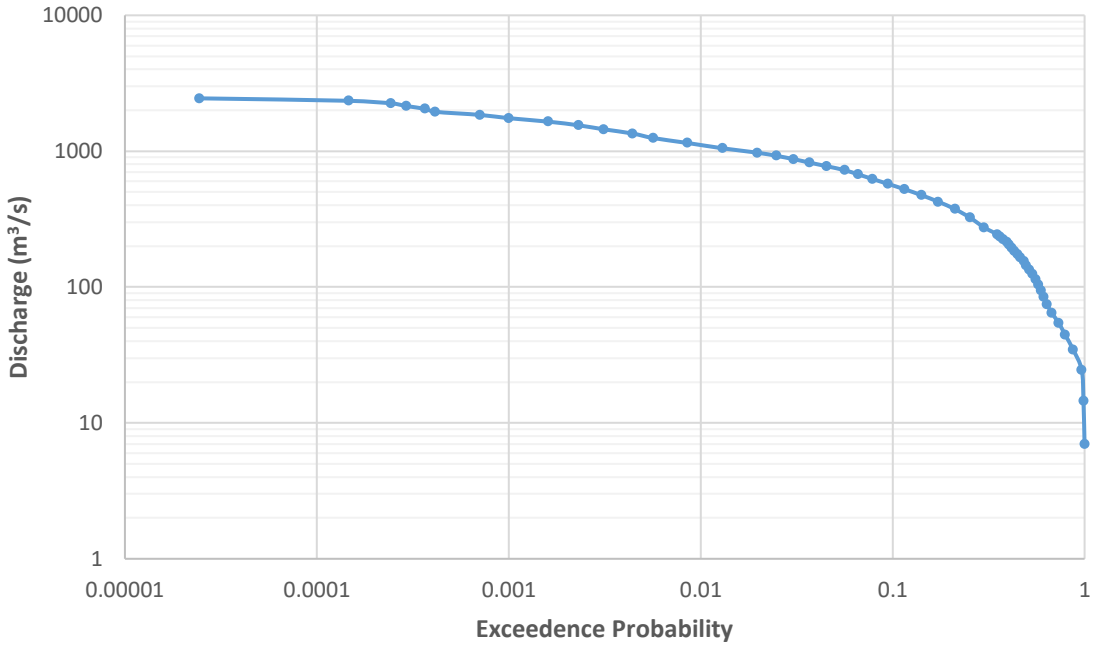

Figure 22 *Flow duration curve of the Porong River*

3.2.2 Hydraulic properties of the Porong River

The typical cross-section of the Porong River is shown in **Figure 23**. The location of the cross-section, KP 168, is 30 m downstream of the Ginonjo Outlet. The bankfull width is about 160 m. The hydraulic parameters for three flow conditions are presented in **Table 5** which includes the discharge (Q), average depth (h), top width (W), flow area (A), energy slope (S_f), average flow velocity (V), and shear velocity (u_*). The low flow Q_l, which takes place in dry season between June to November, has a flow depth, width, and velocity of 6.3 m, 106 m, and 0.1 m/s, respectively. With limited flow velocity, the diverted mud was expected to have more time for mixing and settling. This is the main concern for this research. The medium flow (Q_m = 250 m^3/s), which usually takes place during wet season, would have a flow depth, width, and average velocity of 6.33 m, 106 m, and 0.57 m/s, respectively. In this condition, the diverted mud would have less

time to mix and settle. The high flow Q_h, which would happen only under extreme conditions, would have a flow depth, width, and velocity of 12.25 m, 134 m, 2.16m/s, respectively. The high velocity would cause the diverted mud to flow quickly to the estuary, with a little time to settle in the river.

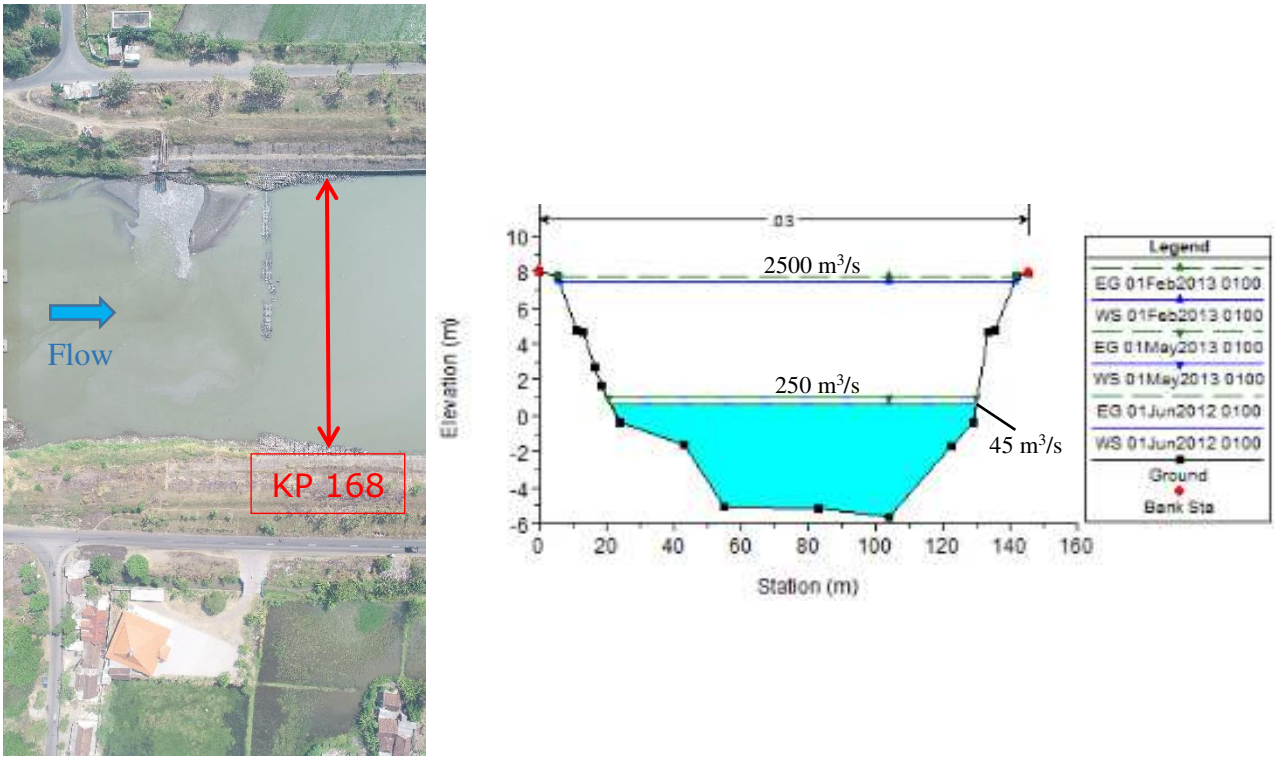

Figure 23 *Cross-section of the Porong River*

Table 5 *Hydraulic properties of the Porong River*

	Time	Q (m^3)	h (m)	W (m)	A (m^2)	S_f (cm/km)	V (m/s)	u_* (m/s)
Low Flow	06-01-12	45	3.5	105	370	0.3	0.12	0.01
Medium Flow	05-01-13	250	3.7	107	400	6.6	0.64	0.05
High Flow	02-01-13	2500	8.6	135	1160	25	2.15	0.14

3.2.3 Characteristics of bed materials

We investigated the particle size distribution of the bed material at three different locations, as described in **Figure 24**: Bed1, which is located at 500 m upstream of the Pejarakan Outlet (original condition), Bed2, which is located at 10 km downstream of the Ginonjo Outlet, and Bed3, which is located at 13 km downstream of the Ginonjo Outlet. The results are presented on **Figure 25** (Laboratorium Mekanika Tanah dan Batuan, 2018). Bed1 was found to consist of 0.2% gravel, 43.2% sand, 47.7% silt, and 8.9% clay. Bed2 was found to consist of 15.6% sand, 69.9% silt, and 14.5% clay. Bed3 was found to consist of 0.2% gravel, 47.8% sand, 48.7% silt, and 3.3% clay.

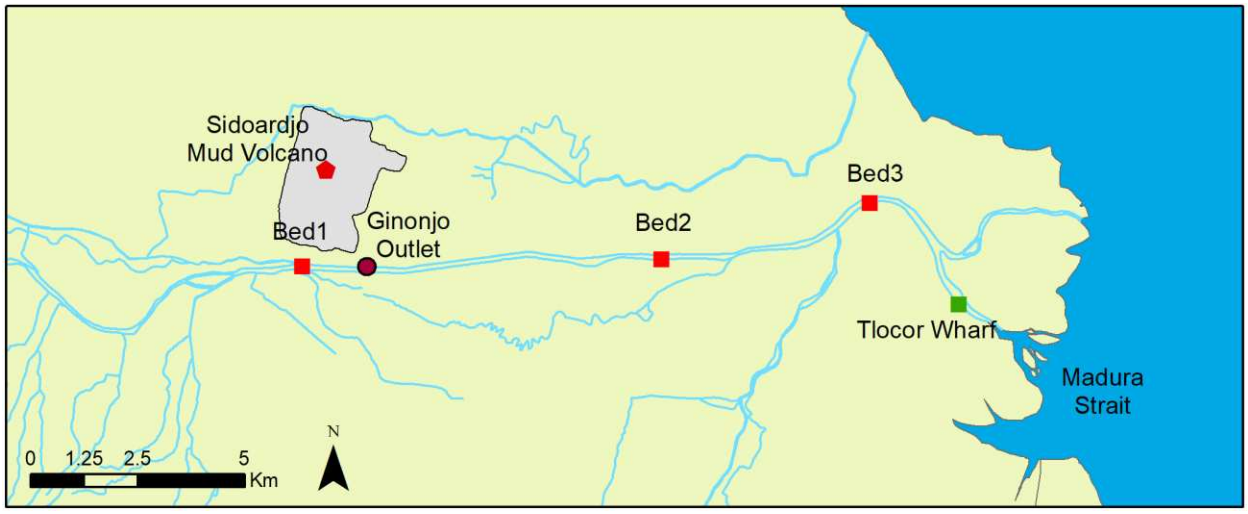

Figure 24 *Location of the sampling of bed material in the Porong River, Sidoardjo, East Java*

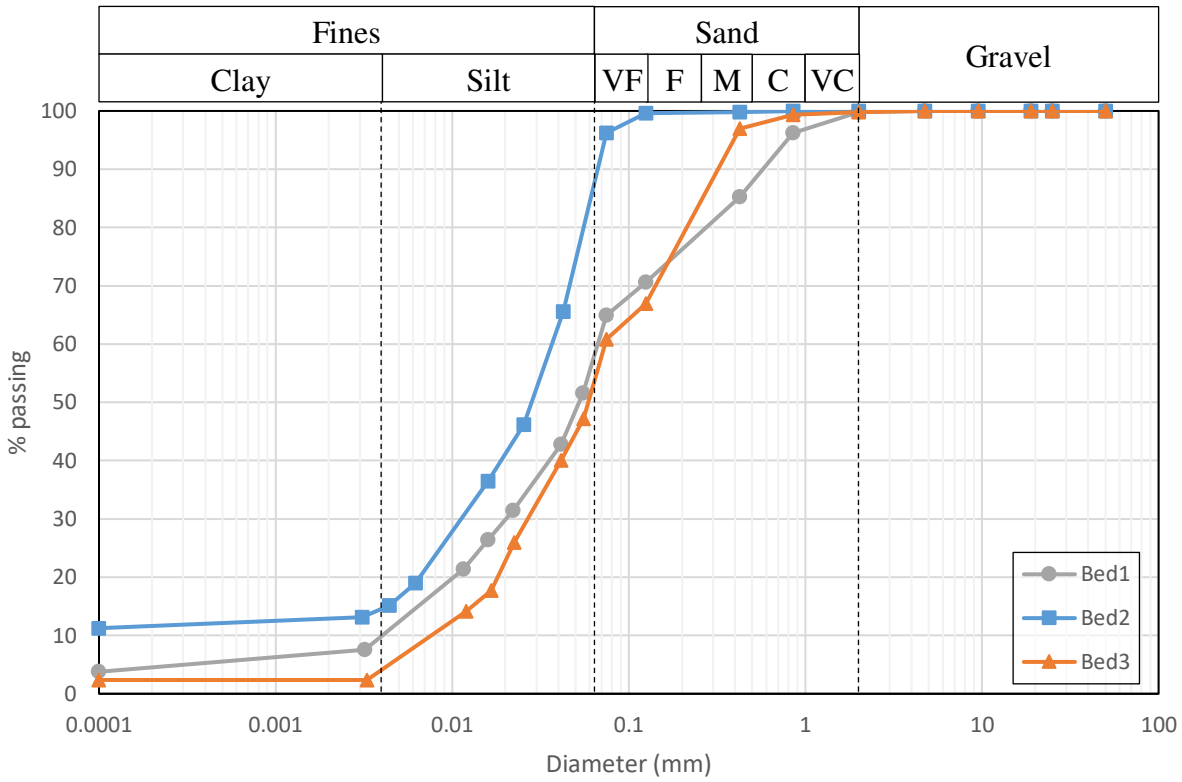

Figure 25 *Particle size distribution of bed materials of Porong River*

3.2.4 Temperature of the Porong River

The author observed the temperature of the diverted mud from the Ginonjo Outlet on September 12, 2020. It was presented in **Figure 26**. The temperature was between 28^0C to 30.5^0C. The lowest temperature of the diverted mud was approximately 28^0C at 10:00. The temperature gradually rose until it reached 30.5^0C at 16:00 and started to decrease at 17:00. In addition, the temperature of the Madura Strait was about 30^0C.

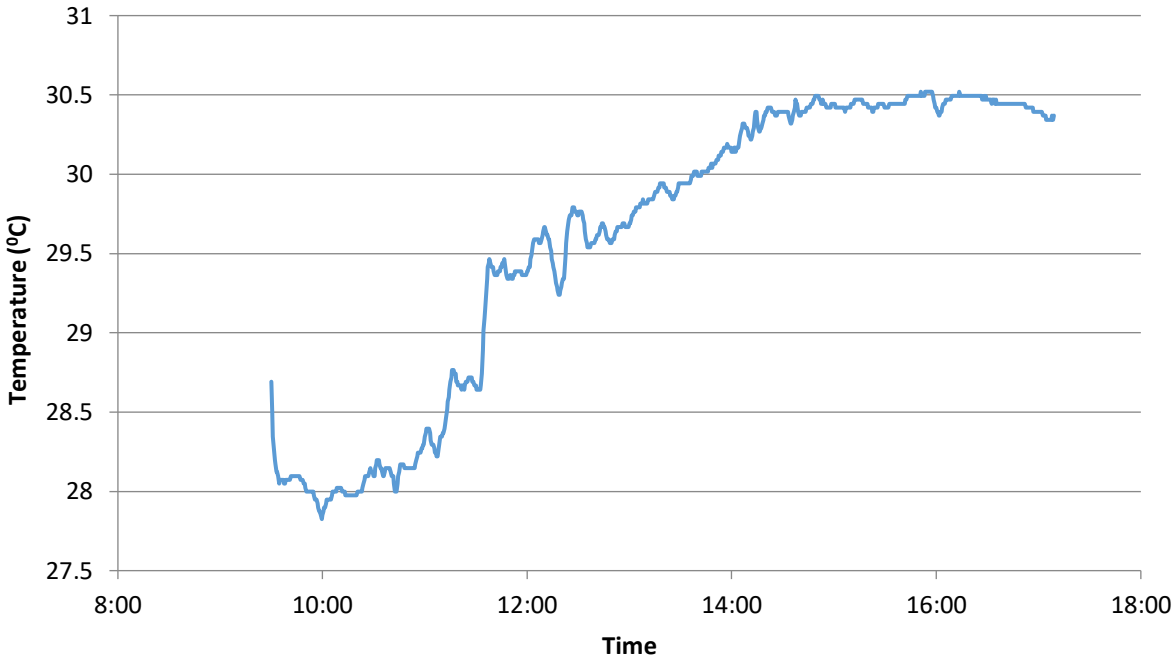

Figure 26 *Temperature of the diverted mud from Ginonjo Outlet on September 12, 2020*

The temperature of flow of the Porong River on September 12, 2020 is presented in **Figure 27**. Based on **Figure 27**, the range of temperature of the flow ranged between 29.1^{0}C to 29.8^{0}C. The lowest temperature was observed at around 9:00 to 10:00 while the highest temperature was recorded at 14:00 to 17:00. The average temperature of this day was 29.5^{0}C.

The temperature of flow of the Porong River also had been observed on October 14-15, 2020 as shown in **Figure 28**. In these two days, the temperature was between 31^{0}C to 34^{0}C with an average temperature of 32.5^{0}C. The highest temperature was recorded at 15:00 on October 14, 2020. Even though there were fluctuations at around 23:00, the temperature gradually decreased to 33^{0}C at 13:00 and more rapidly decreased to 31^{0}C at 7:00 on October 15, 2020. Then, the temperature slowly increased at 11:00. Based on the data from September 12 and October 14-15, the lowest temperature occurs around 10:00 in the morning and the highest temperature usually occurs at 15:00.

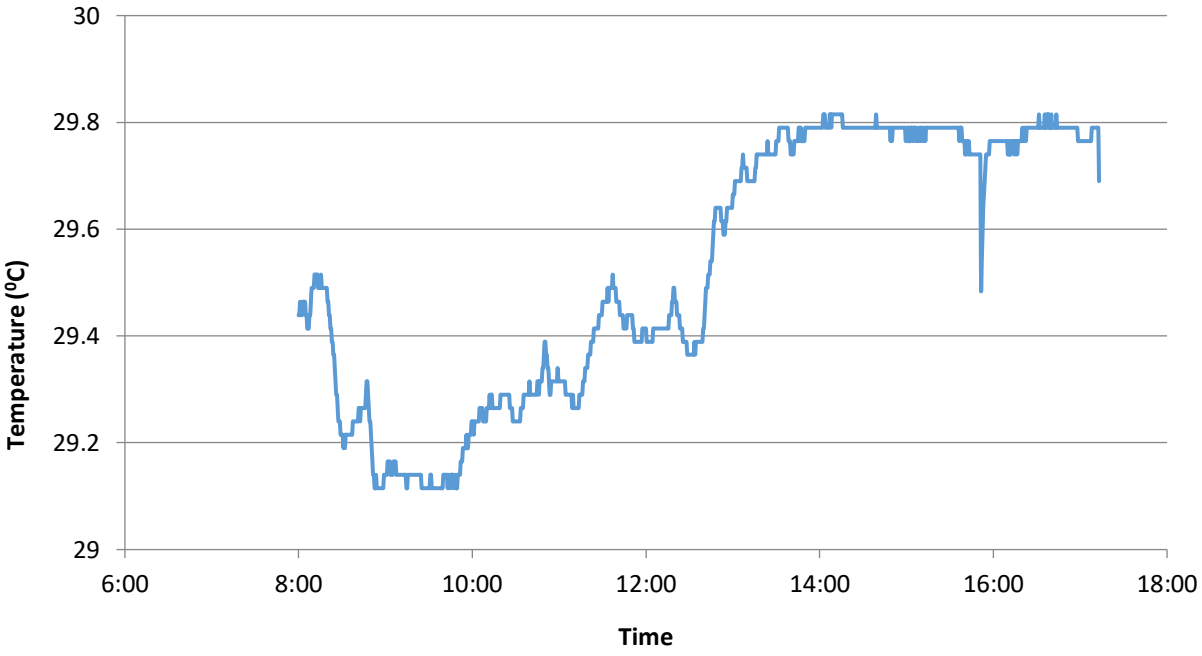

Figure 27 *Temperature of flow of the Porong River on September 12, 2020*

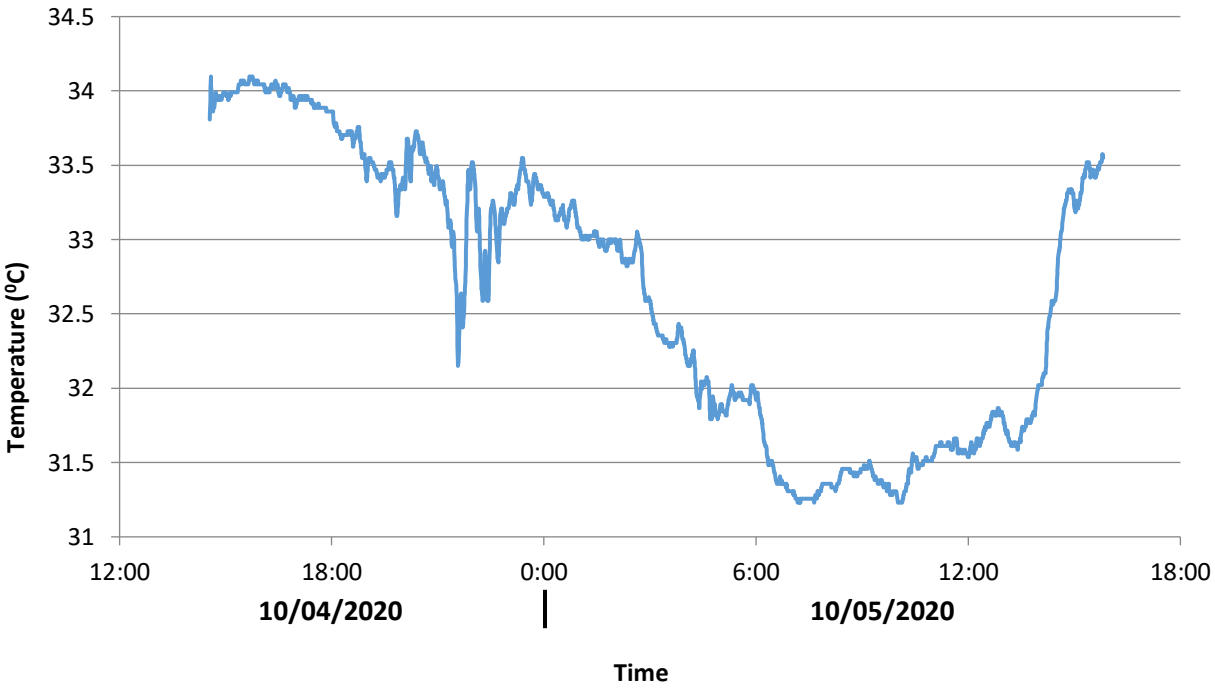

Figure 28 *Temperature of flow of the Porong River on October 4-5 , 2020*

CHAPTER 4 THE PROPERTIES OF THE DIVERTED MUD

4.1 Particle Size Distribution of Mud Samples

To determine the physical characteristics of the mud, a particle size distribution analysis of the mud was completed. The author sampled the extruded mud, taken near the main crater (P25), and mud that had been diverted from the Pejarakan and Ginonjo Outlets. The particle size distribution analysis was completed at Transportation and Geotechnical Laboratory of Civil Engineering of Sepuluh November Institute of Technology in Manyar, Surabaya. **Figure 29** shows the particle size distributions for these samples (Laboratorium Transportasi dan Geoteknik, 2018), which consists mainly of silts and clays. The extruded mud has 17.1% sand, 44% silt, and 38.9% clay; mud diverted from the Pejarakan Outlet has 5.2% sand, 41.2% silt, and 53.6% clay; and mud diverted from the Ginonjo Outlet has 0.8% gravel, 13.3% sand, 34.1% silt, and 51.8% clay. The median grain size or d_{50} and the gradation coefficient for these samples are shown in **Table 6**.

Table 6 *The grain size and gradient coefficient of mud samples*

Sample	d_{10} (mm)	d_{50} (mm)	d_{80} (mm)	G_r (-)
Extruded Mud	0.0013	0.0080	0.0526	6.48
Diverted Mud – Pejarakan	0.0010	0.0034	0.0216	5.63
Diverted Mud - Ginonjo	0.0011	0.0047	0.0556	8.85

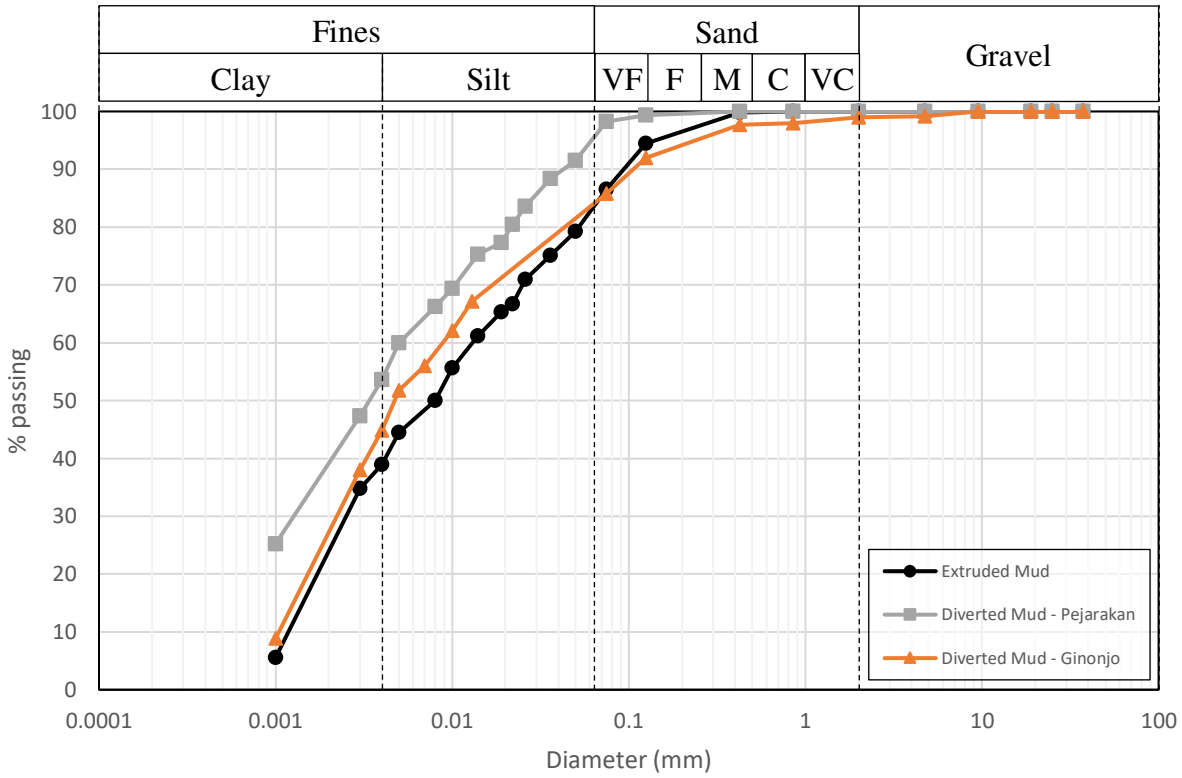

Figure 29 *Particle size distribution of mud samples (VC: very coarse, C: coarse, M: medium, F: fine, and VF: very fine)*

4.2 The Relationship of Turbidity and Sediment Concentration

4.2.1 Data Collection

The relationship between turbidity and sediment concentration was determined through a laboratory experiment by diluting a full bottle of sediment sample from the mud reservoir with the Porong River water. The following instruments were used for this laboratory experiment: 1. HACH 2100P turbidimeter; 2. Mettler Toledo laboratory balance; 3. Glass beaker; and 4. Flask – 100 ml. The laboratory experiment was done in 2018 as the result were shown in **Table 7**. There are 2 sets of turbidity data. Set 1 was used to construct the relationship through regression analysis while the set 2 was used to calculate the error of the regression analysis. This is explained in **Appendix A**.

4.2.2 Regression Analysis for the Relationship of Turbidity and Sediment Concentration

The relationship between turbidity and sediment concentration was identified through a regression analysis. Turbidity, in NTU, serves as the independent variable while sediment concentration, in mg/l, is the dependent variable. Four types of regression were used: linear, power, logarithmic, and exponential regression. **Figure 30** shows the regression analysis used to assess the turbidity and sediment concentration relationship in the Porong River in 2018. Based on the coefficient of determination r^2, the best fitted relationship between the turbidity (NTU) and sediment concentration (mg/l) in Porong River is linear regression, marked with blue rectangle:

$$C = 5.3 \times Tur + 24 \tag{29}$$

with $r^2 = 0.99$. This indicates the linear regression can accurately predict the sediment concentration. This relationship will be used later on to calculate data from the field measurement. The second best fitted relationship is the power regression:

$$C = 5.32 \times Tur^{1.01} \tag{30}$$

with $r^2 = 0.99$. While it has a good accuracy for the lower values of concentration, it tends to overpredict the concentration at higher values.

Table 7 *Turbidity (NTU) of the sediment mixture of the corresponding sediment concentration from the laboratory experiment in 2018*

No.	C (mg/L)	Turbidity (NTU)	
		1	2
1	5000.0	949.0	962.0
2	2500.0	469.0	504.0
3	1666.7	255.0	295.0
4	1250.0	245.0	243.0
5	1000.0	189.0	180.0
6	833.3	172.0	143.0
7	714.3	119.0	94.7
8	625.0	110.0	108.0
9	555.6	94.5	107.0
10	500.0	69.4	75.1
11	476.2	84.4	90.3
12	454.5	88.3	84.6
13	416.7	66.6	68.7
14	384.6	64.0	70.4
15	357.1	56.8	59.3
16	333.3	61.9	59.7
17	312.5	54.4	57.9
18	277.8	51.4	47.3
19	250.0	42.4	39.1
20	166.7	24.9	28.1
21	125.0	22.8	22.6
22	100.0	17.2	18.0
23	83.3	16.0	17.1
24	71.4	11.9	12.8
25	62.5	10.9	11.4
26	55.6	10.7	10.4
27	50.0	8.2	8.4
28	45.5	7.8	7.8
29	41.7	7.0	7.5
30	35.7	7.1	6.6
31	31.3	6.3	6.1
32	27.8	5.6	6.1
33	25.0	6.7	6.1

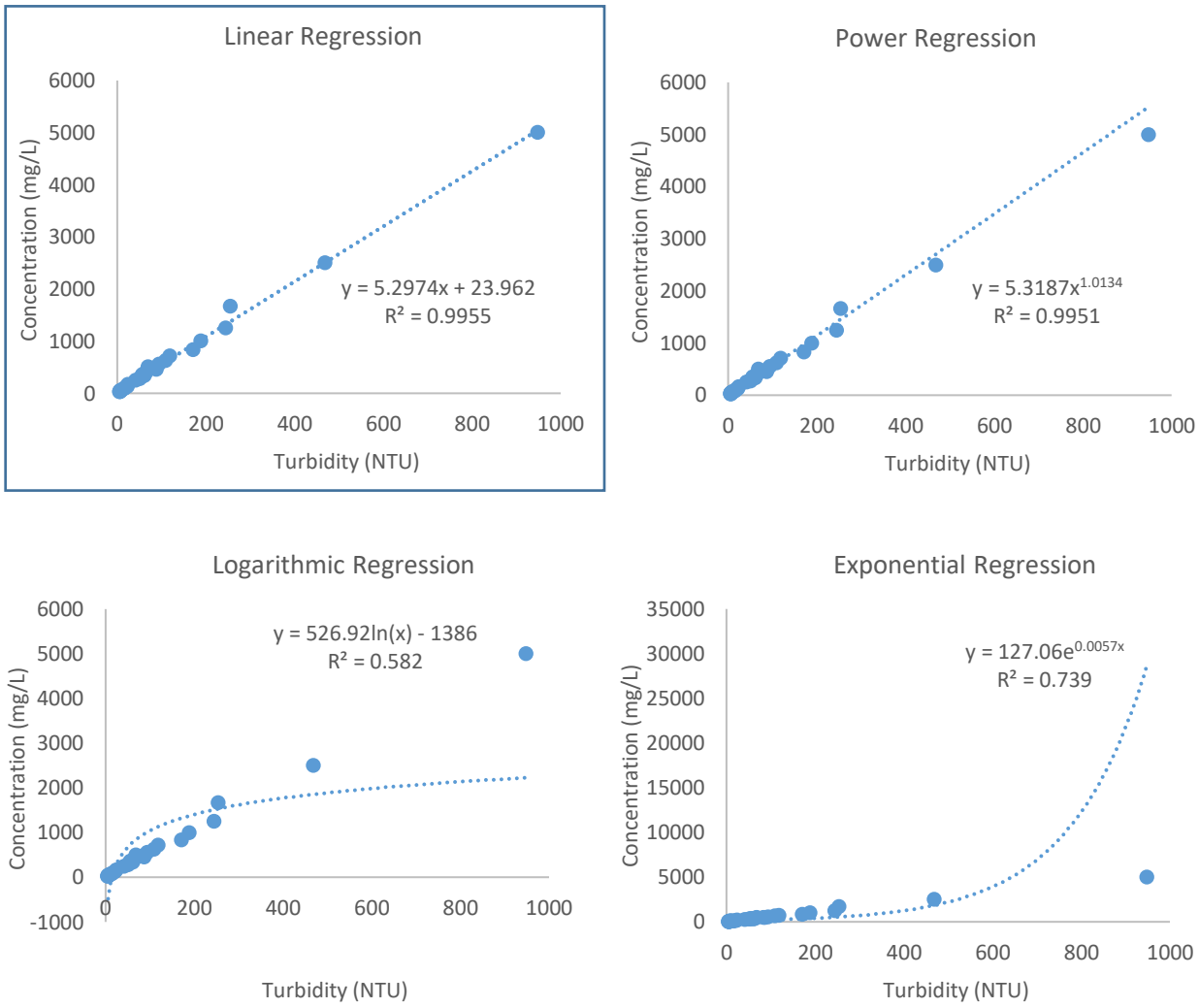

Figure 30 *Regression analysis for turbidity and sediment concentration in Porong River in 2018*

Figure 31 compares preliminary results from previous studies of the relationship of turbidity and sediment concentration. The preliminary results (red circle) is plotted in the middle of the previous studies.

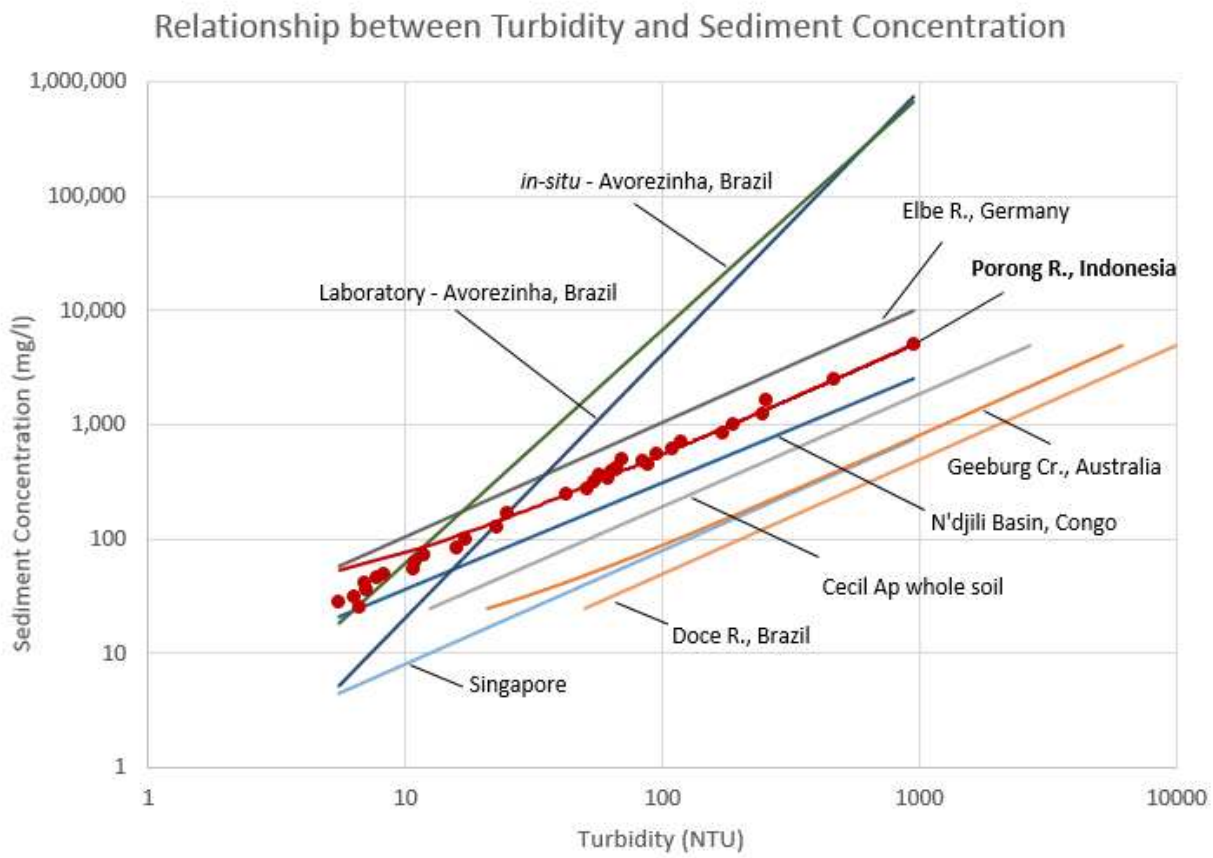

Figure 31 *Comparison of the relationship of turbidity and sediment concentration between the preliminary result and previous studies*

4.3 Flocculation

Flocculation tests were conducted in December 2019 to determine the flocculation processes in the mixture. Two samples were prepared for flocculation tests. The deflocculant agent (specified in the previous chapter) was added to one of the samples while leaving the other sample untouched. Both samples were shaken to resuspend the sediment to compare the settling time and settling distance time. If flocculation occurs, the sample with deflocculant should settle slower than the sample without deflocculant. Otherwise, both will settle around similar time frame. The hyphotesis was that flocculation occurs because fine sediments dominate the mud mixtures.

Water samples from each diversion outlet were gathered and poured into 500ml bottles and catalogued to identify the diversion outlet, as shown in **Figure 32**. Two bottles containing water collected from Pejarakan Outlet were named P1 and P2 and two bottles containing water collected from Ginonjo Outlet were named G1 and G2. P1 and G1 were without the deflocculant while P2 and G2 were mixed with 5 ml of the deflocculant. The sediment was left to settle and the settling distance and settling time were recorded.

Figure 32 *Samples from Pejarakan and Ginonjo Outlet. Sample from left: P1, P2, G1 and G2; deflocculant were added to P2 and G2.*

Figure 33 shows the comparative result of the flocculation test during the first 4 hours of the experiment. The settling velocity is settling distance divided by settling time. Comparing the result of those samples, the settling velocity of sample mixed with deflocculant P2 was slower than the settling velocity of the natural sample P1. The settling velocity of P2 was 0.015 mm/s while P1

was 0.032 mm/s. Both were recorded 10 minutes after the test was started. For G1 and G2, the fastest settling velocity were at 0.028 mm/s and 0.013 mm/s, respectively. By comparing the settling velocity between the samples from Pejarakan and Ginonjo, it is possible to summarize that samples from Pejarakan had a slightly faster settling velocity. Thus, the mud from Pejarakan Outlet settled faster than the mud from Ginonjo. The settling velocity value of the two outlets was miniscule compared to the general settling velocity, which is 0.15 – 0.6 mm/s. Nevertheless, the test concluded that the mud has a very slight tendency to flocculate.

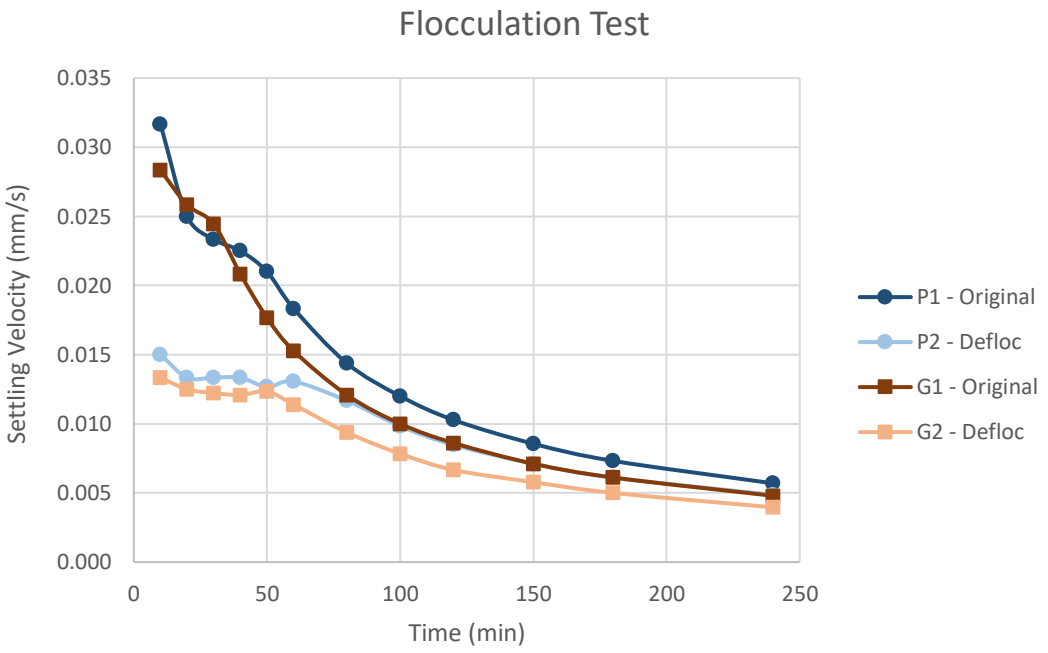

Figure 33 *Results of flocculation test*

Furthermore, the settling velocity gradually decreased after 60 minutes because the coarser particles have settled to the bottom of the bottle. The research also analyzed ratios of settling velocity between the samples with and without deflocculant as presented in **Figure 34**. The settling velocity of samples without deflocculant were 2.1 times higher than the settling velocity of samples with deflocculant. These ratio kept decreasing over 60 minutes until it reached 1.4 and 1.3 for

sample from Pejarakan and Ginonjo, respectively. After 60 minutes, the ratio stabilized at an average of 1.2 for Pejarakan's sample and 1.25 for Ginonjo's sample. This indicated that a portion of sediment forms a bigger floc, as a flocculation process, and settled after 60 minutes. The non-flocculated sediments started to become visible after 60 minutes.

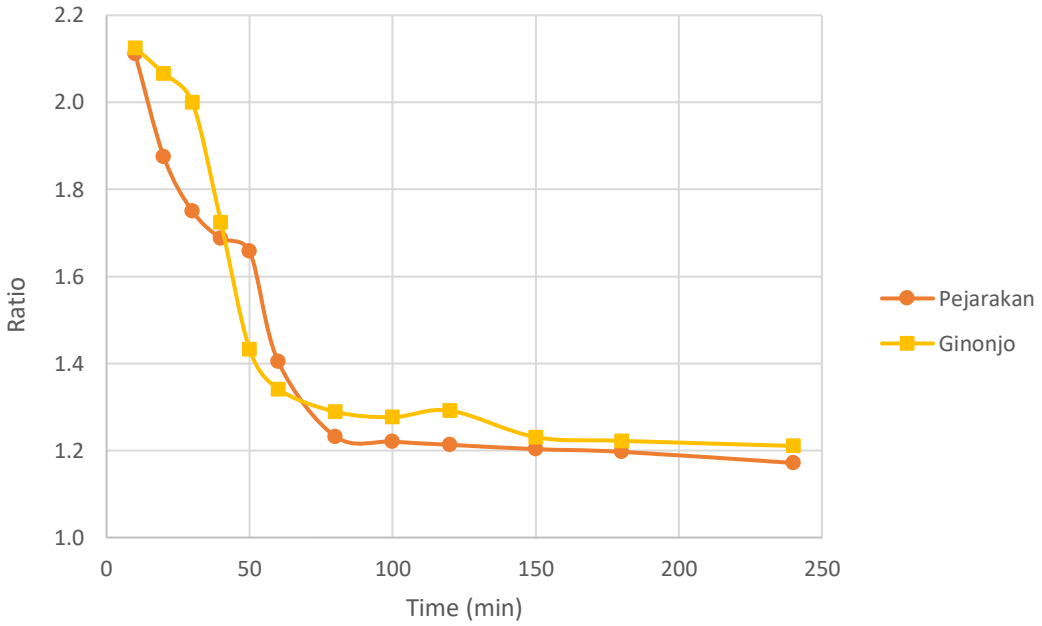

Figure 34 *Ratio of settling velocity of deflocculated samples and original samples*

CHAPTER 5 FIELD MEASUREMENTS

The objective of the field measurements was to validate the computational model. The field measurements were needed because a comprehensive data set was not available. Two field measurements were conducted in the study reach: Field measurement program #1 in July 10-14, 2018 and Field measurement program #2 in September 10-12, 2019.

5.1 Field Measurement Program #1 (July 10-14, 2018)

The field program measured turbidity along the whole study reach. The turbidity data can be easily measured and are used as a surrogate of sediment concentration. At the time of the measurements #1, the discharge of the Porong River is 45.2 m^3/s with flow velocity of 0.16 m/s and shear velocity of 0.01 m/s. The upstream sediment concentration was 56.7 mg/l. The sediment concentration of the diverted mud at Ginonjo Outlet is 57,000 mg/l and the discharge was 0.33 m^3/s. The following is the field survey program with point measurements.

The river reach of 15.8 km was surveyed at 106 cross-sections with a distance between cross-sections of 150 m. The first cross-section of the measurement was located at 30 m upstream of Ginonjo Outlet and was intended to capture the undisturbed sediment concentration in the Porong River. The second cross-section was at 80 m downstream of the Ginonjo Outlet. The following cross-section up to the 106^{th} cross-section were located 150 m downstream of the previous cross-section. Each cross-section had 4 point of measurements with a lateral distance between point measurements of 25 m as illustrated in **Figure 35**. For example, cross-section 1 consists of points 1A, 1B, 1C, and 1D. Cross sections were offset by 5 m from the left and right bank to avoid additional sediment concentration from the river bank.

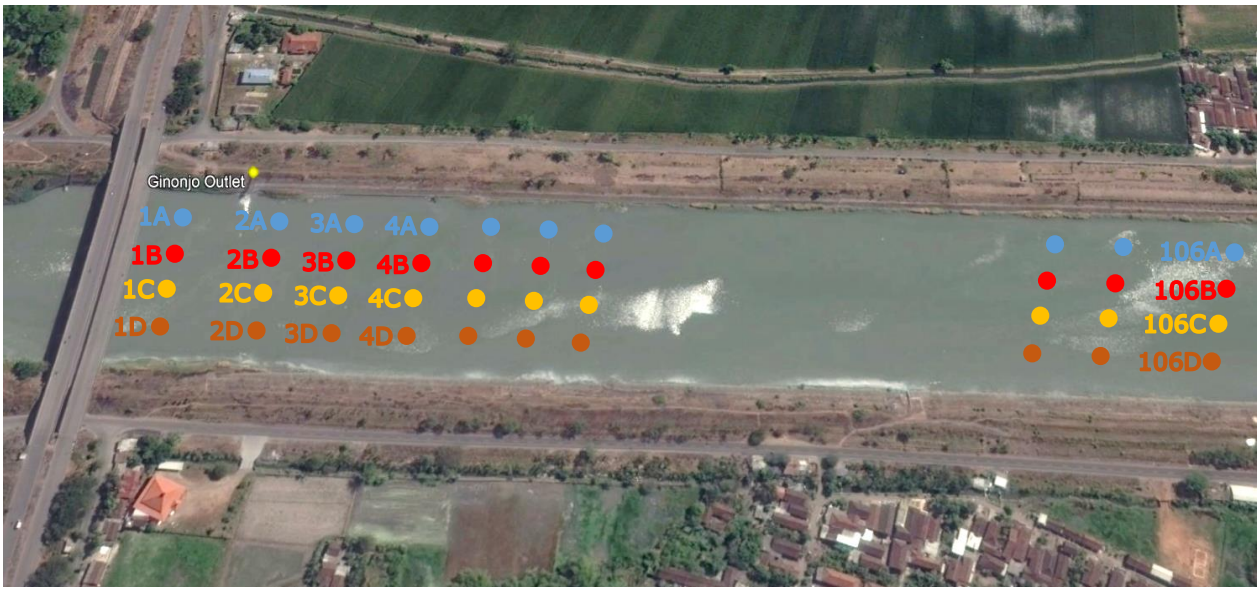

Figure 35 *Illustration of field measurement #1 in the study reach; not to scale (point A, B, C, and D illustrated the 4 points of measurement in one cross-section)*

The field measurements were carried out at 1 m below the water surface. An instantaneous sampler was used with a product name of water sampler horizontal "bit" type WSH-BIT 22 that had a capacity of 2.2L as shown in **Figure 36**. Then, the turbidity of the sample was measured by using a turbidimeter and the coordinate at the collection point were recorded. **Figure 37** presents the pictures when the measurements were completed on the field. The turbidity data from field measurement #1 were presented in **Appendix B**.

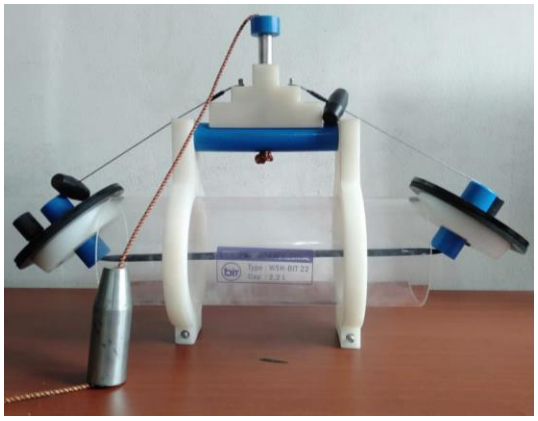

Figure 36 *Water sampler horizontal for field measurements*

Figure 37 *Photos of the field measurements #1*

The turbidity data from the field measurement were converted to sediment concentration by using Equation 30:

$$C = 5.3 \times Tur + 24$$

The sediment concentration profiles along the 16 km Porong River is shown in **Figure 38**. The measured concentrations in line A, B, C, and D indicate a same pattern. All four had high sediment concentration in the first 2 km and gradually decreased to about 90 mg/l 3 km from the point source at the Ginonjo Outlet. The highest measured sediment concentration was actually located in line C at 4,198 mg/l, followed by line D at 2,704 mg/l, line B at 2,021 mg/l, and line A with 691 mg/l. There were slight fluctuations at 12 km downstream of the Ginonjo Outlet which could be caused by the presence of fish farms in the area.

5.2 Field Measurement Program #2 (September 10-12, 2019)

Based on Field Measurement Program #1, the sediment in the Porong River became fully-mixed at 4 km. The sediment concentration at line A, B, C and D were observed at the same level.

However, from 0 to 4 km, there were different sediment concentrations laterally and perhaps vertically. Therefore, the Field Measurement Program #2 aimed to capture the vertical variability of sediment concentration, or the vertical sediment concentration profile for the first 4 km of the study reach. Field Measurement Program #2 was completed in September 20-12, 2019. The discharge of the Porong River was 47.7 m/s, flow velocity was 0.16 m/s and the shear velocity was 0.01 m/s.

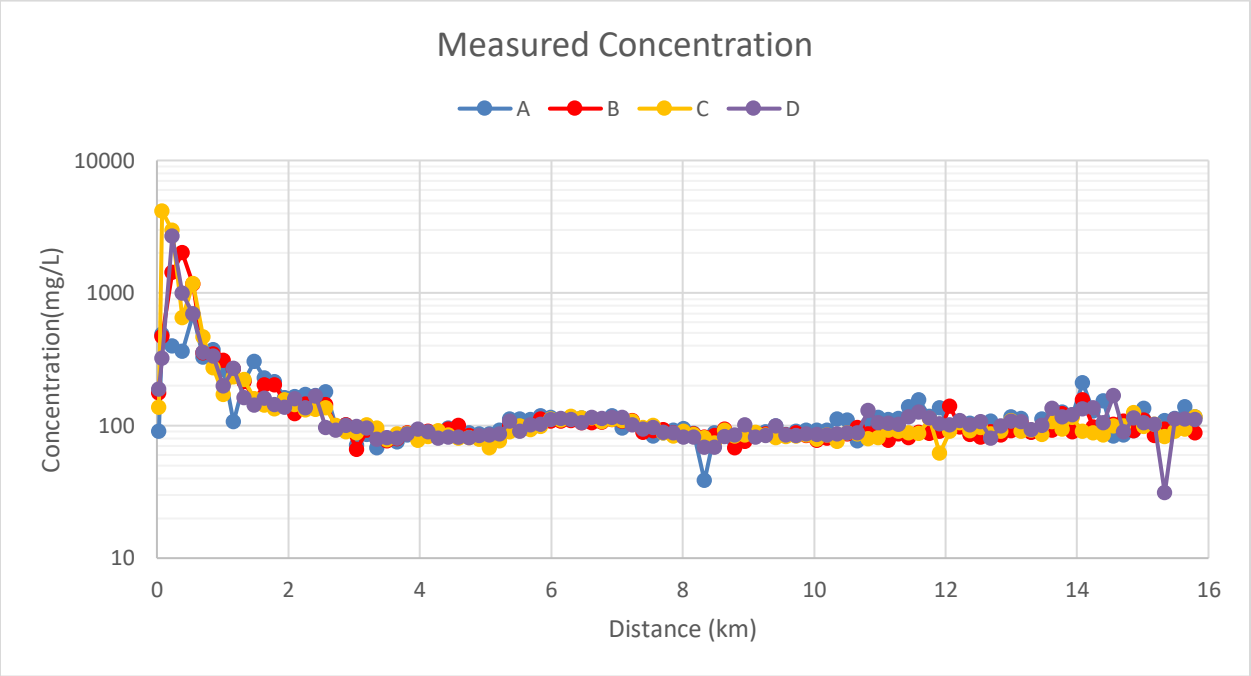

Figure 38 *The measured sediment concentration in the study reach*

The points of measurements in field measurement #2 were presented in **Figure 39**. Similar to Field Measurement #1, each cross-section had 4 point of measurements with the lateral distance between each point was 25 m and had 5 m offset from the left and right bank. The first cross-section was at 130 m downstream of the Ginonjo Outlet. For the first 4 km, the following cross-section was located 100 m downstream of the previous cross-section. After 4 km, the distance between cross-section was 200 m. The first cross-section could not be closer to the Ginonjo Outlet because there

were a ground sill or river bed protection consists of many tetrapods at 30 m downstream of the outlet. To capture the vertical sediment concentration, the sample were taken every 1 m depth until the bed of the Porong River. This action was done at each point measurement. Field Measurement #2 also utilized the instantaneous sampler as shown in **Figure 36**. Documentations of the measurement were shown in **Figure 40**. In total 301 bottles os sample were collected.

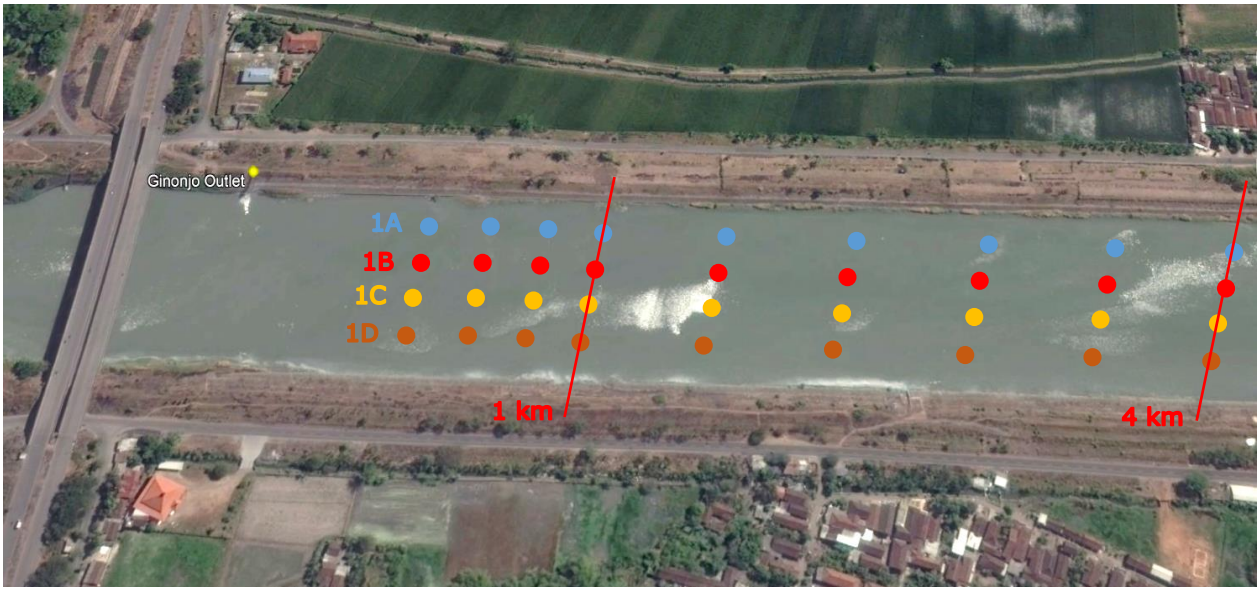

Figure 39 *Illustration of field measurement #2 in the study reach; not to scale (point A, B, C, and D illustrated the 4 points of measurement in one cross-section)*

Figure 40 *Photos of field measurements and bottles of samples*

The longitudinal sediment concentration per 1 m depth from Field Measurement #2 were displayed in **Figure 41**. In general, the sediment concentration was high at the beginning of the study reach, particularly in the deeper water. Beyond 1 km, most of the sediment concentration was in range between 10 mg/l to 100 mg/l. The two highest sediment concentrations of line B were 700 mg/l at 6m in depth and 400 mg/l at 4m in depth where it were located 200m downstream from the outlet. The trend of line C was similar to line B with the two highest sediment concentration close to 1 km downstream from the Ginonjo Outlet with 1,500 mg/l at 6 m in depth and 1,450 mg/l at 3 m in depth. These values proved that the coarser sediments are settled in the first kilometer.

To capture a viable sediment concentration profile, we selected the point of measurements that had at least 3 m depth. Thus, we could get at least 4 points of depth for each measurement point. Line A and D, which have limited numbers of depth measurement, were left out of the analysis. Out of 24 points of measurement in line B and line C, only 12 points and 11 points met the requirement of 4 different points of depth, respectively. The sediment concentration profile parameters, such as Rouse number, were obtained by plotting the suspended sediment concentration versus $(h - z)/z$ in power function as shown in **Figure 42**. A summary of this analysis is presented in **Table 8**. The Rouse number obtained from this method was called the plotted Rouse number Ro_p. The Rouse number Ro is the power indice in the following Equation 31.

$$C = C_{mid}\left(\frac{h - z}{z}\right)^{Ro} \tag{31}$$

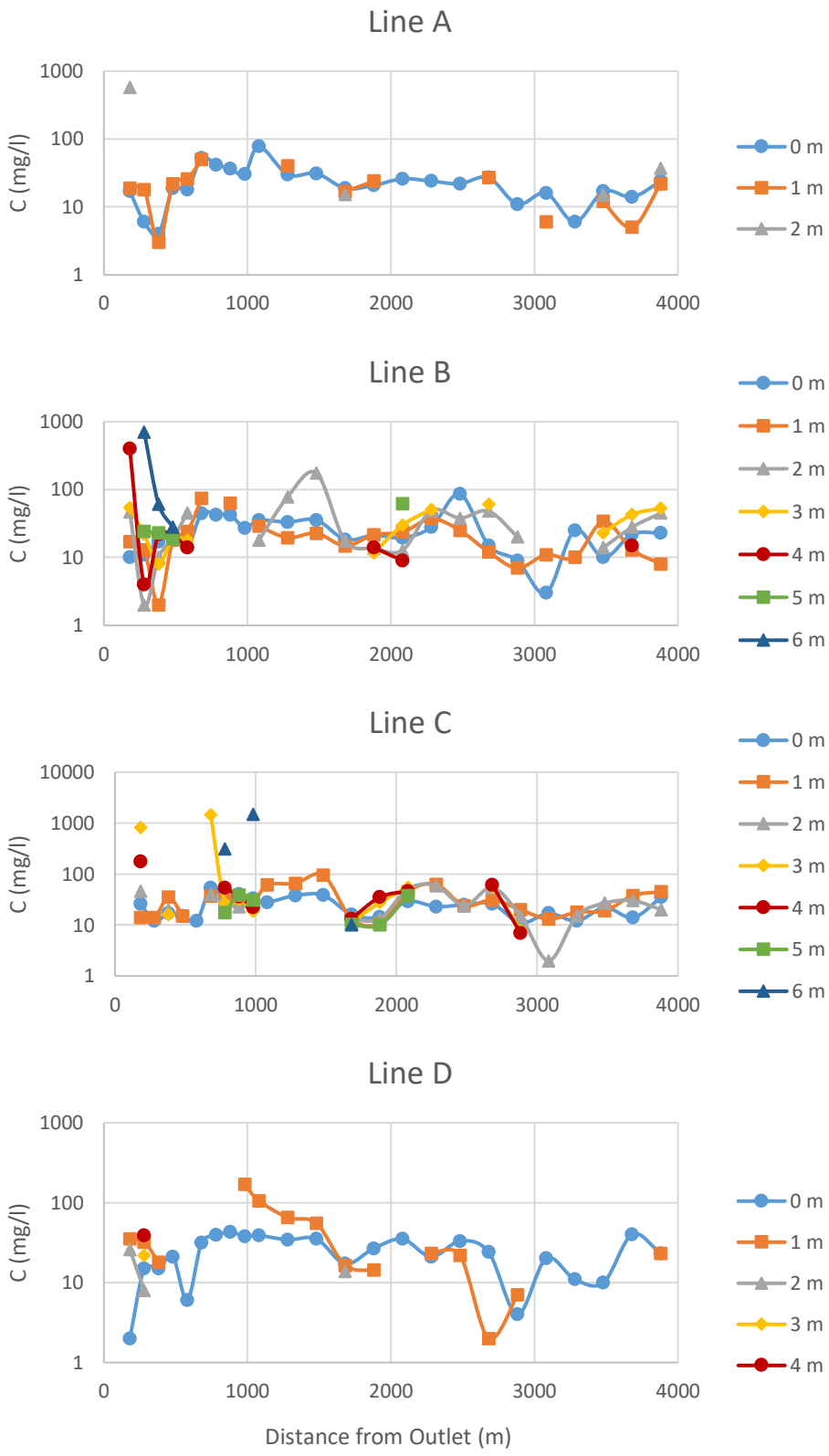

Figure 41 *The longitudinal sediment concentration per 1 m depth*

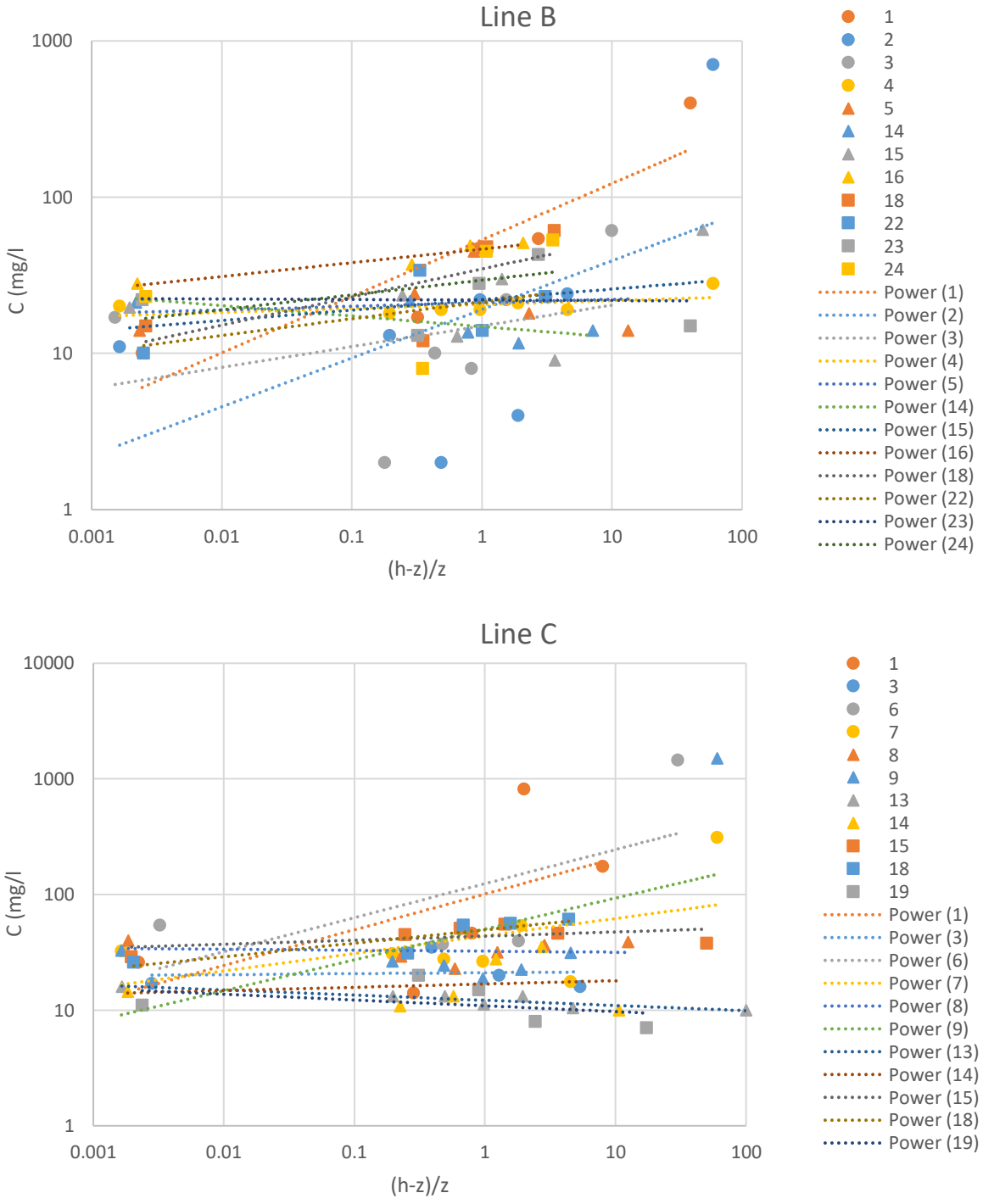

Figure 42 *Plot of suspended sediment concentration versus* $(h-z)/z$

Table 8 *Summary of the analysis of sediment concentration parameter (h is the flow depth;Ro_p is the plotted Rouse number; C_{mid} is the mid-depth sediment concentration; C_a is the reference sediment concentration which in this case is the near-bed concentration)*

XS	Line B				Line C			
	h (m)	Ro_p	C_{mid} (mg/l)	C_a (mg/l)	h (m)	Ro_p	C_{mid} (mg/l)	C_a (mg/l)
1	4.1	0.36	53.23	401	4.5	0.31	101.09	175
2	6.1	0.31	19.13	702	-	-	-	-
3	6.6	0.13	15	61	3.6	0.01	21.1	16
4	6.1	0.03	20.56	28	-	-	-	-
5	4.3	0.02	21.09	14	-	-	-	-
6	-	-	-	-	3.1	0.29	124.29	1448
7	-	-	-	-	6.1	0.16	43.85	310
8	-	-	-	-	5.4	0	32.34	39
9	-	-	-	-	6.1	0.27	50.37	1504
13	-	-	-	-	6.1	0	12.16	10
14	4.6	0	14.85	14	5.5	0.03	16.85	10
15	5.1	0.07	22.13	62	5.1	0.04	43.73	38
16	4.5	0.09	46.57	51	-	-	-	-
18	3.8	0.18	34.67	61	4.9	0.11	19.54	61
19	-	-	-	-	4.2	0	10.91	7
22	4.0	0.11	21.34	23	-	-	-	-
23	4.1	0	21.98	15	-	-	-	-
24	3.9	0.09	29.42	53	-	-	-	-

Based on **Figure 42** and **Table 8**, the plotted Rouse number Ro_p ranged from 0 to 0.36, which is smaller than 1.25 as the limit of the mixed load. Therefore, the mode of sediment transport in the study reach is suspended load. It can be assumed that the concentration profile are a uniform ($Ro = 0$).

A deeper investigation for 6 cross-section with the highest plotted Rouse number was completed. These were cross-section (XS) B-1, B-2, B-18, C-1, C-6, and C-9 as presented in **Table 9** and **Figure 43**. There were 3 types of sediment concentration profiles in **Figure 43**: measured concentration profiles from sampling or measurements, fitted concentration profiles obtained by

utilizing the Rouse number Ro_f with the smalles root mean square of the concentration, and plotted concentration profile from the calculated Rouse number Ro_p.

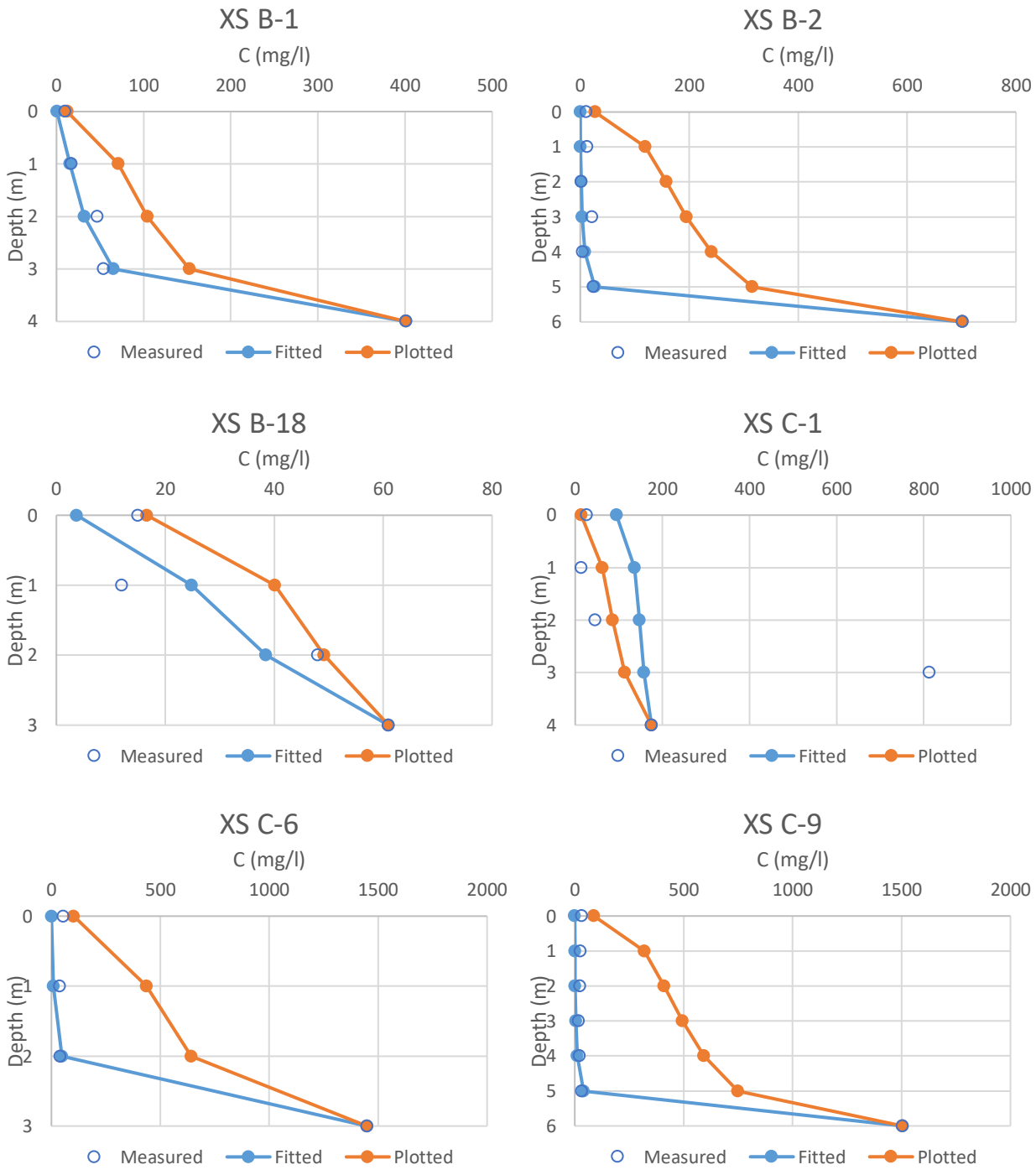

Figure 43 *Suspended sediment profiles for 6 cross-sections in the study area*

Table 9 *Suspended sediment concentration parameters for 6 cross-sections in the study area*

XS	h (m)	C_{mid} (mg/l)	C_a (mg/l)	Ro_f	d_s (mm)	RMS_f	Ro_c	d_s (mm)	RMS_c
B-1	4.1	53	401	0.68	49	9	0.36	36	56.37
B-2	6.1	19	702	1.27	68	10	0.31	33	171.94
B-18	3.8	35	61	0.39	50	10	0.18	25	14.10
C-1	4.5	101	175	0.07	16	303	0.31	33	313.96
C-6	3.1	124	1448	1.22	67	31	0.29	32	361.99
C-9	6.1	50	1504	1.40	72	19	0.27	31	431.72

Figure 43 shows that the plotted sediment concentration profiles did not fit the measured concentration profiles. The root mean square between those two profiles ranged from 14.1 to 431. Meanwhile, the root mean square between the fitted concentration profiles and the measured concentration profiles ranged from 9 to 303. The results of median grain size for fitted concentration profiles ranged from very fine sand to medium silt, while for the plotted concentration profiles ranged from coarse silt to medium silt. Therefore, the results from the fitted concentration profiles is more appropriate to use for modeling. The median grain size of the diverted mud was very fine silt, as mentioned in **Table 6**. It then changed into medium silt because of flocculation.

CHAPTER 6 SEDIMENT PROPAGATION MODEL FOR THE PORONG RIVER

6.1 HEC-RAS

The objective of the HEC-RAS model used in this research is to understand the hydraulic properties in the Porong River. To achieve this objective, the HEC-RAS model with the quasi unsteady flow and the sediment transport was utilized. The results obtained from the HEC-RAS, such as the river width, flow depth, and average flow velocity, are therefore necessary for the sediment propagation model. There are three main inputs for the HEC-RAS simulation. They are: geometric data, quasi unsteady flow data, and sediment data. The geometric data were obtained from the study reach characteristics with a plan view of the Porong River as in **Figure 44.**

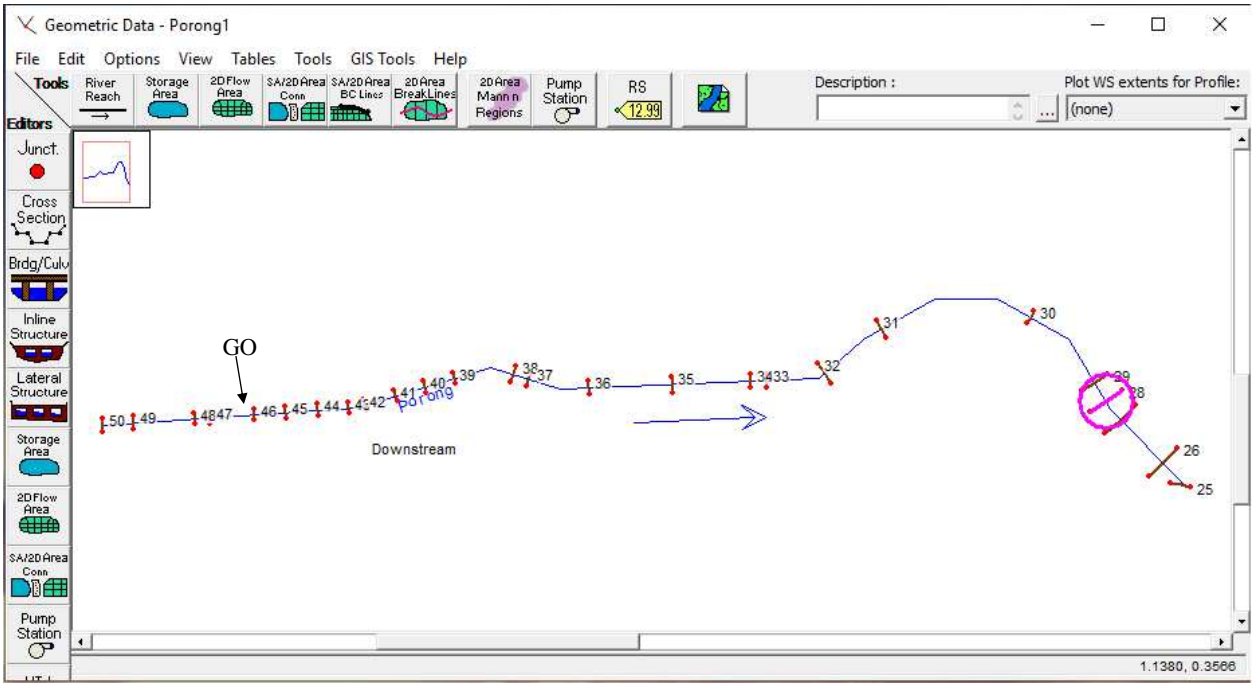

Figure 44 *Plan view of the study reach in HEC-RAS (GO is Ginonjo Outlet)*

The cross-section in the study reach are featured in **Figure 45**. We analyzed 26 cross-sections throughout the study reach. The Ginonjo Outlet is located just upstream of KP 168 (or cross-section 46) in HEC-RAS and there are 4 cross-sections upstream of the outlet. The bed slope of the study

reach is 28 cm/km. A Manning's coefficient n of 0.030 was selected for the first 6 km of the reach (until KP 186 or cross-section 37) where there was an excavated channel with some sand deposit and weeds. Beyond that cross-section, the n of 0.035 was used for natural major streams (Chow, 1959).

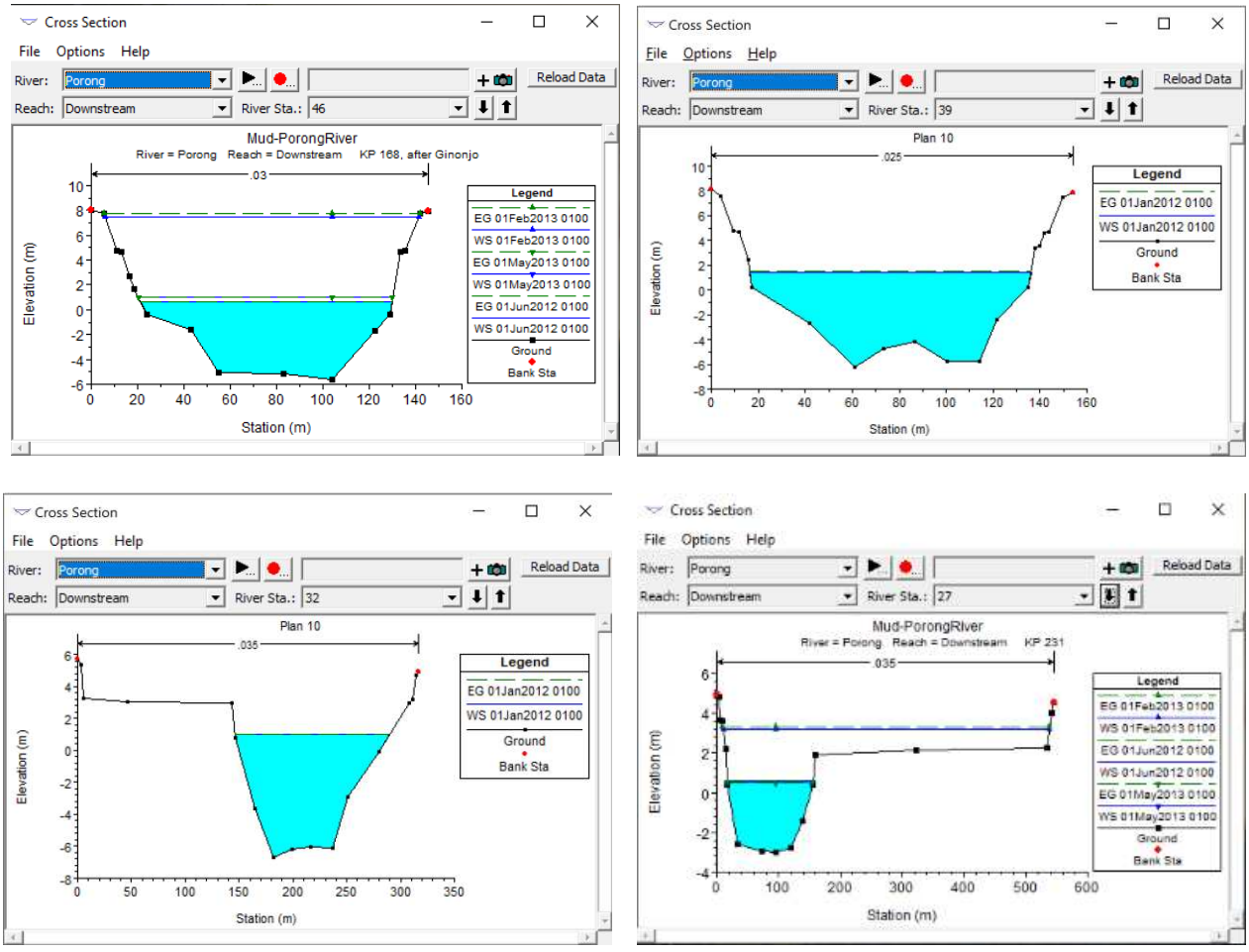

Figure 45 *The cross-sections of the study reach*

The quasi unsteady flow data used a flow series as shown in **Figure 46**. It was based on the hydrograph data of Porong River from January 2012 to December 2016 in **Figure 21**. The tides

prediction data (Geospatial Information Agency, 2019) were used for the downstream boundary condition as shown in **Figure 47** with 0.0 m indicates the mean sea level.

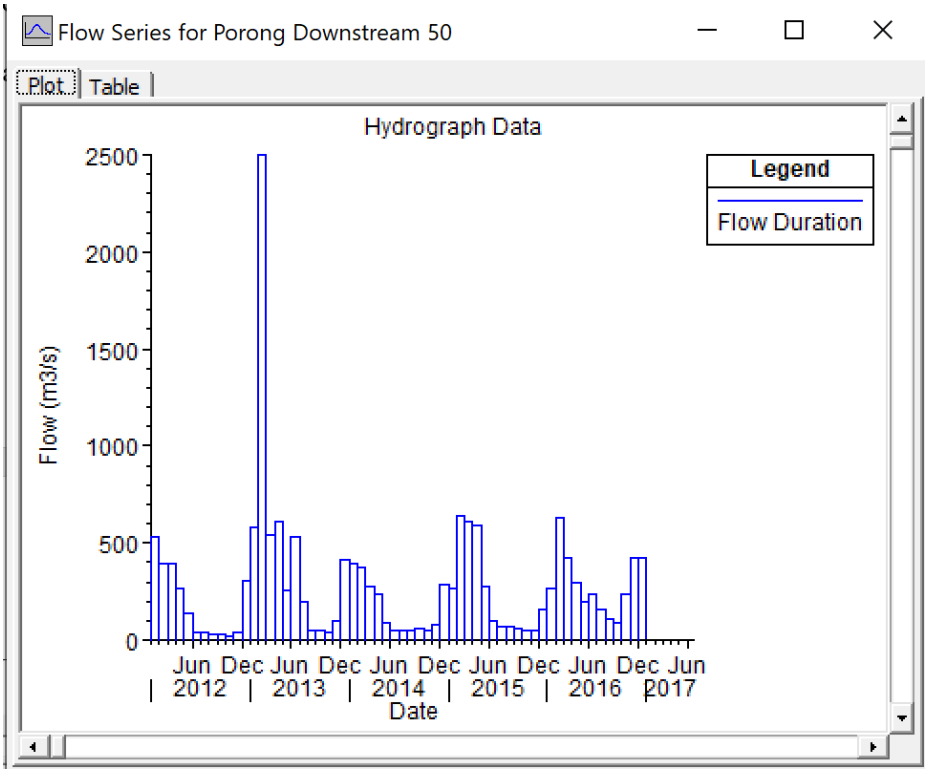

Figure 46 *Flow series of the study reach for 2012-2016*

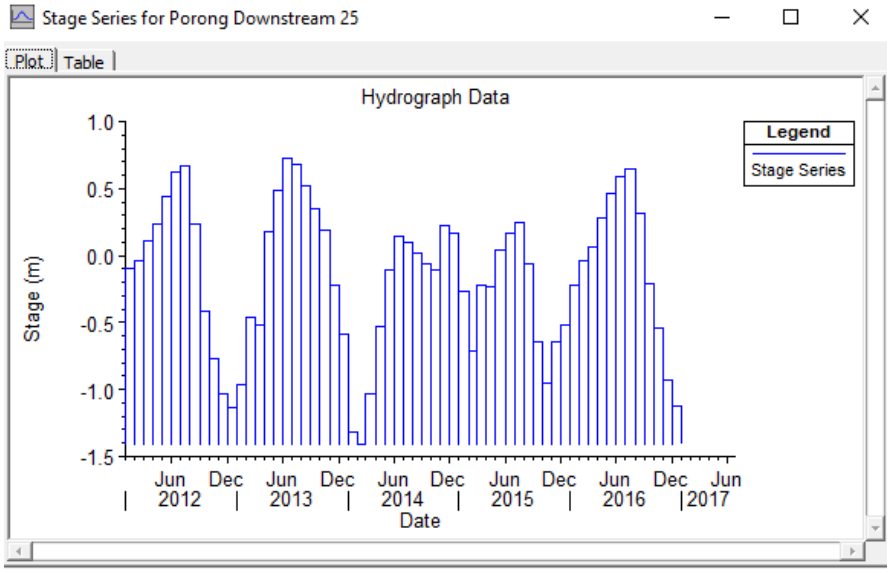

Figure 47 *Tides in Madura Strait*

The sediment data for HEC-RAS simulation is presented in **Figure 48** with Bed2 in **Figure 25** as the bed material. The maximum depth of degradation of the cross-section 50 to 47 were set at 0 because of the presence of scour protection structure just before cross-section 46. It maintains the bed level of the upstream reach. The simulation was done for 5 years, from January 2012 to December 2016.

Sediment Data - porongsediment4

File Options View Help

Initial Conditions and Transport Parameters | Boundary Conditions | USDA-ARS Bank Stability and Toe Erosion Model (BSTEM) (Beta)

River: (All Rivers) Transport Function: Toffaleti Define/Edit Bed Gradation ...

Reach: Sorting Method: Thomas (Ex5)

Number of mobile bed channels: 1 Fall Velocity Method: Report 12 Define Layers...

	River	Reach	RS	Invert	Max Depth	Min Elev	Left Sta	Right Sta	Bed Gradation
1	Porong	Downstream	50	-2.276	0		0	160.72	Bed2
2	Porong	Downstream	49	-2.519	0		0	173.35	Bed2
3	Porong	Downstream	48	-2.811	0		0	148.51	Bed2
4	Porong	Downstream	47	-1.799	0		0	147.16	Bed2
5	Porong	Downstream	46	-5.622	10		0	145.75	Bed2
6	Porong	Downstream	45	-5.592	10		0	146.43	Bed2
7	Porong	Downstream	44	-5.795	10		0	146.54	Bed2
8	Porong	Downstream	43	-2.105	10		0	147.41	Bed2
9	Porong	Downstream	42	-3.2211	10		0	150.35	Bed2
10	Porong	Downstream	41	-5.975	10		0	153.92	Bed2
11	Porong	Downstream	40	-6.752	10		0	151.63	Bed2
12	Porong	Downstream	39	-6.252	10		0	154.08	Bed2
13	Porong	Downstream	38	-2.281	10		0	213.04	Bed2
14	Porong	Downstream	37	-7.208	10		0	175.22	Bed2
15	Porong	Downstream	36	-6.311	10		0	177.03	Bed2
16	Porong	Downstream	35	-6.12	10		0	206.59	Bed2
17	Porong	Downstream	34	-5.374	10		0	169.03	Bed2
18	Porong	Downstream	33	-6.174	10		0	170.54	Bed2
19	Porong	Downstream	32	-6.694	10		0	317.03	Bed2
20	Porong	Downstream	31	-6.661	10		0	250.72	Bed2
21	Porong	Downstream	30	-6.722	10		0	181.57	Bed2
22	Porong	Downstream	29	-2.101	10		0	388.91	Bed2
23	Porong	Downstream	28	-5.859	10		0	489.29	Bed2
24	Porong	Downstream	27	-3.019	10		0	545.23	Bed2
25	Porong	Downstream	26	-6.456	10		0	505.25	Bed2
26	Porong	Downstream	25	-3.886	10		0	257.26	Bed2

Use Banks for Extents | Interpolate Gradations

Figure 48 *The sediment data of HEC-RAS simulation*

The results of the HEC-RAS are shown in **Figure 49**. It shows the bed elevation changes and water surface elevation in longitudinal plane for 4 different dates: (a) January 1, 2012, as the initial condition; (b) June 1, 2012, for the low flow condition; (c) Feb 1, 2013, for the high flow condition; and (d) May 1, 2013, for the medium flow condition. Aggradation was spotted in the first km from the Ginonjo Outlet (GO) while degradation was spotted at approximately 1.5 km and at the downstream end of the study reach. At cross-section 46, there were about 4 m of aggradation over 5 years due to the sedimentation of coarse sediment. There were no significant change in the bed elevation for cross-section 39 and 32. At cross-section 27, high degradation was spotted only at the first day. **Appendix C** presents the sediment time series for 4 cross-sections.

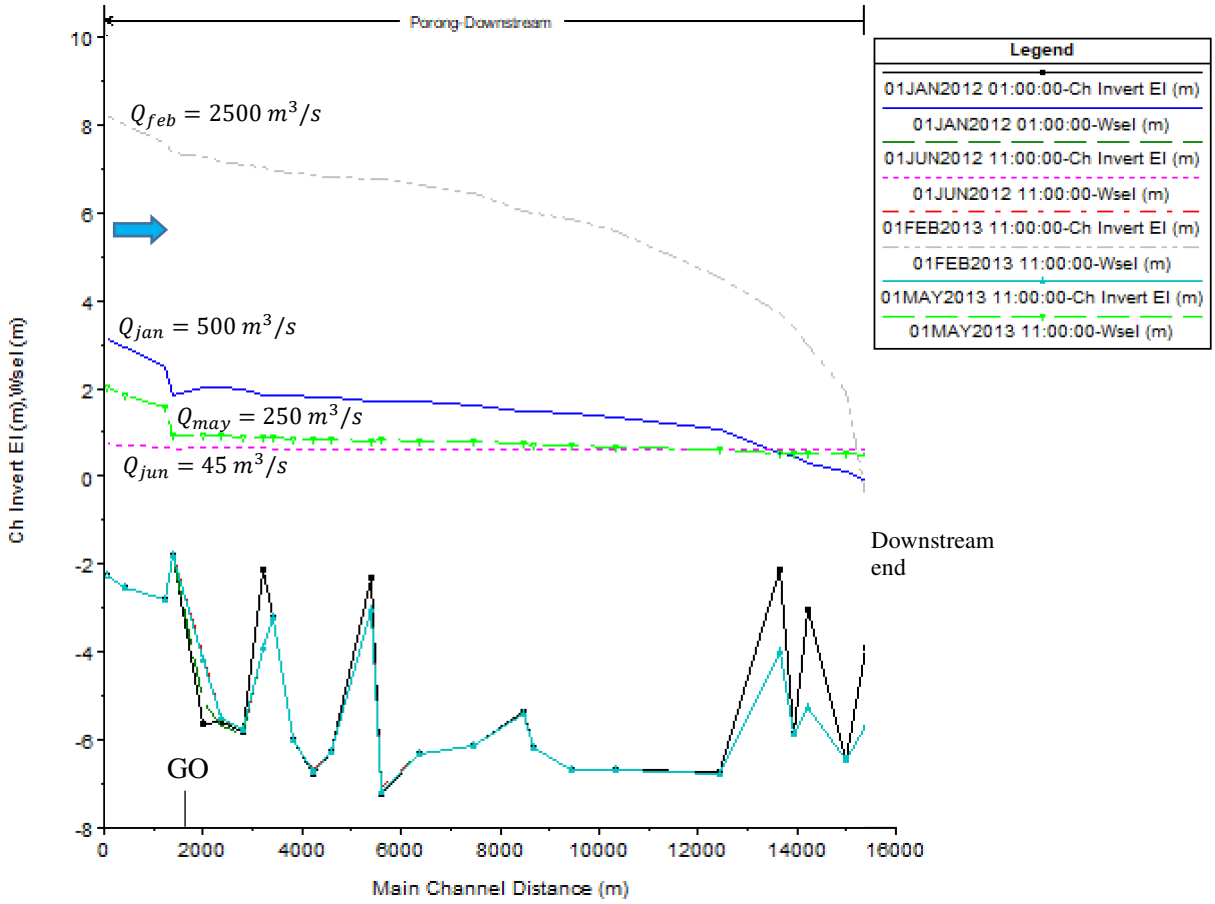

Figure 49 *The water surface elevation of the study reach from HEC-RAS simulation (➡ indicates flow direction and GO is Ginonjo Outlet)*

6.2 Two-Dimensional Mixing Model

Results from HEC-RAS simulation such as the hydraulic properties of the Porong River are used to solve the advection-diffusion equation. **Table 10** summaries the first order approximation of the coefficient, length and time scale of longitudinal dispersion, vertical and transversal mixing of the Porong River.

Table 10 *Summary of the coefficitent, length and time scale of longitudinal dispersion, vertical and transversal mixing of the Porong River*

	K_d (m^2/s)	ε_v (m^2/s)	ε_t (m^2/s)	X_d (m)	X_v (m)	X_t (m)	t_d (s)	t_v (s)	t_t (s)
Low Flow	85	0.02	0.20	1,420	43	3,920	11,800	355	32,660
Medium Flow	95	0.03	0.23	300	240	19,260	460	370	30,100
High Flow	330	0.09	0.80	290	1,200	29,250	145	560	13,600

As described in the site description, the Ginonjo Outlet is located in the left bank with 57,000 mg/l sediment concentration of the diverted mud. This corresponds to 0.02 concentration by volume C_v. Theoretically, the sediment concentration should be high near the left bank because it is close to the outlet and should be low at the right bank of the river. This phenomena should be found in the first couple km of the reach, or before the diverted mud becomes fully-mixed. The fully-mixed sediment concentration C_b was calculated by using Equation 24. Assume a low flow condition of the Porong River of 45 m^3/s, initial sediment concentration was 56.7 mg/l, the discharge of the diverted mud from Ginonjo outlet was 0.33 m^3/s and the sediment concentration of the diverted mud was 57,000 mg/l. Thus:

$$C_b = \frac{C_{outlet} \times Q_{outlet} + C_{river} \times Q_{river}}{Q_{outlet} + Q_{river}} = \frac{57{,}000 \times 0.33 + 56.7 \times 45}{(0.33 + 45)} = 470\ mg/l$$

The fully-mixed sediment concentration C_b for low flow condition was 470 mg/l. With the same parameters except for the river's discharge, the medium flow ($Q = 250\ m^3/s$) and high flow ($Q =$

$2500\ m^3/s$) would have the fully-mixed sediment concentration C_b of 130 mg/l and 64 mg/l, respectively.

To elaborate this phenomena, it is important to recall Equation 22 and 23 for the two-dimensional model without settling. These equations calculates the sediment concentration variability in x and y direction.

$$\frac{C}{C_b} = \frac{1}{\sqrt{4\pi x'}} \sum_{n=-\infty}^{\infty} \left\{ \exp\left[-\frac{(y' - 2n - y_0')^2}{4x'} \right] + \exp\left[-\frac{(y' - 2n + y_0')^2}{4x'} \right] \right\}$$

$$C_b = \frac{\dot{m}}{UhW} \quad x' = \frac{x\varepsilon_t}{UW^2} \quad y' = \frac{y}{W} \quad y_0' = \frac{y_0}{W}$$

Because the diversion outlet is located on the left bank, then $y_0' = 0$. The y', or y/W, for the left bank, centerline and right bank is $0, 0.5,$ and 1, respectively. For n value, we would use $\pm 4, \pm 3, \pm 2, \pm 1,$ and 0 to accurately model the sediment propagation in Porong River. Applying those value in our study reach, we found a sediment propagation in Porong River such as **Figure 50** for low flow, medium flow and high flow. These prediction were completed for the left bank line ($y' = 0$), centerline ($y' = 0.5$) and right bank ($y' = 1$).

The expected trends of all 3 flow conditions would be: at the start of study reach (the location of diversion outlet), the sediment concentration at left bank would be very high and the concentration at the centerline and right bank would be 0. As sediment propagates through the reach, it would be mixed transversally and longitudinally, causing the sediment concentration at the left bank to decrease gradually while the concentration at the centerline and right bank would increase. Eventually, the diverted mud would be fully-mixed and the sediment concentration would be the same across one cross-section (third stage of the mixing processes). The low flow, medium flow, and high flow conditions would have a fully-mixed mud at 4 km, 19 km, and 29 km, respectively. Thus, by the end of the Porong River, the diverted mud would be fully-mixed laterally in low flow

and medium flow conditions. However, lateral mixing would not be done along Porong River in high flow condition. Because the required reach for high flow condition was 7 times longer than the required for low flow condition.

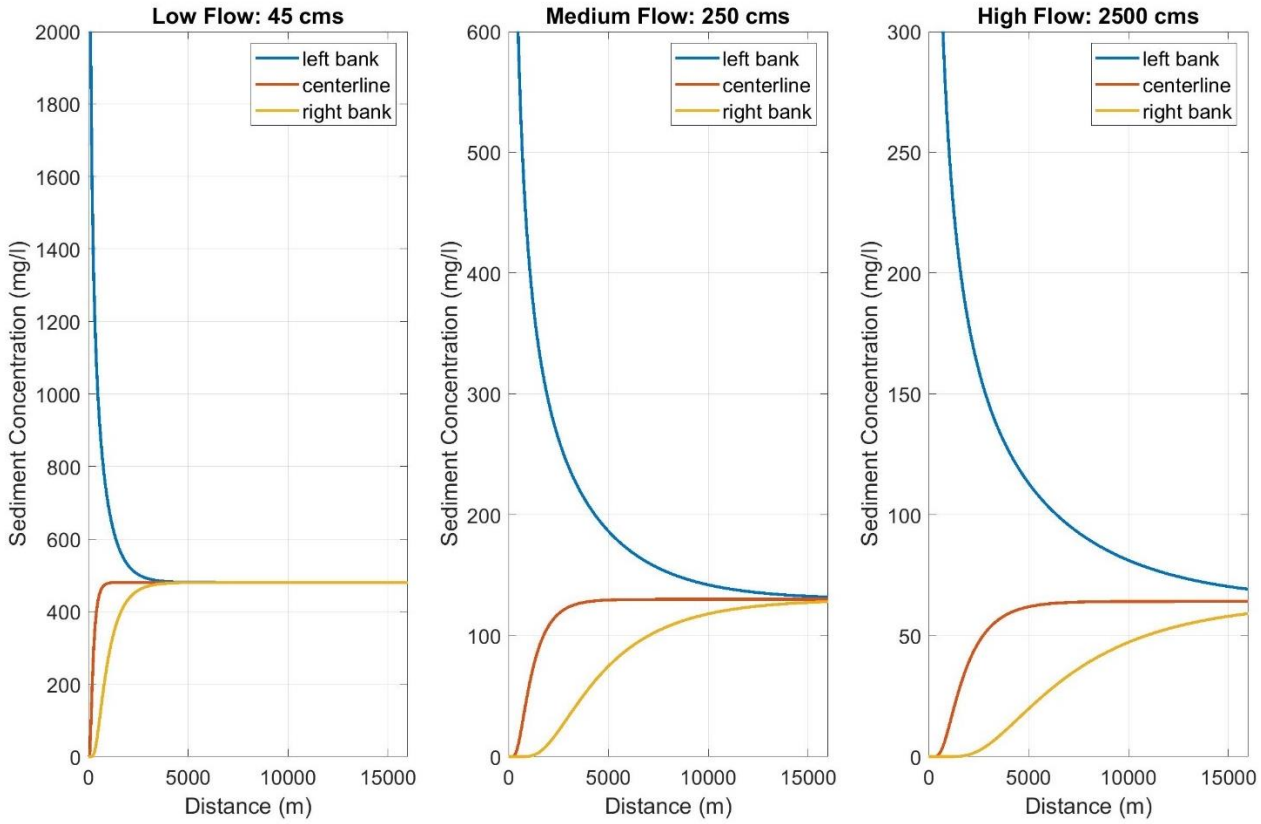

Figure 50 *Expected sediment propagation in left bank, centerline and right bank in Porong River for three flow conditions*

We used this model to predict the sediment concentration at certain distance (one cross-section) for different flow condition. In **Figure 51**, the expected sediment concentration at 5 km, 10 km and 15 km downstream from the Ginonjo Outlet for low flow (blue line), medium flow (red line) and high flow condition (orange line) is presented. The x-axis was the y' or y/W, which was the y-coordinate over river width. The left bank was indicated by $y' = 0$ and the right bank was indicated by $y' = 1$. The y-axis was the normalized sediment concentration, which was the

sediment concentration over the fully-mixed sediment concentration C_b. The normalized sediment concentration was used because there is a significant diffirence between the the fully-mixed sediment concentration C_b for low flow (480 mg/l), medium flow (130 mg/l) and high flow (64 mg/l). These differences would enlarge the scale of y-axis. Therefore, the dynamics of sediment concentration could not be captured without the normalized sediment concentration.

The top graph showed the expected sediment concentration at 5 km downstream of the Ginonjo Outlet. At this location, the fully-mixed sediment concentration had been achieved along the cross-section at the low flow condition. However, the fully-mixed sediment concentrations for the medium and high flow were only achieved at the centerline. The sediment concentration at the left bank were as much as 1.4 times C_b for medium flow and 1.7 times C_b for high flow. At the right bank, the sediment concentration were as low as 0.6 times C_b for medium flow and 0.3 times C_b for high flow. The same pattern was also observed for the cross-section at 10 km and 15 km, but with smaller range of sediment concentration between left bank and right bank. At the 10 km, the range of sediment concentration for medium flow was 0.9 – 1.1 times C_b and for high flow was 0.73 – 1.27 times C_b. Meanwhile, at 15 km, the range was 0.98 – 1.02 times C_b for medium flow and 0.9 – 1.1 times C_b for high flow. The author expected to have a same pattern of sediment concentration across all cross-section with high discharge condition. It would have a larger difference of sediment concentration between left bank and right bank.

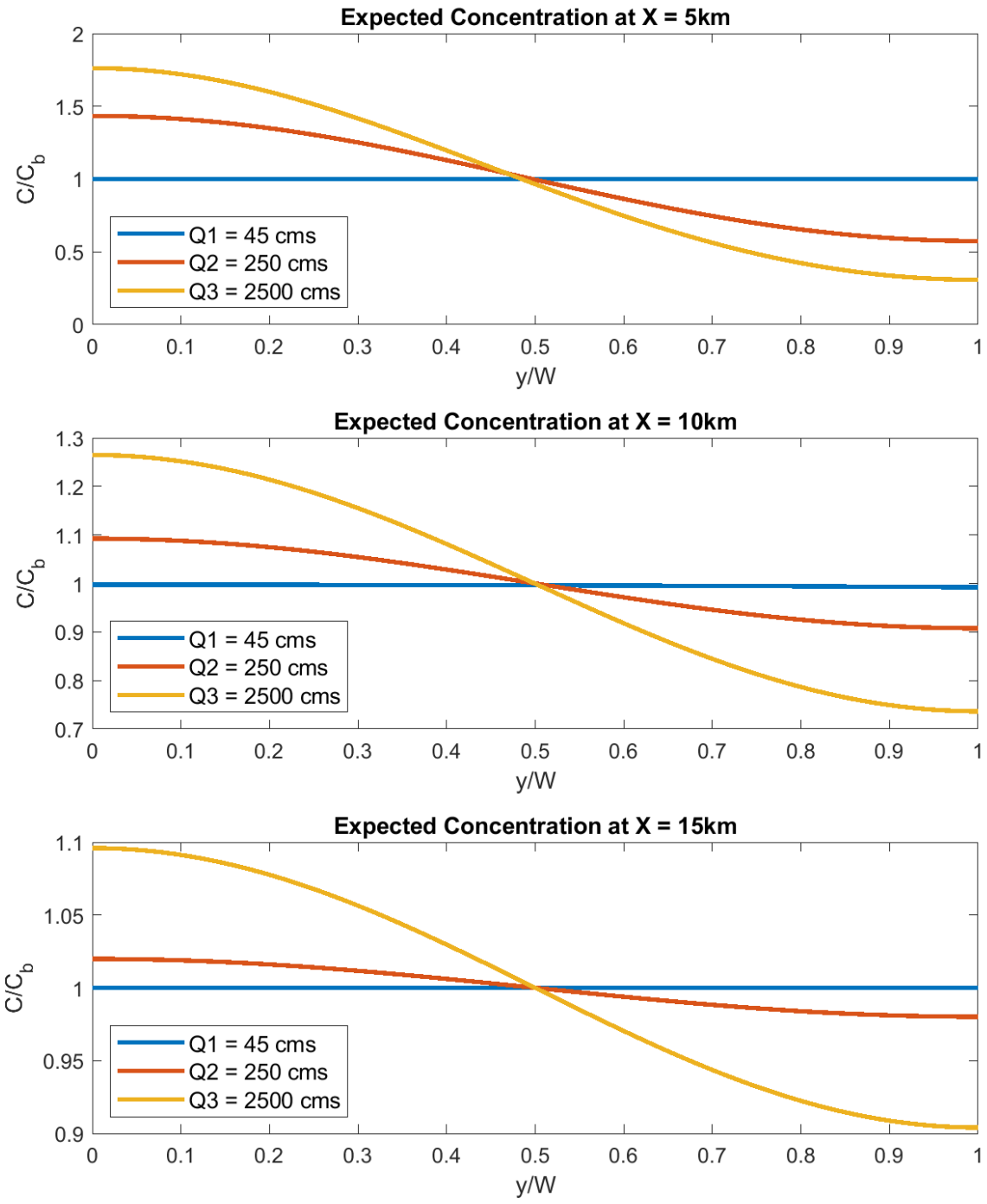

Figure 51 *Expected sediment concentration at 5km, 10 km and 15 km in Poromg River for three flow conditions*

Another way to look at the sediment propagation in Porong River is by presenting it as a surface graph. In this graph, the reach is divided into 2 subreaches: Subreach 1 and Subreach 2. Subreach 1 represents the sediment concentration from 0 to 100 m downstream from the Ginonjo Outlet and

Subreach 2 represents the concentration from 100 m to the downstream end of the Porong River. For the subreach 1 as presented in **Figure 52**, the trend of sediment propagation across the three flow conditions was same, which they had a high sediment concentration at left bank and low concentration at the right bank.

Because low flow condition has a low velocity, the diverted mud has more time to mix transversally. This caused the concentration at 100 m downstream from the outlet at the left bank side to decrease to about 2,000 mg/l, which equaled 3.5% of the initial concentration by the diverted mud. The sediment concentration at the right bank side was 57 mg/l because the mud had not reached that side. For medium flow, the sediment concentration at 100 m downstream from the outlet at the left bank side was 800 mg/l, which equaled to 1.3% of the initial sediment concentration. In the high flow condition, the sediment concentration at 100 m downstream from the outlet at the left bank side was 150 mg/l, which was 0.2% of the initial concentration. We could see that in the high flow condition, the sediment concentration at 100 m decrease 20 times more dramatically than in low flow condition.

For the subreach 2 as depicted in **Figure 53**, the trend of sediment concentration in low flow condition was different than the trend in medium and high flow condition. In low flow condition, the diverted mud had fully-mixed transversally 4 km downstream from the outlet, which allowed for a relatively identical sediment concentration in a cross-section beyond that point. The added sediment concentration at 100 m downstream from the outlet was 2,000 mg/l and by the downstream end of the Porong River was 475 mg/l. This means that there was a 76% loss of sediment concentration in Subreach 2 for low flow condition. Meanwhile, medium flow and high flow had a length scale of transversal mixing of 19 km and 29 km, respectively. These means that a gradual reduction of sediment concentration was found moving downstream and laterally to the

right bank in one cross-section, until the required length scale of transversal mixing have achieved. At the mouth of Porong River, the sediment concentrations were 130 mg/l and 65 mg/l for the medium and high flow, respectively. There were 84% (from 800 mg/l) and 57% (from 150 mg/l) loss in sediment concentration in subreach 2 for medium and high flow conditions, respectively.

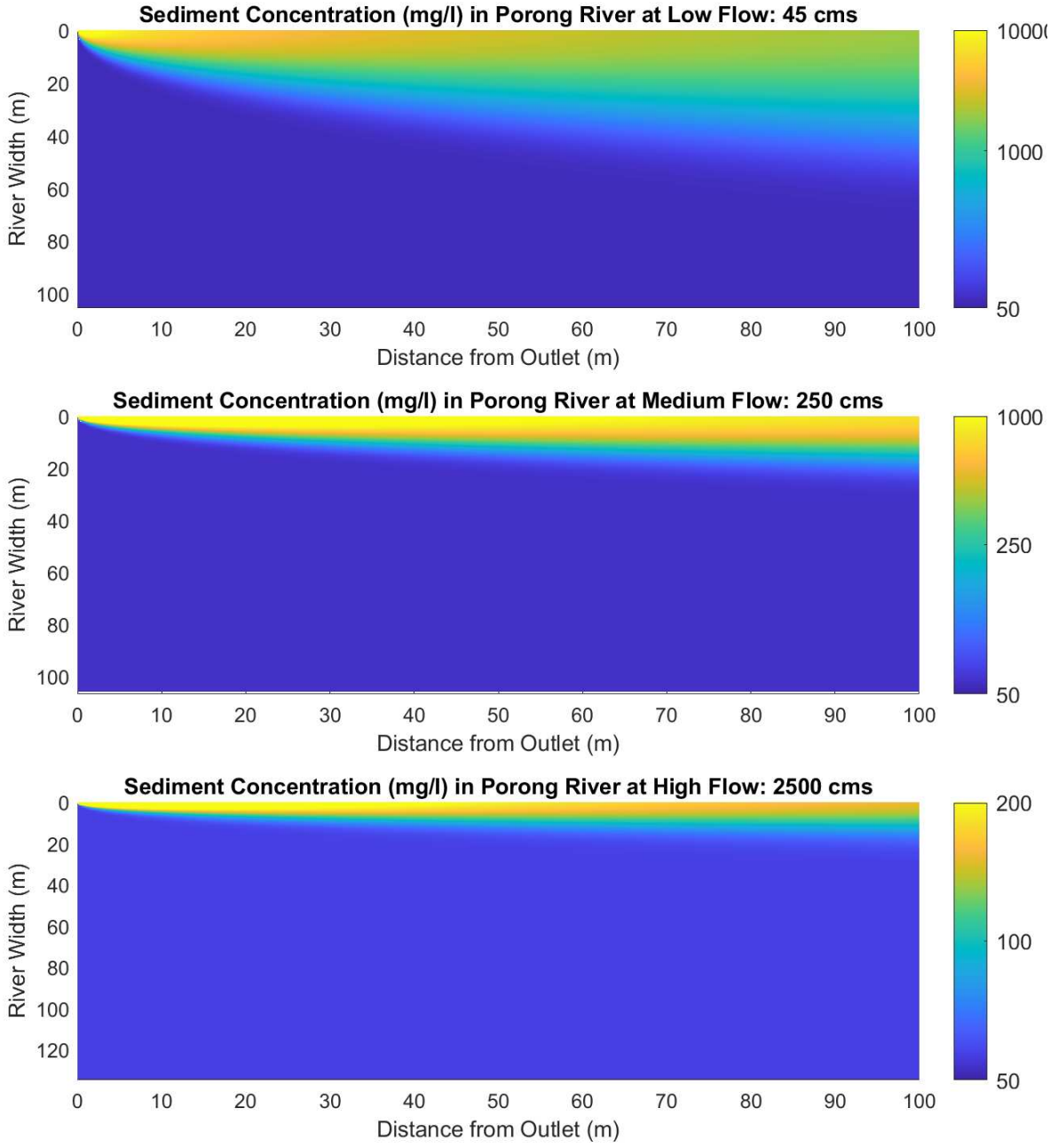

Figure 52 *Two-dimensional model without settling in the first 100 m of study reach for 3 flow conditions*

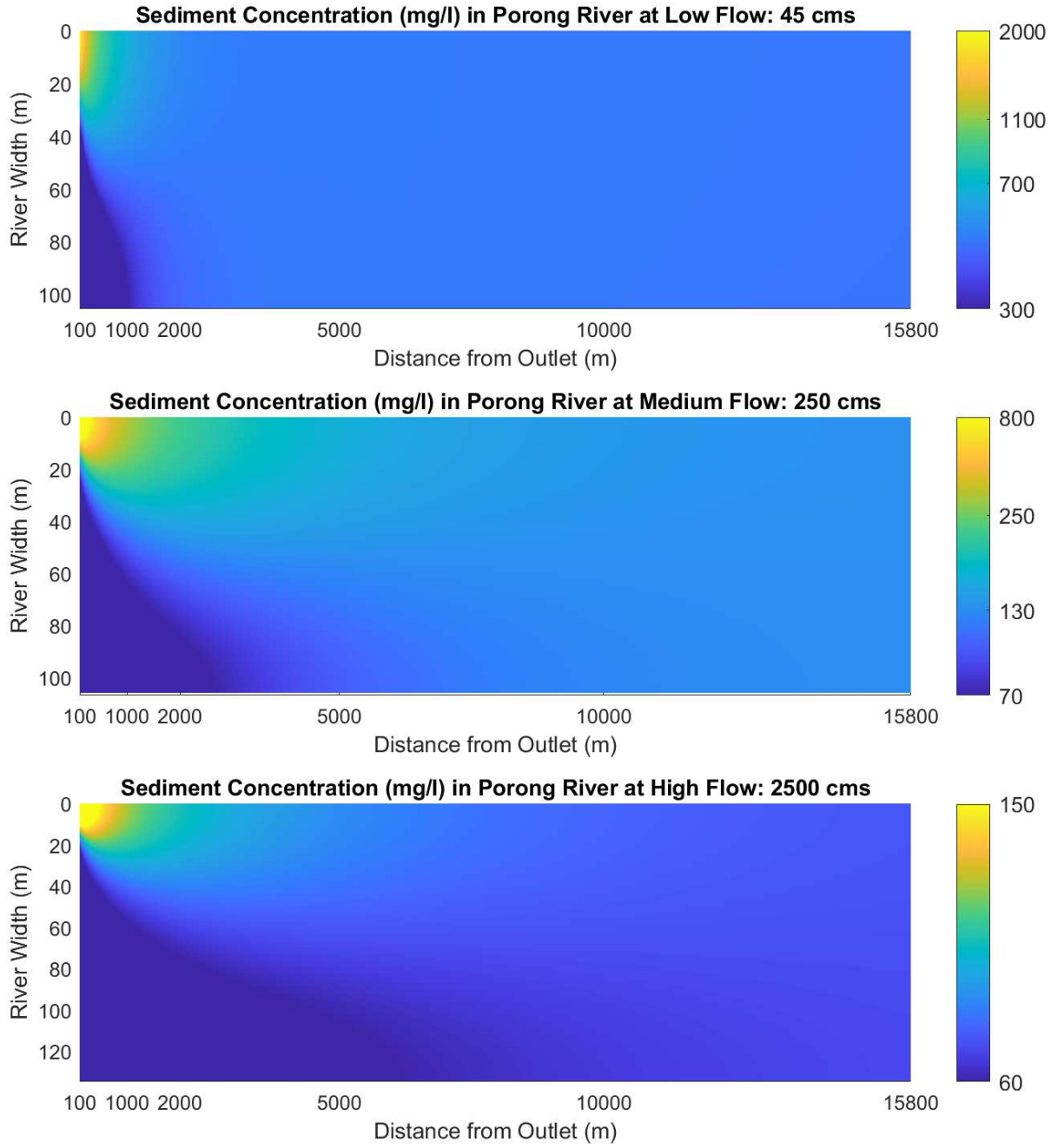

Figure 53 *Two-dimensional model without settling from 100 m to 15800 m of study reach for 3 flow conditions*

This line graph in **Figure 54** indicates sediment propagation along the Porong River for lines A, B, C, and D based on the two-dimensional model without settling. The graph includes the observed sediment concentration of line A to D. The sediment concentration at point 0, or just before the diversion outlet was assumed 0 for all lines. The concentration increased after the diversion as discussed in the previous chapter. According to this model, the concentration should reach equilibrium around 4 km downstream from the point source with an average concentration of 470 mg/l. However, the observed sediment concentration from field measurements after 4 km downstream from the Ginonjo Outlet was 90 mg/l. There was a 380 mg/l of difference in the sediment concentration between the model results and the field measurements. This was most likely due to sedimentation in the first 4 km of the study reach. Sediment settling of these fine fractions therefore needs to be considered.

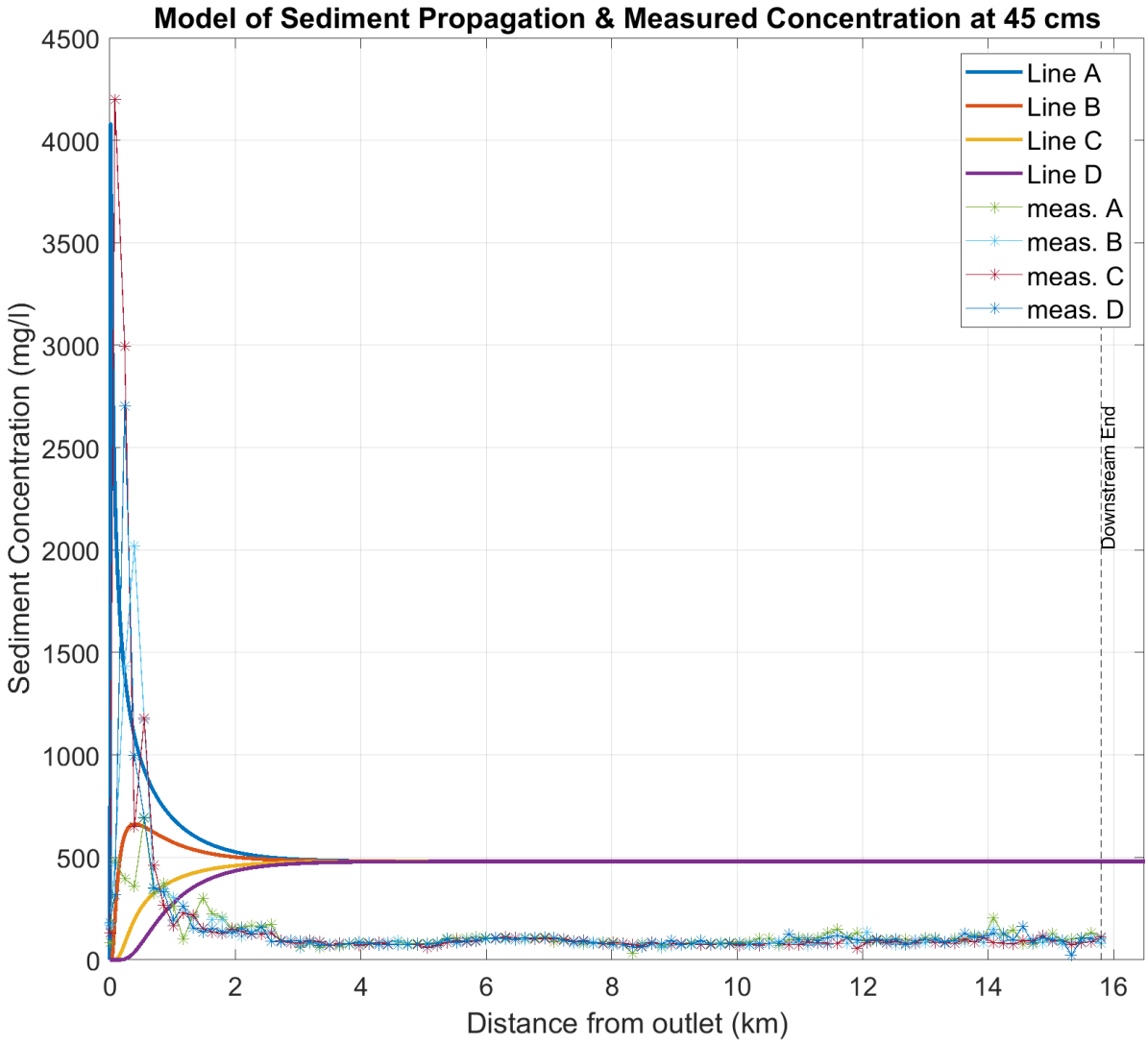

Figure 54 *Sediment propagation model without settling (Line A-D) and the field measurements (meas.)*

6.3 Two-Dimensional Mixing and Settling Model without Flocculation

Based on the analysis of the mud properties, it is clear that the diverted mud had a tendency to flocculate and settle. In this case, the two-dimensional mixing model with finite width was not adequate to predict the sediment propagation in the Porong River. Therefore, this research added the settling factor into the two-dimensional mixing model. The settling factor comes from the solution of advection-diffusion with nonconservative substance, which is:

$$e^{-k_i t_{j+1}} = \frac{C_{i,j+1}}{C_{i,j}}$$

The $C_{i,j+1}$ is the sediment concentration of fraction i at location $j+1$, the $C_{i,j}$ is the sediment concentration of fraction i at location j, the settling rate of fraction i, $k_i = \omega_i/h$, where ω_i is the settling velocity of the fraction i and h is the flow depth. The time t can be defined as X/U, where X is the river length and U is the flow velocity.

Recall the two-dimensional mixing equation for finite width for equation at point j:

$$C_j = C_b \left(\frac{1}{\sqrt{4\pi x_j'}} \sum_{n=-\infty}^{\infty} \left\{ \exp\left[-\frac{(y' - 2n - y_0')^2}{4x_j'} \right] + \exp\left[-\frac{(y' - 2n + y_0')^2}{4x_j'} \right] \right\} \right)$$

If we substitute the sediment concentration at point j, C_j, from the two-dimensional mixing equation into the settling factor, we get:

$$C_{i,j+1} = C_{b,i} e^{-k_i t_{j+1}} \left(\frac{1}{\sqrt{4\pi x_j'}} \sum_{n=-\infty}^{\infty} \left\{ \exp\left[-\frac{(y' - 2n - y_0')^2}{4x_j'} \right] + \exp\left[-\frac{(y' - 2n + y_0')^2}{4x_j'} \right] \right\} \right)$$

By utilizing this equation into our study, we can determine the sediment propagation in the Porong River. Noted that the research computed the sediment concentration for every size fraction from

the particle size distribution to get a better understanding of the settled and unsettled portion of the diverted mud. The total suspended sediment concentration is:

$$C = \sum \Delta p_i C_i$$

where Δp_i is the relative weight of fraction i and C_i is the suspended sediment concentration for fraction *i.*

The result of the model for Line A, the closest to the outlet, was compared to the maximum, mean, and minimum values of the measured concentration as presented in **Figure 55**. However, the measured concentration did not agree with the result from the model. The total sediment concentration from the model at the downstream end of the Porong River was about 195 mg/l as indicated by the cyan line. All of the big sediments, from 4.75 mm to 75 μm, settled at the first 200 m of the Porong River. The fraction of 13 μm and 10 μm mostly settled before 4 km of the Porong River. The fraction of 7 μm and 5 μm mostly settled around 7 km and 15 km, respectively. Only the fraction of 4 μm, 3 μm, and 1 μm were in suspension util the downstream end of the Porong River with concentration of 17 mg/l, 60 mg/l and 108 mg/l, respectively. Note that 8% of the total sediment was the clay fraction. About half of the suspended fractions flocculated and settled in the first 4 km.

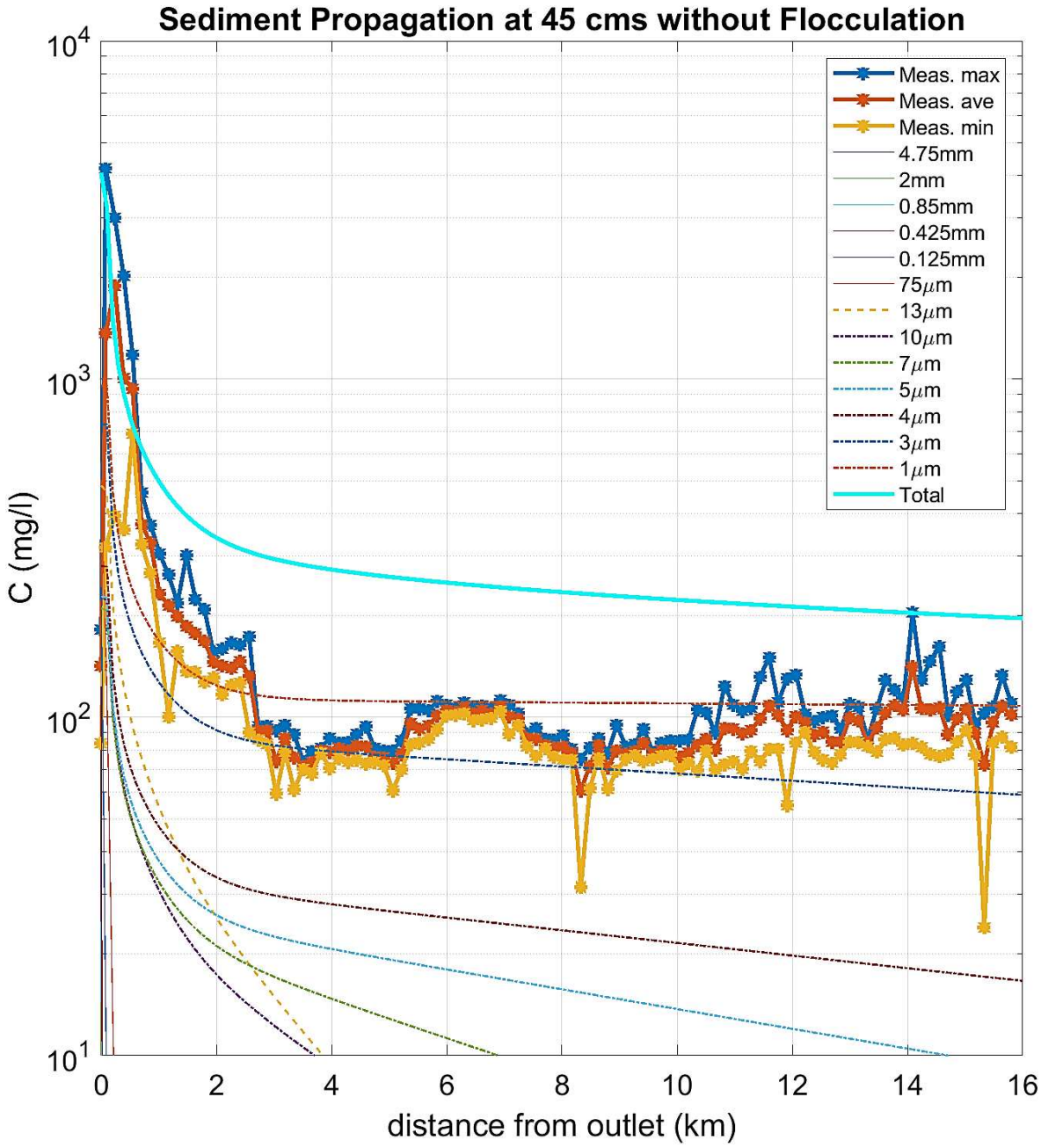

Figure 55 *The result from suspended sediment propagation model by size fraction at low flow (45 m^3/s) without flocculation for Line A compared to the measurement data*

6.4 Two-Dimensional Mixing and Settling Model with Flocculation

The model was advanced by adding the concept of flocculation. The result of the flocculation experiment showed that the diverted mud have a slight tendency to flocculate. Hence, another class of sediment was added to the particle size distribution of the diverted mud as the input for the two-dimenstional mixing and settling model with flocculation. The new class was called floc with the flocculated settling velocity (mm/s) and the floc size (mm) as follows:

$$\omega_f = \frac{250}{d_s^2}\omega$$

$$\omega_f = 10 d_{flocc}^{1.5}$$

where d_s is the particle size in microns and ω is the settling velocity of disperse particles in mm/s. **Figure 56** presents the result of the two-dimensional mixing and settling model with flocculation. At the downstream end of the study reach, the total sediment concentration at the left bank of the Porong River was 90 mg/l as indicated by the black line. It matches the observed data very well, which was between 80 to 100 mg/l . The gravel and sand fractions settled in the first 300 m of the Porong River. The silt fractions of 13 μm and 10 μm mostly settled around 10 km of the Porong River. Meanwhile, some fractions of 7 μm, 5 μm and 4 μm were still in suspension until the end of the study reach. The fractions of 3 μm and 1 μm were the only significant fractions in suspension at the downstream end of the Porong River with concentrations of 24 mg/l and 54 mg/l, respectively.

Table 11 shows the result of the mixing model with settling but in more detail. Column 3 shows the weight of fraction per class. The class with the highest weight was the floc class (92 μm) with about 38% and followed by fraction of 75 μm with 12%. About 50% of the sediment has a similar

size with fine sand due to flocculation. Meanwhile, the clay fraction had been reduced to about 22% of the total sediment.

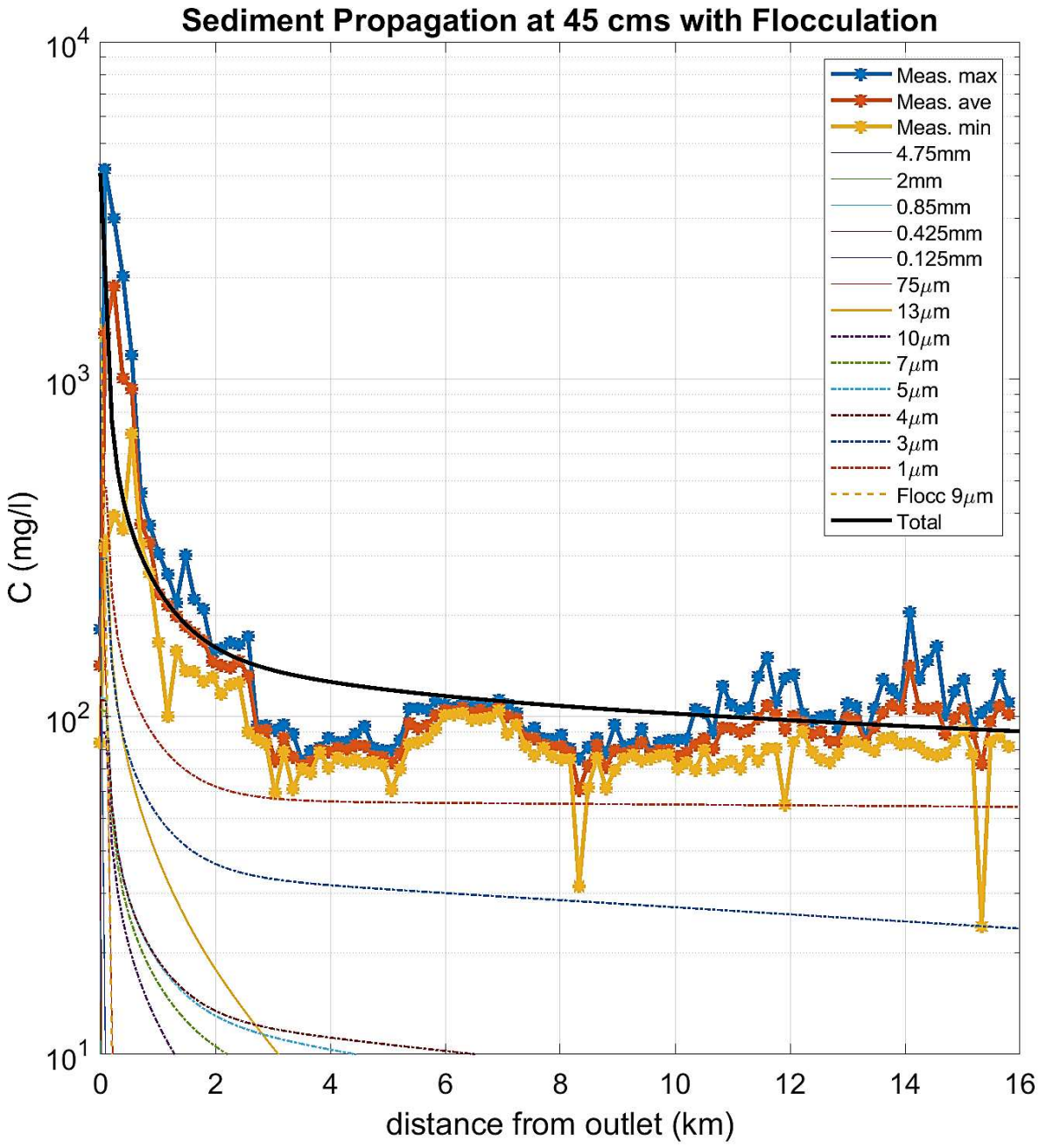

Figure 56 *The result from suspended sediment propagation model by size fraction at low flow (45 m^3/s) without flocculation for Line A compared to the measurement data*

Table 11 *The classes of the diverted mud with its parameter and sediment concentration at certain distance from the Ginonjo Outlet*

Class	d_s (mm)	dP_i (%)	ω (m/s)	k (1/s)	C (mg/l) at X (m) =									
					0	**100**	**300**	**500**	**1000**	**3000**	**5000**	**10000**	**15000**	**15800**
1	4.75	0.9%	0.26	0.075	39	0	0	0	0	0	0	0	0	0
2	2	0.6%	0.17	0.048	23	0	0	0	0	0	0	0	0	0
3	0.85	0.6%	0.10	0.030	25	0	0	0	0	0	0	0	0	0
4	0.425	3.0%	0.06	0.019	123	0	0	0	0	0	0	0	0	0
5	0.125	6.0%	0.02	0.004	243	6	0	0	0	0	0	0	0	0
6	0.075	12.4%	0.01	0.002	505	117	2	0	0	0	0	0	0	0
7	0.013	8.3%	1.9E-04	5.5E-05	339	324	107	71	38	10	4	0	0	0
8	0.01	2.2%	1.1E-04	3.2E-05	91	89	30	21	12	5	3	1	0	0
9	0.007	2.6%	5.5E-05	1.6E-05	105	104	36	26	16	9	6	3	2	2
10	0.005	2.8%	2.8E-05	8.1E-06	114	113	40	29	19	11	10	7	5	5
11	0.004	2.7%	1.8E-05	5.2E-06	112	112	40	29	19	12	11	9	7	7
12	0.003	7.2%	1.0E-05	2.9E-06	294	293	105	76	51	33	31	27	24	24
13	0.001	11.7%	1.1E-06	3.2E-07	478	478	172	125	84	57	56	55	54	54
14	0.092	38.9%	2.8E-04	8.1E-05	1588	183	1	0	0	0	0	0	0	0
Total	-	100%	-	-	4079	1819	535	376	240	138	120	102	92	91

As can be seen in **Figure 57**, the observed data were compared to the result from the two-dimensional mixing and settling model with and without flocculation. The observed data, the model with flocculation and the model without flocculation started at 4100 mg/l. For the most part the sediment concentration of the model without flocculation at the left bank side was twice as large as the sediment concentration of the model with flocculation, which was 90 mg/l. The sediment concentration at the centerline and the right bank side started from very low and reached their apex at 1 km with 150 mg/l and 2 km with 130 mg/l, respectively. After those point, the sediment concentration kept decreasing until it became 90 mg/l. Furthermore, the percentage of the sedimentation in the Porong River was calculatd by using the trap efficiency:

$$T_E = \frac{C_j - C_{j+1}}{C_j}$$

The percentage of settled sediment in the Porong River in the low flow condition at the left bank side was 98%, while at the centerline and the right bank side were 40% and 31%, respectively.

The presence of the mud diversion caused a higher sediment concentration in the Porong River. The additional sediment concentration was very significant at the first 4 km downstream of the diversion outlets and much lower by the end of the Porong River. Without any mud diversion, the sediment concentration would be stagnant at about 50 mg/l based on the observed sediment concentration upstream of the diversion outlets. Then, the observed data agreed with the two-dimensional mixing and settling model with flocculation. It meant that the model can be used to predict the sediment propagation in Porong River primarily because of the diversion from the mud volcano.

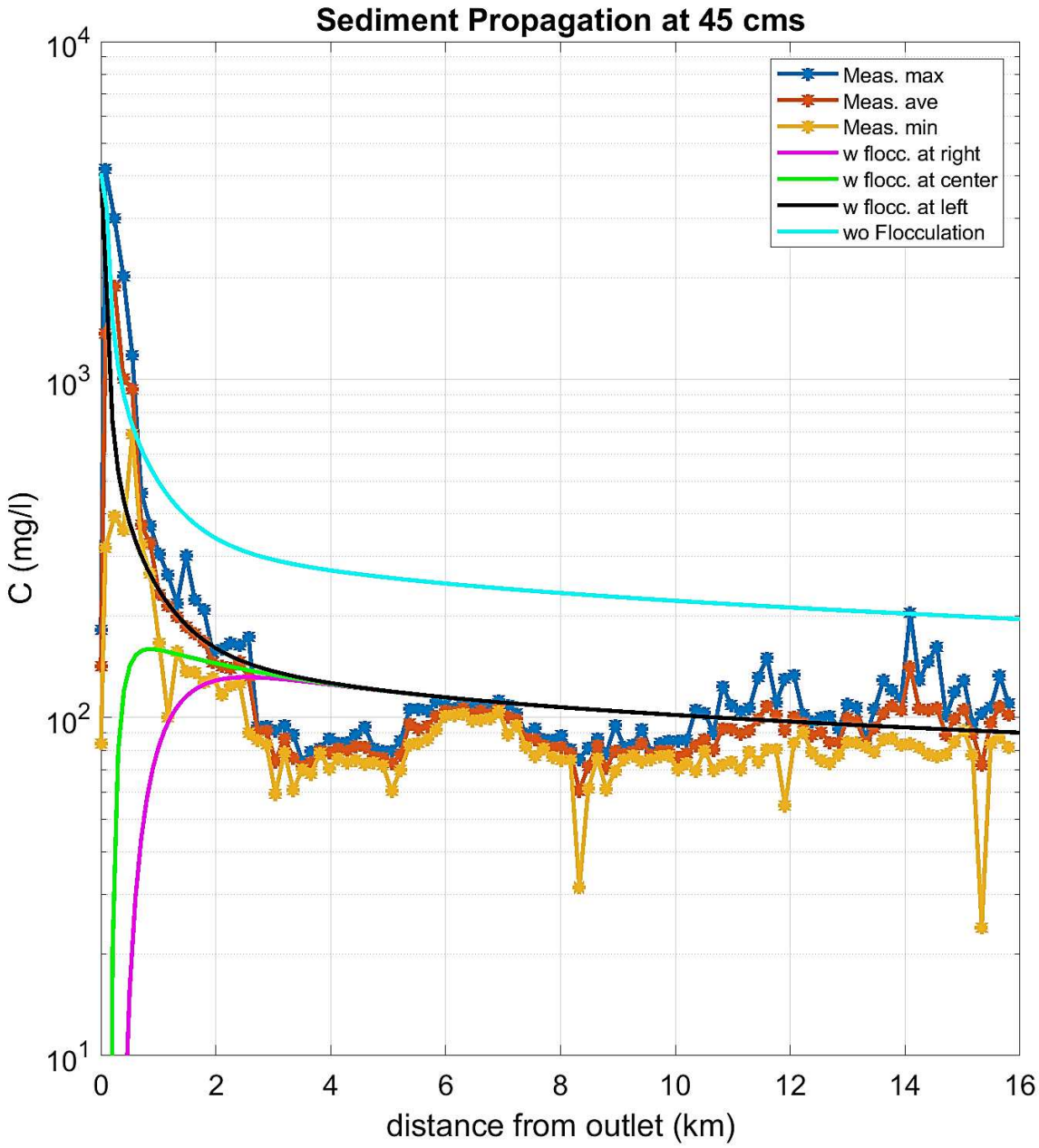

Figure 57 *Comparison of the measurement data, the result of model with flocculation at left bank, centerline, and right bank, and the model without flocculation*

CHAPTER 7 MANAGEMENT

This chapter reviews some management issues and provides recommendations regarding the disaster management of mud volcano.

7.1 Current Condition and Recommendation

7.1.1 Data availability and transparency

Historical data in water resources management field are very important. They are used to analyze and to understand a particular past event or to foresee future scenarios. For example, a comprehensive data set of river stages, discharges, cross-sections, infrastructures and ground elevation of a city can be used to model and analyze the source of a flood event in the city. The data are also useful to analyze the impact of future flood events.

One of the main problems in developing countries, particularly in Indonesia, is the data availability and accessibility. The data are hardly available due to the limited instrumentation and accessibility. Weather radars or stations are only available in urban areas. Meanwhile, a very limited number of meteorological stations is installed in the wide mountain area which force the researchers to extrapolate the data from the nearest point. It reduces the accuracy of model predictions. Moreover, the weather stations or other instruments sometimes are not properly maintained which caused an inability to record extreme events or missing some record data. One of the great values of this dissertation is the effort to collect field measurements of sediment concentration and turbidity at this site. The availability of discharge data at a national level should facilitate future hydrologic and hydraulic studies. The access to topographic data, Digital Elevation Models and LiDAR terrain data will also facilitate the future geo-spatial analysis of hydraulic and sedimentation projects. Indonesia is a large and complex archipelago with a wide variety in altitude and climatic conditions. Data transparency is another common problem in Indonesia. Because the

data are hard to collect, it becomes proprietory and difficult to access and share. At this time a researcher sometimes needs to formally send a request letter or pay a certain fee for the data. Take an example of a research of a flood control in a certain watershed. A researcher can download the rainfall data in Indonesia from the Meteorogical, Climatological, and Geophysical Agency of Indonesia (BMKG in Indonesian). However, for other data such as rating curve (river stages and discharge), the researcher needs to send a request letter to a specific river basin organization who manage the river. On the other hand, a dam structure is usually managed by other institution than the river basin organization. Thus, the researcher has to send another letter to this institution to get a record data of the dam. The request to these institutions will not be answered unless the researchers have a good background or portfolio. This complicated institutional problem should be solved to increase the effectiveness a research.

There are couple recommendations to solve or improve the data-availability and transparency problem. A national program for data collection with public access would be a tremendous asset in the future.

1. Installing a lot of new measurement instrument are essential to have a more comprehensive data. As stated before, Indonesia needa many of rainfall or weather stations and the river stations. The locations can be determine based on the long-term development plan. More importantly, the installation sites should be able to cover the the critical watershed in the water resources management plan in Indonesia. For example, the big city with high frequency of flooding, are with major drought, irrigation land, the central for food production, and the watershed of a dam structure.
2. Application of remote sensing measurement. This concept can be executed to collect a water quality data. For example: to determine the total suspended solid in a river by using

a satellite data. The satellite data can be imported into water quality data through a specific algorithm. In the early stage of the study, the result of the water quality data from the remote sensing or predicted data should be validated by the field observation data. If the deviations between the predicted data and the observed data are small, then the remote sensing is accurate and the algorithm can be used for practical purpose. Furthermore, remote sensing or remote measurement can be applied in the river monitoring field, particularly to monitor the effluent from industry.

3. Technical and engineering data can be compiled in one government institution for external request. The only access for students or researchers to collect data about the river should be the river basin organization. The data include the properties of the river, plan view, cross-sectional drawing, rating curve and the water quality data, including the dam operation plan if there is any dam structure in the river. This could accelerate the data collection step and encourage more research in water resources management or hydraulic topics.

7.1.2 Mud Diversion

Based on the 15 years of experience with the mud diversion from the Sidoardjo Mud Volcano and based on the result of the sediment propagation model, the mud diversion into the Porong River will not clog the river. Furthermore, at the current diversion rates, it will not cause a massive aggradation problem and flood to the surrounding area. The mud is dominated by fine sediment which accounted for about 86% and most of the sediment will settle at the first 4 km. The sediment deposited at low flow gets remobilized and transported to the estuary during floods. Thus, the aggradation and degradation processes will balance each other.

The observed sediment propagation in the Porong River was collected manually by using a water

sampler. The shortcomings of the manual method are the required resources, such as man-power, for the collection and the time to do the sample collection. In this research, the sample collection was completed from 8AM to 5PM in more than 3 days. The unability to collect the sample at night caused a discontinuation in observed data. To overcome this problem, a remote monitoring can be installed and the data can be downloaded for several observation days. The strength of the remote monitoring is the ability to collect a continuous data with a relatively cheaper price than the conventional method.

One problem that occurred in the current mud diversion project is the measurement of sediment concentration of the diverted mud. The sediment concentration is determined by using the a hydrometer which is very inaccurate. A more accurate method to determine the sediment concentration is by Total Suspended Solid (TSS) analysis in laboratory. A relationship between the TSS analysis and the hydrometer analysis might be established for a practical use, but a more detail research should be done regarding this relationship. One important contribution of this dissertation has been the possibility to use turbidity measurements in correlation with sediment concentration measurements. This turbidity versus concentration relationship may be helpful at other similar sites in the future.

Another problem that can occur in the mud diversion phase is the contract of mud diversion project. Due to the contract problem with the contractor, the mud diversion of the Sidoardjo Mud Volcano had to be stopped for a couple months every year. Without a mud diversion, the volume of mud inside the mud reservoir increased rapidly and endangered the stabilty of the mud reservoir. This management issue can be solved by using a multi-year contract with the contractor or the government can start the tender of the project before the end of the current project. Another solution is the government divert the mud by themselves without the

help from contractor. This method gives a flexibility to the government to determine the sediment concentration of the diverted mud. However, the government will need a skillful staff and worker to execute the diversion.

7.2 Mud Volcano Disaster Guidelines

The Sidoardjo Mud Volcano is the first mud volcano that inflicted an urban area, in this case is the Sidoardjo District. At the beginning of the eruption, the government did not have any guidelines or policies to mitigate the damage of the Sidoardjo Mud Volcano. The mitigation action was purely based on a trial and error basis with priority for human welfare. However, in order to mitigate a huge social, economic, and environmental losses due to a mud volcano disaster, a proper mitigation guidelines are essential. Thus, after decades of research regarding the growth of the Sidaordjo Mud Volcano, including this research, proper guidelines can be constructed.

The following are some proposed mud volcano disaster guidelines. Please note that the main priority for these guidelines is human welfare.

1. The first step after the mud volcano is reported should be a preliminary study, which includes the study of the characteristics of the mud volcano and the properties of the mud sediment. In this preliminary study, the chamber and the source of the extruded mud, the volume of extruded mud, the longevity of the mud volcano, and the subsidence area can be studied and predicted for the basis of the mud volcano disaster policy. The preliminary study should be finished in 2 to 3 months. In the meantime, the government can start to relocate the neighborhood in the radius of 0.5 km from the main crater.

2. The second step is securing the affected zone of the mud volcano by land acquisition and creating a mud reservoir. The affected zone include the required land for the mud reservoir, which is based on the volume prediction of the extruded mud with a sufficient embankment, and the subsidence area. The government have to complete the construction of the reservoir in 6 months. This might be hard, but the construction can be divided into several phases based on the total affected zone. The first phase is the land acquisition and constuction of the inner mud reservoir which should be done in less than 2 weeks. The second phase is for the middle reservoir which can be constructed in 2 months and the third phase is for the outer reservoir with a construction time of 3 months. The design of the mud reservoir must consider the mud flow movement inside the reservoir and the mud diversion plan. At this step, the number of refugees should be finalized as the affected zone have been implemented and the social problem should be solved.
3. The third step is initiating the mud diversion to an ocean through the nearest possible river. A feasibility study is important to look for the most effective and efficient procedure to divert the mud. The study includes the physical and chemical properties of the mud, the bathymetri of the river, the maximum allowable diverted mud into the river, the possible aggradation and degradation of the river, and the sediment transport of the river. Moreover, the sediment propagation of the diverted mud in the river should be modeled to get a better understanding about the sediment transport in the river.
4. The fourth step is river monitoring. It could be completed daily or, at least, weekly in order to maintain and prevent any future damage to the river. The monitoring includes the river discharge, the particle size distribution of the diverted mud, the sediment concentration of the diverted mud, the aggradation and degradation of the river bed, the sediment

propagation, and the sedimentation at the estuary. The weekly monitoring is important because the particle size and sediment concentration of the diverted mud are changing in daily basis.

Nowadays, many mud volcanoes are still springing up on the Java and across the globe. Sometimes, it appears inside a house but only lasts a couple of hours. However, a mud volcano similar to the Sidoardjo Mud Volcano can occur again in the future, maybe in Indonesia or elsewhere around the world. Thus, a document providing guidelines for managing mud volcanoes is urgently needed to give a better framework to mitigate the damage of a mud volcano to the human welfare.

CHAPTER 8 CONCLUSIONS

This research addresses an interesting issue in the field of civil and environmental engineering; namely the impact of diverting large flows of mud from the point source to the downstream 16 km of the Porong River towards an open strait. Using the Sidoarjo Mud Volcano eruption as a case study, this research has attempted to answer several scientific questions as stated in the Chapter 1. To this end, the research has analyzed the dynamics of sediment propagation along the Porong River. These actions have been done through analysis and through field measurement programs that were used to test the computational model and establish sediment concentration data sets. By completing this research, the idea of diverting the mud from the mud volcano into the Porong River will not cause any major disturbance to the river. It works well to reduce the volume of the mud inside the mud reservoir and the aggradation – degradation processes are balancing each other.

8.1 Properties of the Diverted Mud

a. The results of the particle size distribution analysis were: the median particle size of the extruded mud, Pejarakan's diverted mud, and Ginonjo's diverted mud were 8 μm, 3.4 μm, and 4.7 μm, respectively.

   Laboratory experiments were conducted on July 5, 2019 on the soil sample from the Sidoardjo mud volcano. The experiments of turbidity and sediment concentration concluded that the linear regression, $C = 5.297 \times Tur + 23.96$, was the best fitted regression with coefficient of determination $r^2 = 0.99$.

b. Flocculation tests using deflocculant agents, sodium hexametaphosphate and sodium carbonate, were completed in 2019. For the samples from Ginonjo Outlet, the recorded deflocculated settling velocity was 0.013 mm/s which was 2 times slower than the natural settling velocity of 0.028 mm/s. This value was one order slower than the general settling

velocity for flocculated particles which is between 0.15 to 0.6 mm/s. The test concluded that the mud has a slight tendency to flocculate.

8.2 Field Measurements

a. Field Measurement Program #1 was conducted at 106 cross-sections with 150 m distance between each cross-section, covering16 km of the Porong River to measure sediment concentration. There were 4 points of measurement in each cross-section with 25 m distance between each point and 5 m offset from the left and right bank. The highest sediment concentration should be higher at the left bank of the Porong River. However, the maximum observed sediment concentration for each line was located at cross-section 2 (80 m downstream from the Ginonjo Outlet) was 4,198 mg/l at line C, 2,704 mg/l at line D, 2,021 mg/l at line B, and 691 mg/l at line A. It means that the lateral mixing is much larger along the first 4 km of the study reach. It might ce caused by the river bed protection immediately downstream from the Ginonjo Outlet.

b. Field Measurement Program #2 was conducted to capture the vertical sediment concentration profiles for the first 4km and to look into possible flocculations. The water was collected at every 1 m in depth. Total number of samples were 307 bottles. The highest near-bed sediment concentration was 1,500 mg/l at Line C cross-section 9, followed by 1,450 mg/l at Line C cross-section 6. The results of Field Measurement Program #2 shows that the sediment concentration are uniform along the Porong River except for the first 4 km where the bottom sediment concentration is high.

8.3 Sediment Propagation Model for Porong River

a. HEC-RAS was used to calculate the hydraulic properties of the Porong River, such as the flow depth, width and average velocity. Three flow conditions based on the hydrograph of

the Porong River were defined: low flow with 45 m^3/s, medium flow with 250 m^3/s, and high flow with 2500 m^3/s. For low flow condition, the average flow velocity was 0.12 m/s, the average flow depth was 3.5 m, the top width was 105 m, the energy slope was 0.3 cm/km and the shear velocity was 0.01 m/s. The simulation was done from January 2012 to December 2016. No significant bed change was observed along the simulation time.

b. Sediment concentration of the diverted mud at Ginonjo Outlet was 57,000 mg/l. The results of the mixing model without settling show that the fully-mixed concentration for low flow condition (45 m^3/s) were achieved at 4 km downstream from the outlet with a concentration of 470 mg/l. However, the average observed sediment concentration was about 90 mg/l and the sediment concentration difference was 380 mg/l.

c. The two-dimensional mixing and setting model without flocculation was used by applying the settling factor into the mixing model with finite width. The gravel, sand, and coarser silt fractions were settled in the first 4 k m of the study reach while the finer silt fraction was settled at 7 km. Only the clay fraction was in suspension by the end of study reach with the sediment concentration of 195 mg/l. The clay fraction was accounted for about 48% of the total sediment. The sediment concentration difference between this model and observed data is 105 mg/l.

d. The two-dimensional mixing and setting model with flocculation was then used to advance the previous model. The sediment concentration at the left bank of the Porong River was about 90 mg/l, which matched the observed data. The gravel, sand, and coarser silt fractions settled along the first 4 k m of the study reach, including the flocculated particle with a size of 92 μm. Only clay fraction were in suspension by the end of study reach with a

concentration of 24 mg/l and 54 mg/l, respectively. The flocculated particle accounted for 38% of the total sediment while the clay particle reduced to about 22%.

8.4 Mud Volcano Disaster Guidelines

a. The idea of diverting mud into the Porong River will not cause any damage to the river because the aggradation will occur in the rainy season and degradation will occur in dry season. The diversion works well to reduce the volume of sediment insdie the mud reservoir.
b. The current problem on mud diversion work in the Sidoardjo Mud Volcano, and generally in Indonesia, includes the data availability and data transparency. These problems can be solved with sheer effort from the government and the private sector by installing many new measurement instruments.
c. A guidelines for the future mud volcano disaster has been established with the priority for the human welfare. It is based on the technical findings in and recommendation of this thesis. It includes the preliminary study, securing the affecting zone for mud reservoir, mud diversion work, and the river monitoring.

BIBLIOGRAPHY

Aboubakr, S., Reda Taha, M. M., and Kandil, U. (2013) Creep of epoxy-clay nanocompsite at FRP interface. *Ninth International Conference of Composite Science and Technology, ICCST 9.*

Akalin, S. (2002). Water temperature effect on sand transport by size fraction in the lower Mississippi River. Ph.D. dissertation, Colorado State University.

Allen, G. P., Salomon, J. C., Bassoullet, P., Penhoat, Y. D., and Grandpre, C. D. Effect of tides on mixing and suspended sediment transport in microtidal estuaries. *Sedimentary Geology, 26,* p. 69-90.

Aniekan, E. I., Ebunilo, P. O., and Okovido, J. (2018). Geotechnical evaluation of bentonite clay for municipal solid waste landfill lining membrane. *J. Envir. Eng. Sci. 4,* p. 337-351.

Aris, R. (1956). On the dispersion of a solute in a fluid flowing through a tube. *Proceeding of the Royal Society of London. Series A. Mathematical and Physical Sciences.*

Armijos, E., Crave, A., Espinoza, R., Fraizy, P., Dos Santos, A. L. M. R., Sampalo, F., De Oliveira, E., Santini, W., Martinez, J. M., Autin, P., Pantoja, N, Oliveira, M., and Filizola, N. (2017). Measuring and modeling vertical gradients in suspended sediments in the Solimões/Amazon River. *Hydrological Processes, 31,* p. 654-667.

Bioresita, F., Pribadi, C. B., Firdaus, H. S., Hariyanto, T., and Puissant, A. (2018). The use of Sentinel-2 imagery for total suspended solids (TSS) estimation in Porong River, Sidoardjo. *Elipsoida: Jurnal Geodesi dan Geomatika, vol. 01, no. 01*, p. 1-6.

Blouin, A., Imbert, P., Sultan, N. and Callot, J.-P. (2019). Evolution model for the Absheron Mud Volcano: from in situ observations to numerical modeling. *Journal of Geophysical Research: Earth Surface, 124,* p. 766-794.

Brandon, C. D., and Karathanasis, A.D. (2002). Clay minerals. *Encyclopedia of Soil Science,* p. 187-192.

Breen, N. A., Silver, E. A., and Hussong, D. M. (1986). Structural styles of an accretionary wedge south of the island of Sumba, Indonesia, revealed by SeaMARC II side scan sonar. *Geological Society of America Bulletin, v. 97,* p. 1250-1261.

Brunner, G. W. (2016). *HEC-RAS, river analysis system hydraulic reference manual*. US Army Corps of Engineers Hydrologic Engineering Center (HEC). California: Davis.

Chapra, S. C. (1997). *Surface Water-Quality Modeling*. USA: McGraw-Hill.

Cheng, N-S. (1997). Effect of concentration on settling velocity of sediment particles. *Journal of Hydraul. Engineering, vol. 128*, p. 728-731.

Chow, V.T. (1959). *Open-Channel Hydraulics.* New Jersey: The Blackburn Press.

Christensen, V. G., Rasmussen, P. P., and Ziegler, A. C. (2002). Comparison of estimated sediment loads using continuous turbidity measurements and regression analysis. *Turbidity and Other Surrogates Workshop*.

Cody, C. A., and Magauran, E. D. (1990). *Method of treating waste water for organic contaminants with water dispersible organically modified smectite clay compositions*, US5130028A.

Daphne, L. H. X., Utomo, H. D., and Kenneth, L. Z. H. (2011). Correlation between Turbidity and Total Suspended Solids in Singapore Rivers. *Journal of Water Sustainability, vol. 1, Issue 3.*

Davies, R. J., Mathias, S. A., Swarbrick, R. E., and Tingay, M. J. (2011). Probabilistic longevity estimate for the LUSI mud volcano, East Java. *Journal of Geological Society, vol. 168,* p. 517-523.

Davies, R. J., Swarbrick, R. E., Evans, R. J., and Huuse, M. (2007). Birth of a mud volcano: East Java, 29 May 2006. *GSA Today, v. 17, no. 2,* p. 4-9.

Davies, R., Manga, M., Tingay, M., Lusianga, S., and Swarbrick, R. (2010). Sawolo et al. (2009) the Lusi mud volcano controversy: Was it caused by drilling? *Marine and Petroleum Geology, v. 27*, p. 1651-1657.

Dimitrov, L. I. (2002). Mud volcanoes – the most important pathway for degassing deeply buried sediments. *Earth-Science Reviews, 59,* 49-76.

Ettema, R. (2006). Hunter Rouse – His work in retrospect. *J. Hydraul. Eng., 132,* 1248-1258.

Fischer, H. B., List, E. J, Koh, R. C. Y., Imberger, J., and Brooks, N. H. (1979). *Mixing in inland and coastal waters*. New York: Academic Press, Inc.

Foster, I. D. L., Millington, R., and Grew, R. G. (1992). The impact of particle size controls on stream turbidity measurement; some implications for suspended sediment yield estimation. *Erosion and Sediment Transport Monitoring Programmes in River Basin (Proceedings of the Oslo Symposium). IAHS Publ. no. 210*, p. 51-62.

Geospatial Information Agency. (2019). *Online tidal prediction.* Retrieved from: http://tides.big.go.id/pasut/index.html

Gippel, C. J. (1989). The use of turbidimeters in suspended sediment research. *Hydrobiologia 176/177*, p. 465-480.

Gujarati, D. N., Porter, D. C., and Gunasekar, S. (2012). *Basic Econometrics (5th ed.).* Tamil Nadu: McGraw Hill Education (India) Private Limited.

Guo, C., He, Q., Guo, L., and Winterwerp, J. C. (2017) A study of in-situ sediment flocculation in the turbidity maxima of the Yangtze Estuary. *Estuarine, Coastal and Shelf Science, vol. 191,* p. 1-9.

Guy, H. P. (1969). Laboratory theory and methods for sediment analysis. *United States Geological Survey Techniques of Water Resources Investigations, Book 5*.

Hadimuljono, M. B. (2008). *Sidoardjo's Hot Mudflow Catastrophe: Lessons from a Disaster.*

Hamilton, L. J., Shi, Z., and Zhang, S. Y. (1998). Acoustic backscatter measurements of estuarine suspended cohesive sediment concentration profiles. *Journal of Coastal Research, 14,* p. 1213-1224.

Harnanto, A. (2011). *Peranan Kali Porong dalam mengalirkan lumpur Sidoardjo ke laut.* Badan Pelaksana – Badan Penanggulangan Lumpur Sidoarjo (BAPEL-BPLS).

Hermawan, C. (2012). *Debit minimum Kali Porong untuk menjamin angkutan sedimen sampai ke muara Kali Porong* (Bachelor Thesis). Retrieved from digilib.uns.ac.id.

Hernawan, U., and Budiono, K. (2012). Karakteristik dan distribusi lumpur Sidoardjo sepanjang sungai, estuary dan perairan Porong. *Jurnal Geologi Kelautan, vol 11, no 2,* p. 91-100.

Hidayati, D., Sulaiman, N., Ismail, B. S., Shuhaimi-Othman, M., and De Bellard, M. E. (2017). Evaluation of the effect of Sidoardjo Mud on aquatic life using chromatophores and the microstructure of fish scales. *Sains Malaysiana, 46(3)*, p. 373-380.

Hoekstra, P. (1988). Hydrodynamics and depositional processes of the Solo and Porong Deltas, East Java, Indonesia. *Proceedings KNGMG Symposium 'Coastal Lowlands, Geology and Geotechnology',* p. 161-173.

Holliday, C. P., Rasmussen, T. C., and Miller, W. P. (2003). Establishing the relationship between turbidity and total suspended sediment concentration. *Proceedings of the 2003 Georgia Water Resources Conference,* April 23-24, 2003. Athens, Georgia.

Hunt, J. N. (1954) The turbulent transport of suspended sediment in open channels. *Proc., Royal Society, 224,* p. 322-335.

Indonesian Government. (2001). *Peraturan Pemerintah Republik Indonesia Nomor 82 Tahun 2001 tentang Pengelolaan Kualitas Air dan Pengendalian Pencemaran Air.* Jakarta: State Secretariat.

Indrawan, D., Chayono, M., and Moerwanto, A. S. (2013). Analisis gerak mula pertikel sedimen kohesif (studi kasus lumpur Lapindo Sungai Porong). *Jurnal Teknik Hidraulik, vol 4, no 1,* p. 39-50.

International Organization for Standardization. (2016). *Water quality – determination of turbidity – part 1: quantitative methods.* ISO 7027-1.

Istadi, B. P., Pramono, G. H., Sumintadireja, P., and Alam, S. (2009). Modeling study of growth and potential geohazard for LUSI mud volcano: East Java, Indonesia. *Marine and Petroleum Geology, 26,* p. 1724-1739.

Jansson, M. B. (1992). Turbidimeter measurements in a tropical river, Costa Rica. *Erosion and Sediment Transport Monitoring Programmes in River Basin (Proceedings of the Oslo Symposium). IAHS Publ. no. 210*, p. 71-78.

Jennerjahn, T. C., Jänen, T., Propp, C., Adi, S., and Nugroho, S. P. (2013). Environmental impact of mud volcano inputs on the anthropogenically altered Porong River and Madura Strait coastal waters, Java, Indonesia. *Estuarine, Coastal and Shelf Science, 130,* p. 152-160.

Julien, P. Y. (2010). *Erosion and sedimentation (2nd ed.).* New York: Cambridge University Press.

Julien, P. Y. (2018). *River Mechanics*. New York: Cambridge University Press.

Julien, P. Y., and Mendelsberg, A. (2003). Sediment in Arroyo Pasajero and San Luis Canal. Report. Dept. of Civil Engineering. Colorado State University.

Jung, S. H., Seo, I. W., Kim, Y. D., and Park, I. (2019). Feasibility of velocity-based method for transverse mixing coefficients in river mixing analysis. *J. Hydraul. Eng., 145.*

Kineke, G. C., and Sternberg, R. W. (1989). The effect of particle settling velocity on computed suspended sediment concentration profiles. *Marine Geology, 90,* p. 159-174.

Kociuba, W. (2017). Determination of the bedload transport rate in a small proglacial High Arctic stream using direct, semi-continuous measurement. *Geomorphology, 287,* p. 101-115.

Kopf, A. J. (2002). Significance of mud volcanism. *Rev. Geophys., 40*(2), 1005.

Kure, S., Winarta, B., Takeda, Y., Udo, K., Umeda, M., Mano, A., and Tanaka, H. (2014). Effects of mud flows from the LUSI mud volcano on the Porong River estuary, Indonesia. *Journal of Coastal Research, 70,* p. 568-573.

Laboratorium Mekanika Tanah dan Batuan. (2018) *Laporan hasil uji analisa pembagian butir.* Institut Teknologi Sepuluh November – Fakultas Teknik Sipil dan Lingkungan.

Laboratorium Transportasi dan Geoteknik. (2018). *Laporan hasil tes laboratorium PPLS (Pusat Pengendalian Lumpur Sidoardjo).* Intitut Teknologi Sepuluh November – Fakultas Vokasi.

Lewis, J. (1996). Turbidity-controlled suspended sediment sampling for runoff-event load estimation. *Water Resources Research, vol. 32, no. 7,* p. 2299-2310.

Lupi, M., Saenger, E. H., Fuchs, F., and Miller, S. A. (2013). Lusi mud eruption triggered by geometric focusing of seismic waves. *Nature Geoscience, vol. 6,* p. 642-646.

Manga, M. (2007). Did an earthquake trigger the May 2006 eruption of the Lusi mud volcano? *Eos, vol. 88,* p. 201.

Manga, M., Brumm, M., and Rudolph, M. L. (2009). Earthquake triggering of mud volcanoes. *Marine and Petroleum Geology, vol. 26,* p. 1785-1798.

Marchuk, S. (2016). The Dynamics of potassium in some Australian soils. Ph.D. Dissertation, The University of Adelaide.

Mazumder, B. S., and Ghoshal, K. (2006). Velocity and concentration profiles in uniform sediment-laden flow. *Applied Mathematical Modelling, 30,* p. 164-176

Mazzini, A., Svensen, H., Akhmanov, G. G., Aloisi, G., Planke, S., Malthe-Sørenssen, A., and Istadi, B. (2007). Triggering and dynamic evolution of the LUSI mud volcano, Indonesia. *Earth and Planetary Science Letters, 261,* p. 375-388.

McCarthy, J. C., Pyle, T. E., and Griffin, G. M. (1974). Light transmissivity, suspended sediments and legal definition of turbidity. *Estuarine and Coastal Marine Science 2,* p. 291-299.

McMichael, H. (2009). The Lapindo mudflow disaster: environmental, infrastructure and economic impact. *Bulletin of Indonesian Economic Studies, 45(1),* p. 73-83.

Mellors, R., Kilb, D., Aliyev, A., Gasanov, A., and Yetirmishli, G. (2007). Correlations between earthquakes and large mud volcano eruptions. *J. Geophys. Res., 112, B04304*.

Meyer-Peter, E., and Muller, R. (1948). Formulas for bed-load transport. Proc. 2nd Meeting IAHR, Stockholm, p. 39-64.

Migniot, C. (1989). Tassement et rheologie des vases. *La Houille Blanche*, *no. 1,* p. 11-29.

Milkov, A. V. (2000). Worldwide distribution of submarine mud volcanoes and associated gas hydrates. *Marine Geology, 167,* p. 29-42.

Minella, J. P. G., Merten, G. H., Reichert, J. M., and Clarke, R. T. (2008). Estimating suspended sediment concentrations from turbidity measurements and the calibration problem. *Hydrological Processes 22,* p. 1819-1830.

Mori, J., and Kano, Y. (2009). Is the 2006 Yogyakarta earthquake related to the triggering of the Sidoardjo, Indonesia mud volcano? *Journal of Geography, vol. 118(3),* p. 492-498.

Ndolo Goy, P. (2015). *GIS-based soil erosion modeling and sediment yield of the N'djili River Basin, Democratic Republic of Congo* (Masters Thesis). Retrieved from https://www.engr.colostate.edu/~pierre/

Ni, J. R., and Wang, G. Q. (1991). Vertical sediment distribution. *J. Hydraul. Eng., 117,* p.1184-1194.

O'Loughlin, E. M., and Bowmer, K. H. (1975). Dilution and decay of aquatic herbicides in flowing channels. *Journal of Hydrology, 26,* p. 217-235.

Odom, I. E. (1984). Smectite clay minerals: properties and uses. *Trans. R. Soc. Lond., A 311,* p.391-409.

Pahlevi, A. M., and Wiweka. (2010). Analisa sedimentasi di muara Kali Porong akibat pembuangan lumpur Lapindo menggunakan data citra satelit ASTER. *Jurnal Ilmiah Geomatika, vol 16, no 2,* p. 23-42.

Palu, M. (2019). *Floodwave and sediment transport assessment aling the Doce River after the Fundao Tailings Dam collapse (Brazil).* (Ph.D. Dissertation). Retrieved from https://www.engr.colostate.edu/~pierre/

Palu, M. C., Julien, P. Y. (2019). Modeling the sediment load of the Doce River after the Fundao Tailing Dam collapse, Brazil. *J. Hydraul. Eng., 145.*

Pavanelli, D., and Bigi, A. (2005). Indirect methods to estimate suspended sediment concentration: reliability and relationship of turbidity and settleable solids. *Biosystems Engineering 90(1),* p. 75-83.

Pejrup, M., and Mikkelsen, O. A. (2009). Factors controlling the field settling velocity of cohesive sediment in estuaries. *Estuarine, Coastal and Shelf Science, vol. 87,* p. 177-185.

Pfannkuche, J., and Schmidt A. (2003). Determination of suspended particulate matter concentration from turbidity measurements: particle size effects and calibration procedures. *Hydrological Processes 17,* p. 1951-1963.

Plumlee, G. S., Casadevall, T. J., Wibowo, H. T., Rosenbauer, R. J., Johnson, C. A., Breit, G. N., Lowers, H. A., Wolf, R. E., Hageman, P. L., Goldstein, H., Anthony, M. W., Berry, C. J., Fey, D. J., Meeker, G. P., and Morman, S. A. (2008). *Preliminary analytical results for a mud sample collected from the LUSI mud volcano, Sidoardjo, East Java, Indonesia*. USGS.

Reichert, J. M., Norton, L. D., Favaretto, N., Huang C., and Blume, E. (2009). Settling velocity, aggregate stability, and interrill erodibility of soils varying in clay mineralogy. *Soil Sci. Soc. Am. J., vol. 73,* p. 1369-1377.

Riley, S. J. (1998). The sediment concentration – turbidity relation: its values in monitoring at Ranger Uranium Mine, Northern Territory, Australia. *Catena 32*, p. 1-14.

Rouse, H. (1937). Modern conception of the mechanics of turbulence. *Trans. ASCE*, 102, p 463-543.

Rudolph, M. L., Karlstrom, L., and Manga, M. (2011). A prediction of the longevity of the Lusi mud eruption, Indonesia. *Earth and Planetary Science Letters, 308,* p. 124-130.

Sasaki, Y. and Yamamoto, O. (2017). Bacterial adsorption effect of smectite for wound-healing application. *Journal of the Ceramic Society of Japan, 125 [9],* p. 710-712.

Satyana, A. H., and Asnidar (2008). Mud diapirs and mud volcanoes in depressions of Java to Madura: origins, nature, and implications to petroleum system. *Proceedings, Indonesian Petroleum Association Thirty-Second Annual Convention and Exhibition.*

Sawolo, N., Sutriono, E., Istadi, B. P., and Darmoyo, A. B. (2009). The LUSI mud volcano triggering controversy: Was it caused by drilling?, *Marine and Petroleum Geology, 26,* p. 1766-1784.

Sawolo, N., Sutriono, E., Istadi, B. P., and Darmoyo, A. B. (2010). Was Lusi caused by drilling? – Authors reply to discussion. *Marine and Petroleum Geology, vol. 27,* p. 1658-1675.

Shah-Fairbank, S. C., Julien, P. Y., and Baird, D. C. (2011). Total sediment load from SEMEP using depth-integrated concentration measurements. *J. Hydraul. Eng.,* p. 1606-1614.

Shen, Y., Zhu, Y., Ge, D., and Shen, X. (2016). Effects of initial concentration on flocculation size and settling velocity of marine hydraulic fill clay. *Thalasssas, 32,* p. 117-122.

Shi, J. Z. (2010). Tidal resuspension and transport processes of fine sediment within the river plume in the partuakky-mixed Changjian River estuary, China: A personal perspective. *Geomorphology, 121,* p. 133-151.

Shirzaei, M., Rudolph, M. L., and Manga, M. (2015). Deep and shallow sources for the Lusi mud eruption revealed by surface deformation. *Geophysical Research Letters, vol. 42,* p. 5274-5281.

Silver, E. A., Breen, N. A., and Prasetyo, H. (1986). Multibeam study of the Flores backarc thrust belt, Indonesia. *Journal of Geophysical Research, vol. 91, no. B3,* p. 3489-3500.

Suntoyo, Ikhwani, H., Zikra, M., Sukmasari, N. A., Angraeni, G., Tanaka, H., Umeda, M., and Kure, S. (2015). Modelling the COD,TSS, Phosphate and Nitrate distribution due to the Sidoardjo Mud Flow into Porong River estuary. *Procedia Earth and Planetary Science 14,* p. 144-151.

Sutherland, B. R., Barrett, K. J., and Gingras, M. K. (2014). Clay settling in fresh and salt water. *Environmental Fluid Mechanics, vol. 15.* P. 147-160.

Tanaka, S., and Sugimoto, S. (1958). On the distribution of suspended sediment in experimental flume flow. *Memoirs of the Faculty of Engineering,* Kobe University.

Tingay, M., Heidbach, O., Davies, R., and Swarbrick, R. (2008). Triggering of the Lusi mud eruption: Earthquake versus drilling initiation. *Geology, vol. 36, no. 8,* p. 639-642.

Tingay, M. R. P., Rudolph, M. L., Manga, M., Davies, R. J., and Wang, C. (2015). Initaition of the Lusi mudflow disaster. *Nature Geoscience, vol. 8,* p. 493-494.

Usman, E., Salahuddin, M., Ranawijaya, DAS., and Hutagaol, J. P. (2016). *Lokasi pengendapan akhir dan evaluasi pengelolaan lumpur Porong*. Retrieved Feb 19, 2018. www.mgi.esdm.go.id/content/lokasi-pengendapan-akhir-dan-evaluasi-pengelolaan-lumpur-porong.

van Rijn, L. C. (1984a). Sediment transport, Part I: Bed load transport. *J. Hydraul. Eng., 110,* p. 1431-1456.

van Rijn, L. C. (1984b). Sediment transport, Part II: Suspended load transport. *J. Hydraul. Eng., 110,* p. 1613-1641.

Vanoni, V. A. (1962). *Sedimentation Engineering – ASCE Manual and Reports on Engineering Practice No. 54* (Reprinted 1977).

Vercruysse, K., Grabowski, R. C., and Rickson, R.J. (2017). Suspended sediment transport dynamics in rivers: Multi-scale drivers of temporal variation. *Eath-Science Reviews, 166,* p. 38-52.

Williams, P. R., Pigram, C. J., and Dow, D. B. (1984). Melange production and the importance of shale diapirsm in accretionary terrains. *Nature, vol. 309,* p. 145-146.

Winterwerp, H. (1999). On the dynamics of high-concentrated mud suspensions. Report. Dept. of Civil Engineering and Geosciences. Delft University of Technology.

Wren, D. G., Barkdoll, B. D., Kuhnle, R. A., and Derrow, R. W. (2000). Field techniques for suspended-sediment measurement. *J. Hydraul. Eng., 126,* p. 97-104.

Yang, C. T., Molinas, A., and Wu, B. (1996). Sediment transport in the Yellow River. *J. Hydraul. Eng., 122,* p. 237-244.

Zhu, H. W., Cheng, P. D., Li, W., Chen, J. H., Pang, Y., and Wang, D. Z. (2017). Empirical model for estimating vertical concentration profiles of re-suspended, sediment-associated contaminants. *Acta Mech. Sin., 33,* p. 846-854.

APPENDIX A

Laboratory experiment of the relationship between the turbidity and sediment concentration.

The laboratory experiment procedures were:

1. Prepare a 0.5 gram of sediment from the mud reservoir in a glass beaker. Use the balance to accurately prepare the sediment sample.
2. Collect 100 ml Porong River water in the flask, then add it into the sediment sample.
3. Record the sediment concentration (mg/l) and turbidity (NTU) by using the turbidimeter. Do at least 2 turbidity measurements for each corresponding concentration.
4. Add 100 ml Porong River water to decrease the sediment concentration of the mixture and record the sediment concentration and the turbitiy.
5. Repeat step 4 until the turbidity of our mixture remains unchanged or until the mixture is clearer than the water condition in the Porong River.

Error analysis for the relationship of turbidity and sediment concentration.

We would focus on the linear regression as the best fitted regression and power regression for a comparison with the linear regression. The error of regression could be analyzed by using residual plot. Residual e is the difference between the observed or actual value y and predicted or estimated value $\hat{y}$ (Gujarati, 2012), such as,

$$e = y - \hat{y} \tag{32}$$

where the observed sediment concentration data were used as the actual value y and the predicted values $\hat{y}$ come from the regression analysis by applying the turbidity data set 2.

Figure 58 presents the residual plot for the relationship of turbidity and sediment concentration in the Porong River for linear and power regression. The linear regression gains the highest residual

as $-195.9\,mg/l$, followed by $184.1\,mg/l$. Note that negative value in residual means an overestimated value of dependent variable or sediment concentration in this case while positive value means an underestimated value of sediment concentration. The power regression shows that the highest residual is $-724.9\,mg/l$ and followed by$170.6\,mg/l$. Furthermore, the sum of the residuals for linear power regressions are $-427.7\,mg/l$ and $-1321.6\,mg/l$, respectively.

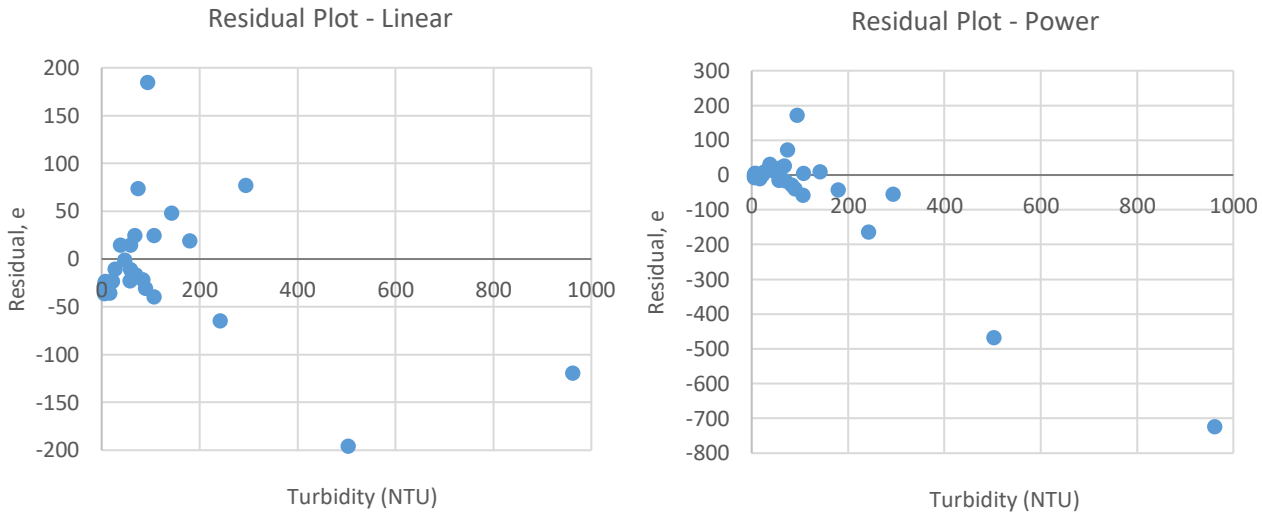

Figure 58 Residual plot for linear and power regression of turbidity – sediment concentration in Porong River

Another method to analyze the error of regression is by comparing the observed values and predicted values of sediment concentration as shown in Figure 59. The predicted values of sediment concentration for linear regression fall closely to the 1:1 line which indicates small errors between the observed values and the predicted values. However, the predited values of sediment concentration for the power regression do not fall on the 1:1 line, particularly at higher values of concentration. Thus, from the regression analysis and it error, we can conclude that the linear regression is the best regression to predict the sediment concentration in Porong River from turbidity based on the laboratory experiment.

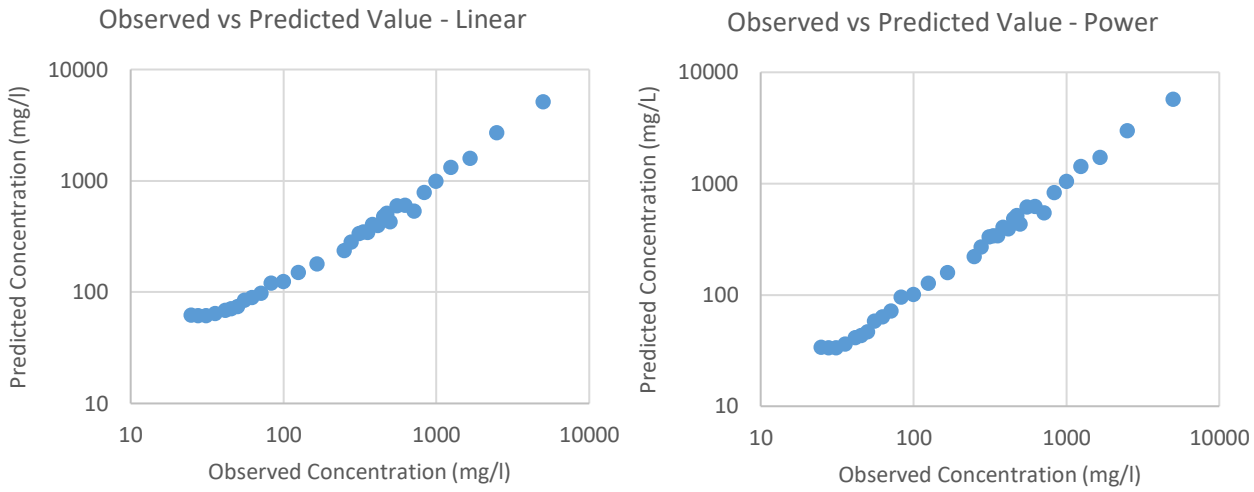

Figure 59 The comparison of observed and predicted value of sediment concentration from laboratory experiment

APPENDIX B

Field Program #1 – Turbidity Data of Porong River (Brantas River Basin Organization)

Date of Measurement: July 10-14, 2018

No	Point	Turbidity (NTU)	No	Point	Turbidity (NTU)
1	P 1 A	134.00	29	P 8 A	32.10
2	P 1 B	40.40	30	P 8 B	26.00
3	P 1 C	32.80	31	P 8 C	26.60
4	P 1 D	25.90	32	P 8 D	27.70
5	P 2 A	52.30	33	P 9 A	31.40
6	P 2 B	27.20	34	P 9 B	21.80
7	P 2 C	41.20	35	P 9 C	25.20
8	P 2 D	22.10	36	P 9 D	64.10
9	P 3 A	31.10	37	P 10 A	38.50
10	P 3 B	36.50	38	P 10 B	23.40
11	P 3 C	29.60	39	P 10 C	28.10
12	P 3 D	27.60	40	P 10 D	27.60
13	P 4 A	49.10	41	P 11 A	32.70
14	P 4 B	39.50	42	P 11 B	22.40
15	P 4 C	33.80	43	P 11 C	30.80
16	P 4 D	24.10	44	P 11 D	38.80
17	P 5 A	27.90	45	P 12 A	27.80
18	P 5 B	24.10	46	P 12 B	24.70
19	P 5 C	25.00	47	P 12 C	26.80
20	P 5 D	33.40	48	P 12 D	33.50
21	P 6 A	31.60	49	P 13 A	11.30
22	P 6 B	26.40	50	P 13 B	27.70
23	P 6 C	27.20	51	P 13 C	20.20
24	P 6 D	26.40	52	P 13 D	29.80
25	P 7 A	35.00	53	P 14 A	87.30
26	P 7 B	45.10	54	P 14 B	84.00
27	P 7 C	28.30	55	P 14 C	788.00
28	P 7 D	25.60	56	P 14 D	55.60

No	Point	Turbidity (NTU)	No	Point	Turbidity (NTU)
57	P 15 A	70.10	93	P 24 A	37.60
58	P 15 B	266.00	94	P 24 B	32.60
59	P 15 C	561.00	95	P 24 C	21.20
60	P 15 D	506.00	96	P 24 D	24.60
61	P 16 A	63.10	97	P 25 A	34.90
62	P 16 B	377.00	98	P 25 B	32.80
63	P 16 C	118.00	99	P 25 C	19.50
64	P 16 D	184.00	100	P 25 D	21.60
65	P 17 A	126.00	101	P 26 A	24.90
66	P 17 B	217.00	102	P 26 B	23.00
67	P 17 C	218.00	103	P 26 C	23.80
68	P 17 D	127.00	104	P 26 D	20.30
69	P 18 A	56.70	105	P 27 A	25.50
70	P 18 B	61.50	106	P 27 B	17.50
71	P 18 C	82.60	107	P 27 C	21.50
72	P 18 D	61.80	108	P 27 D	24.50
73	P 19 A	65.50	109	P 28 A	26.90
74	P 19 B	60.40	110	P 28 B	21.70
75	P 19 C	45.80	111	P 28 C	19.00
76	P 19 D	57.80	112	P 28 D	19.90
77	P 20 A	44.80	113	P 29 A	26.30
78	P 20 B	53.10	114	P 29 B	21.20
79	P 20 C	26.90	115	P 29 C	19.40
80	P 20 D	32.00	116	P 29 D	25.90
81	P 21 A	14.40	117	P 30 A	28.20
82	P 21 B	45.20	118	P 30 B	21.40
83	P 21 C	38.50	119	P 30 C	20.00
84	P 21 D	45.30	120	P 30 D	12.50
85	P 22 A	35.60	121	P 31 A	13.00
86	P 22 B	34.90	122	P 31 B	12.90
87	P 22 C	36.60	123	P 31 C	13.20
88	P 22 D	25.10	124	P 31 D	11.70
89	P 23 A	52.30	125	P 32 A	13.30
90	P 23 B	24.10	126	P 32 B	13.30
91	P 23 C	24.50	127	P 32 C	11.20
92	P 23 D	21.30	128	P 32 D	13.20

No	Point	Turbidity (NTU)	No	Point	Turbidity (NTU)
129	P 33 A	7.61	165	P 42 A	12.30
130	P 33 B	6.71	166	P 42 B	11.90
131	P 33 C	10.90	167	P 42 C	10.20
132	P 33 D	12.80	168	P 42 D	9.67
133	P 34 A	10.40	169	P 43 A	11.70
134	P 34 B	11.60	170	P 43 B	13.20
135	P 34 C	13.40	171	P 43 C	9.30
136	P 34 D	12.30	172	P 43 D	9.62
137	P 35 A	7.03	173	P 44 A	10.80
138	P 35 B	11.10	174	P 44 B	10.10
139	P 35 C	12.30	175	P 44 C	9.48
140	P 35 D	9.03	176	P 44 D	9.45
141	P 36 A	9.22	177	P 45 A	10.60
142	P 36 B	8.74	178	P 45 B	9.68
143	P 36 C	8.90	179	P 45 C	9.11
144	P 36 D	9.51	180	P 45 D	10.10
145	P 37 A	8.39	181	P 46 A	10.60
146	P 37 B	9.29	182	P 46 B	9.50
147	P 37 C	10.50	183	P 46 C	6.97
148	P 37 D	9.42	184	P 46 D	10.20
149	P 38 A	10.30	185	P 47 A	11.60
150	P 38 B	10.80	186	P 47 B	9.92
151	P 38 C	10.70	187	P 47 C	8.68
152	P 38 D	10.60	188	P 47 D	10.60
153	P 39 A	11.10	189	P 48 A	15.50
154	P 39 B	9.77	190	P 48 B	13.20
155	P 39 C	8.84	191	P 48 C	11.20
156	P 39 D	11.90	192	P 48 D	14.60
157	P 40 A	11.00	193	P 49 A	15.50
158	P 40 B	11.40	194	P 49 B	12.00
159	P 40 C	9.76	195	P 49 C	13.00
160	P 40 D	11.20	196	P 49 D	11.40
161	P 41 A	10.50	197	P 50 A	15.30
162	P 41 B	10.80	198	P 50 B	12.90
163	P 41 C	11.50	199	P 50 C	11.80
164	P 41 D	9.42	200	P 50 D	13.30

No	Point	Turbidity (NTU)	No	Point	Turbidity (NTU)
201	P 51 A	16.60	237	P 60 A	14.00
202	P 51 B	15.50	238	P 60 B	14.90
203	P 51 C	12.90	239	P 60 C	14.60
204	P 51 D	13.50	240	P 60 D	13.40
205	P 52 A	16.10	241	P 61 A	12.20
206	P 52 B	14.60	242	P 61 B	11.00
207	P 52 C	15.40	243	P 61 C	12.40
208	P 52 D	15.30	244	P 61 D	11.90
209	P 53 A	15.00	245	P 62 A	10.00
210	P 53 B	14.70	246	P 62 B	11.50
211	P 53 C	15.00	247	P 62 C	13.10
212	P 53 D	15.60	248	P 62 D	12.50
213	P 54 A	16.00	249	P 63 A	10.80
214	P 54 B	14.90	250	P 63 B	11.80
215	P 54 C	16.40	251	P 63 C	10.90
216	P 54 D	15.20	252	P 63 D	11.00
217	P 55 A	15.80	253	P 64 A	11.70
218	P 55 B	14.00	254	P 64 B	10.90
219	P 55 C	15.90	255	P 64 C	9.91
220	P 55 D	14.00	256	P 64 D	10.90
221	P 56 A	15.20	257	P 65 A	12.20
222	P 56 B	14.10	258	P 65 B	10.60
223	P 56 C	15.80	259	P 65 C	11.40
224	P 56 D	16.00	260	P 65 D	9.62
225	P 57 A	15.20	261	P 66 A	10.70
226	P 57 B	14.30	262	P 66 B	10.60
227	P 57 C	14.50	263	P 66 C	10.40
228	P 57 D	15.60	264	P 66 D	9.61
229	P 58 A	16.70	265	P 67 A	1.40
230	P 58 B	15.30	266	P 67 B	9.70
231	P 58 C	15.20	267	P 67 C	9.55
232	P 58 D	16.10	268	P 67 D	7.19
233	P 59 A	12.30	269	P 68 A	10.90
234	P 59 B	14.70	270	P 68 B	10.10
235	P 59 C	14.80	271	P 68 C	8.18
236	P 59 D	16.10	272	P 68 D	7.15

No	Point	Turbidity (NTU)	No	Point	Turbidity (NTU)
273	P 69 A	11.10	309	P 78 A	11.60
274	P 69 B	11.90	310	P 78 B	8.75
275	P 69 C	11.60	311	P 78 C	9.05
276	P 69 D	9.81	312	P 78 D	10.40
277	P 70 A	8.37	313	P 79 A	11.70
278	P 70 B	7.06	314	P 79 B	9.37
279	P 70 C	10.00	315	P 79 C	10.20
280	P 70 D	10.30	316	P 79 D	10.20
281	P 71 A	10.20	317	P 80 A	15.40
282	P 71 B	8.60	318	P 80 B	10.00
283	P 71 C	10.20	319	P 80 C	8.60
284	P 71 D	13.40	320	P 80 D	10.50
285	P 72 A	10.20	321	P 81 A	15.00
286	P 72 B	9.99	322	P 81 B	10.60
287	P 72 C	11.00	323	P 81 C	10.90
288	P 72 D	9.68	324	P 81 D	10.90
289	P 73 A	11.20	325	P 82 A	8.68
290	P 73 B	10.60	326	P 82 B	12.50
291	P 73 C	10.20	327	P 82 C	10.50
292	P 73 D	10.10	328	P 82 D	10.90
293	P 74 A	13.00	329	P 83 A	13.70
294	P 74 B	10.20	330	P 83 B	10.50
295	P 74 C	9.46	331	P 83 C	9.20
296	P 74 D	13.00	332	P 83 D	18.90
297	P 75 A	10.40	333	P 84 A	16.10
298	P 75 B	10.30	334	P 84 B	12.40
299	P 75 C	9.73	335	P 84 C	9.53
300	P 75 D	10.30	336	P 84 D	14.00
301	P 76 A	11.40	337	P 85 A	15.20
302	P 76 B	10.80	338	P 85 B	8.78
303	P 76 C	9.99	339	P 85 C	11.70
304	P 76 D	10.10	340	P 85 D	13.90
305	P 77 A	11.60	341	P 86 A	15.60
306	P 77 B	10.10	342	P 86 B	10.50
307	P 77 C	10.20	343	P 86 C	11.40
308	P 77 D	10.50	344	P 86 D	13.60

No	Point	Turbidity (NTU)	No	Point	Turbidity (NTU)
345	P 87 A	20.40	381	P 95 A	14.60
346	P 87 B	9.47	382	P 95 B	11.20
347	P 87 C	10.90	383	P 95 C	10.60
348	P 87 D	16.20	384	P 95 D	9.31
349	P 88 A	23.90	385	P 96 A	11.20
350	P 88 B	11.00	386	P 96 B	10.20
351	P 88 C	10.70	387	P 96 C	11.40
352	P 88 D	18.10	388	P 96 D	13.00
353	P 89 A	16.40	389	P 97 A	16.20
354	P 89 B	10.70	390	P 97 B	11.50
355	P 89 C	15.70	391	P 97 C	14.90
356	P 89 D	15.90	392	P 97 D	14.70
357	P 90 A	20.10	393	P 98 A	15.70
358	P 90 B	11.40	394	P 98 B	14.00
359	P 90 C	5.86	395	P 98 C	11.40
360	P 90 D	13.70	396	P 98 D	14.40
361	P 90 A	12.30	397	P 99 A	11.10
362	P 90 B	11.60	398	P 99 B	11.00
363	P 90 C	6.14	399	P 99 C	11.60
364	P 90 D	13.50	400	P 99 D	11.80
365	P 91 A	12.70	401	P 100 A	15.50
366	P 91 B	20.80	402	P 100 B	13.00
367	P 91 C	11.40	403	P 100 C	10.40
368	P 91 D	13.30	404	P 100 D	13.20
369	P 92 A	13.40	405	P 101 A	13.70
370	P 92 B	12.60	406	P 101 B	11.70
371	P 92 C	14.00	407	P 101 C	14.40
372	P 92 D	14.80	408	P 101 D	19.80
373	P 93 A	13.90	409	P 102 A	18.20
374	P 93 B	10.40	410	P 102 B	17.40
375	P 93 C	11.50	411	P 102 C	11.90
376	P 93 D	13.30	412	P 102 D	16.30
377	P 94 A	14.10	413	P 103 A	17.10
378	P 94 B	9.61	414	P 103 B	11.10
379	P 94 C	12.40	415	P 103 C	16.00
380	P 94 D	14.40	416	P 103 D	17.10

No	Point	Turbidity (NTU)	No	Point	Turbidity (NTU)
417	P 104 A	34.00	453	P 113 A	15.70
418	P 104 B	23.80	454	P 113 B	12.30
419	P 104 C	11.30	455	P 113 C	11.30
420	P 104 D	19.50	456	P 113 D	15.50
421	P 105 A	18.50	457	P 114 A	20.60
422	P 105 B	12.70	458	P 114 B	15.10
423	P 105 C	10.90	459	P 114 C	12.00
424	P 105 D	19.90	460	P 114 D	15.50
425	P 106 A	23.20	461	P 115 A	16.30
426	P 106 B	13.70	462	P 115 B	10.90
427	P 106 C	10.20	463	P 115 C	16.30
428	P 106 D	14.00	464	P 115 D	15.20
429	P 107 A	9.98			
430	P 107 B	13.50			
431	P 107 C	13.00			
432	P 107 D	26.10			
433	P 108 A	10.20			
434	P 108 B	14.60			
435	P 108 C	13.00			
436	P 108 D	11.10			
437	P 109 A	11.50			
438	P 109 B	11.50			
439	P 109 C	18.00			
440	P 109 D	15.80			
441	P 110 A	19.80			
442	P 110 B	15.10			
443	P 110 C	12.80			
444	P 110 D	14.00			
445	P 111 A	12.70			
446	P 111 B	10.10			
447	P 111 C	13.50			
448	P 111 D	13.50			
449	P 112 A	14.90			
450	P 112 B	11.90			
451	P 112 C	9.73			
452	P 112 D				

APPENDIX C

Output of the HEC-RAS model - sediment time series

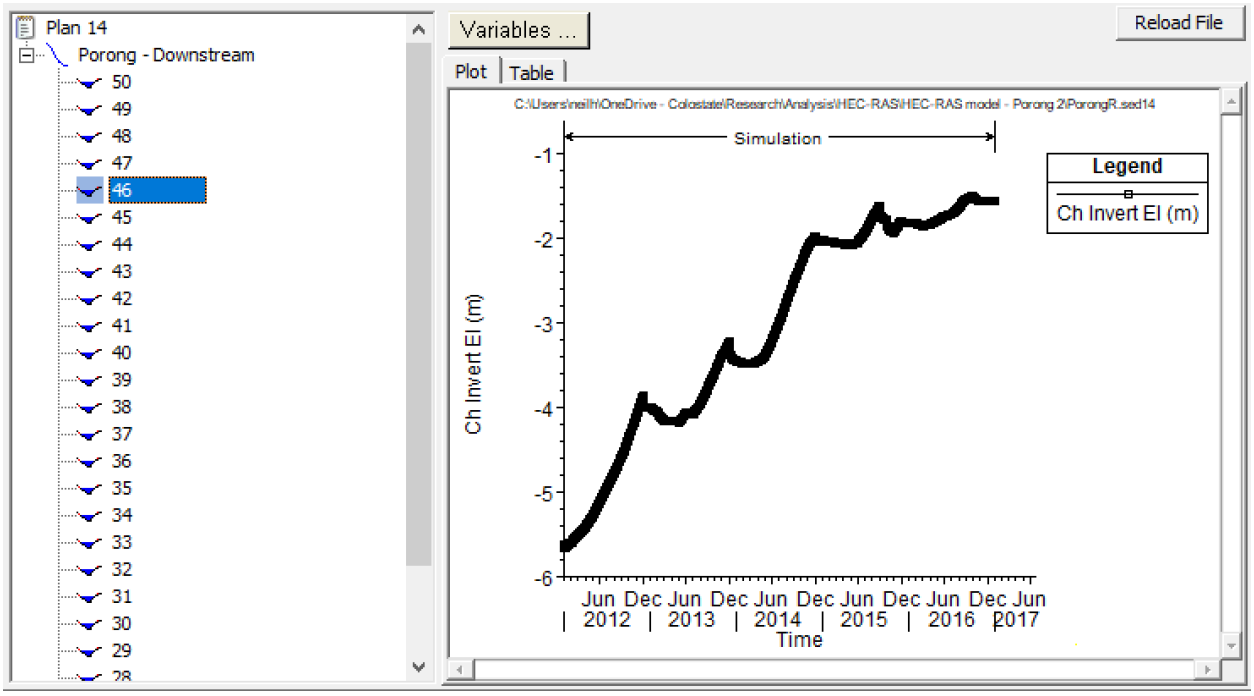

Figure 60 Sediment time series of cross-section 46

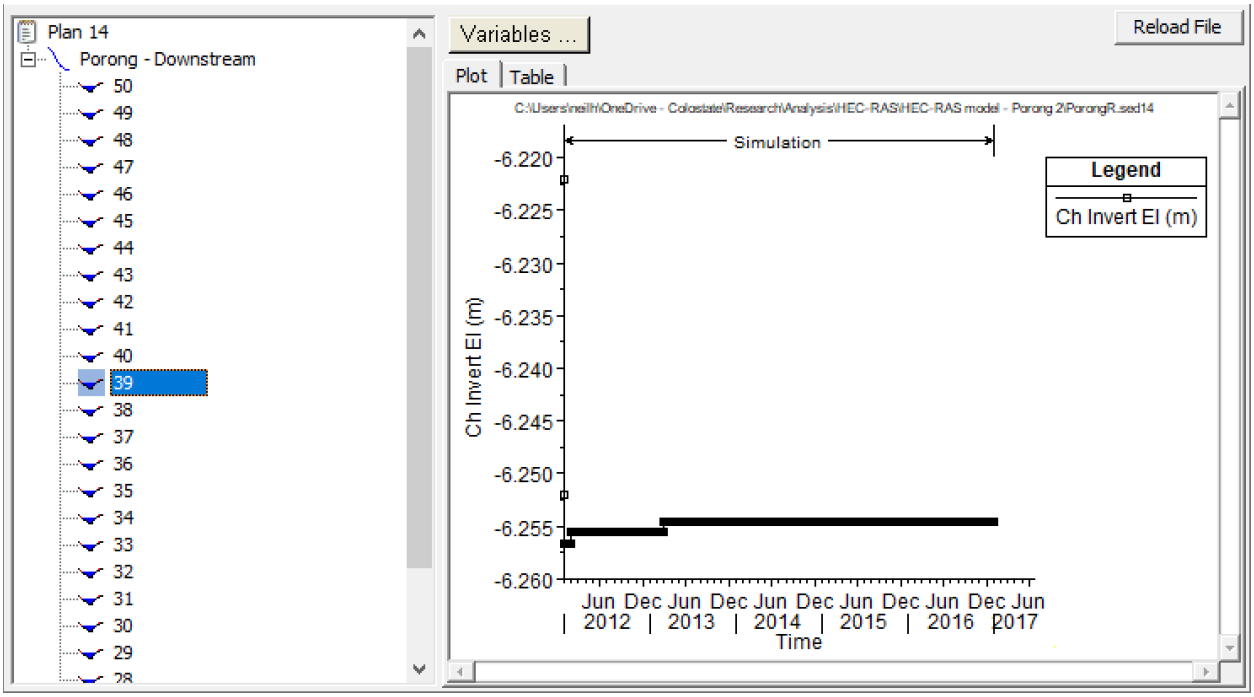

Figure 61 Sediment time series of cross-section 39

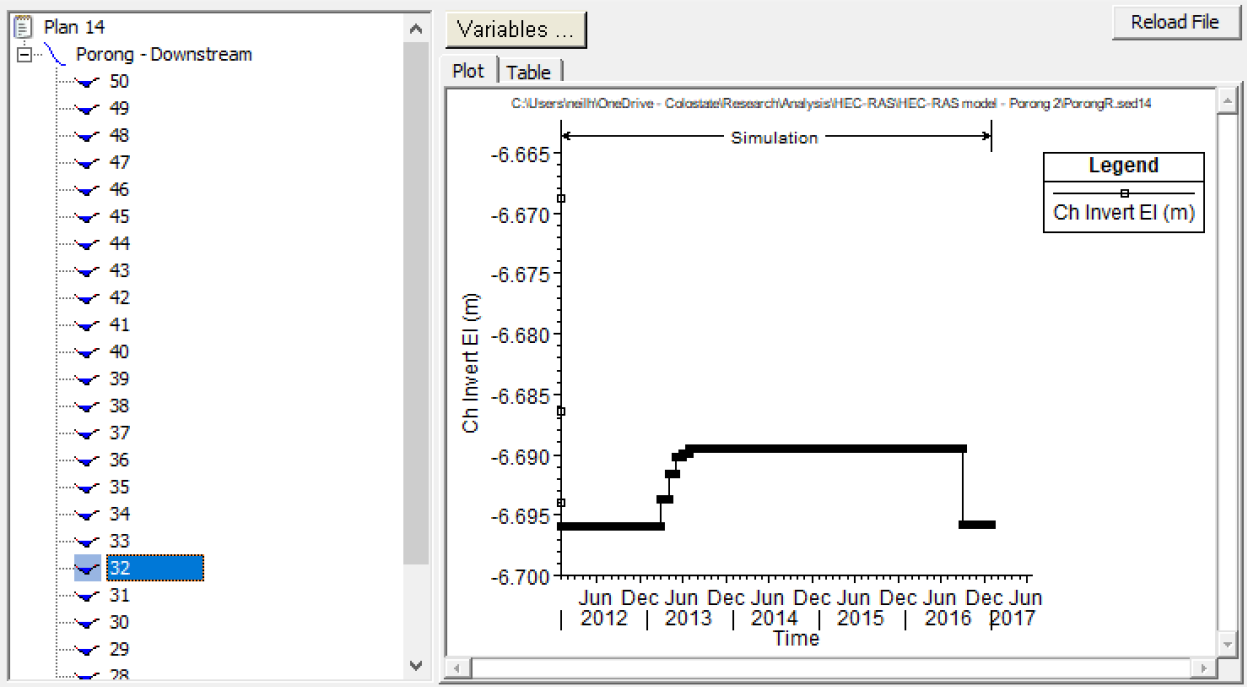

Figure 62 Sediment time series of cross-section 32

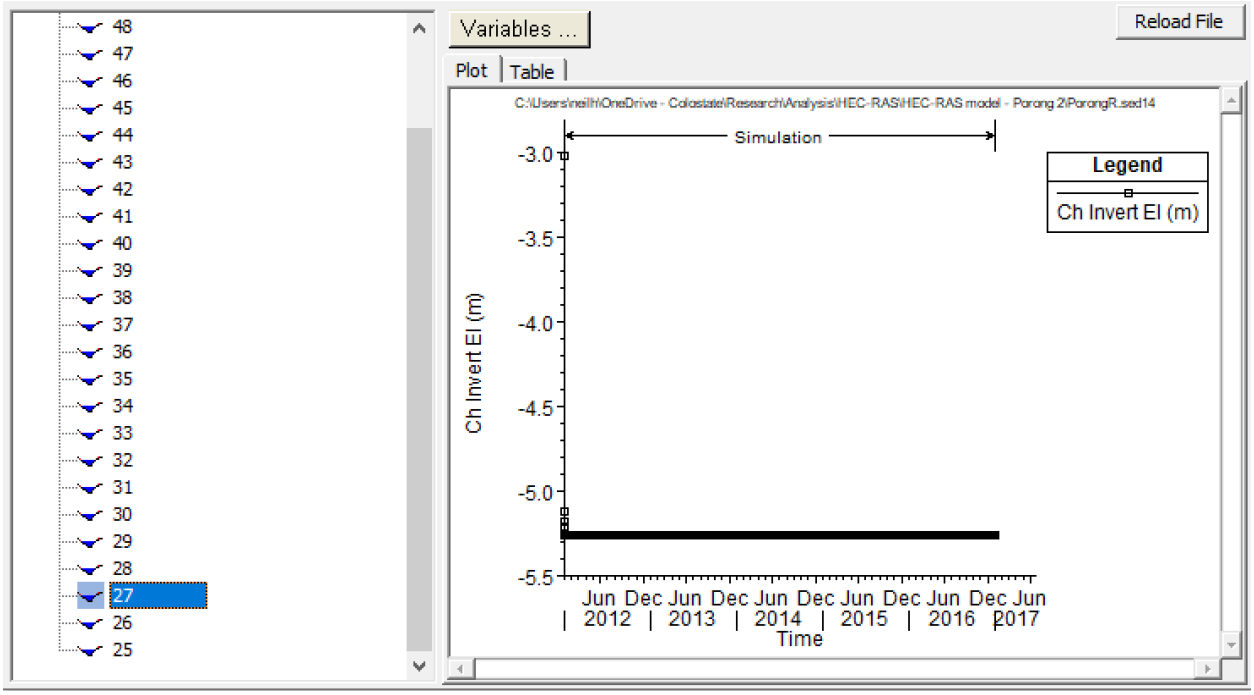

Figure 63 Sediment time series of cross-section 27